



**Anti-aggregation of Gold Nanoparticles for Inorganic Bromide  
Detection in Rice Sample**

**Siwat Plaisen**

**A Thesis Submitted in Partial Fulfillment of the Requirements for the  
Degree of Master of Science in Chemistry  
Prince of Songkla University  
2018  
Copyright of Prince of Songkla University**

**Thesis Title**                      Anti-aggregation of gold nanoparticles for inorganic  
bromide detection in rice sample  
**Author**                                Mr. Siwat Plaisen  
**Major Program**                    Chemistry (Analytical Chemistry)

---

**Major Advisor**

.....  
(Dr. Thitima Rujiralai)

**Examining Committee :**

.....Chairperson  
(Asst. Prof. Dr. Supaporn Sangsrichan)

**Co-advisor**

.....  
(Asst. Prof. Dr. Wilairat Cheewasedtham)

.....Committee  
(Asst. Prof. Dr. Apon Numnuam)

.....Committee  
(Dr. Thitima Rujiralai)

.....Committee  
(Asst. Prof. Dr. Wilairat Cheewasedtham)

The Graduate School, Prince of Songkla University, has approved this thesis as partial fulfillment of the requirements for the Master of Science Degree in Chemistry (Analytical Chemistry)

.....  
(Prof. Dr. Damrongsak Faroongsarng)  
Dean of Graduate School

This is to certify that the work here submitted is the result of the candidate's own investigations. Due acknowledgement has been made of any assistance received.

..... Signature  
(Dr. Thitima Rujiralai)  
Major Advisor

..... Signature  
(Mr. Siwat Plaisen)  
Candidate

I hereby certify that this work has not been accepted in substance for any degree, and is not being currently submitted in candidature for any degree.

..... Signature

(Mr. Siwat Plaisen)

Candidate

ชื่อวิทยานิพนธ์	การต้านการรวมกลุ่มของอนุภาคทองนาโนสำหรับตรวจวัดโบรไมด์อนินทรีย์ในตัวอย่างข้าว
ผู้เขียน	นายศิวัช พลายเสน
สาขาวิชา	เคมี (เคมีวิเคราะห์)
ปีการศึกษา	2560

### บทคัดย่อ

การพัฒนาวิธีตรวจวัดสีที่ง่ายและมีความไววิเคราะห์สูงสำหรับการตรวจวัดโบรไมด์อนินทรีย์ (โบรไมด์ไอออน) ในข้าวสารอาศัยวิธีต้านการรวมกลุ่มของอนุภาคทองนาโน (AuNPs) โดยโบรไมด์ไอออนที่ถูกดูดซับบนผิวอนุภาคทองนาโนเป็นตัวป้องกันไม่ให้อนุภาคทองนาโนรวมกลุ่มที่ขึ้นกับการเกิดสารประกอบเชิงซ้อนระหว่างโครเมียมไอออนกับซิเตรทไอออนที่เคลือบอยู่บนผิวหน้าอนุภาคทองนาโน ทำให้สีของการรวมกลุ่มเปลี่ยนจากน้ำเงินเป็นสีแดงของการต้านการรวมกลุ่มตามความเข้มข้นของโบรไมด์ไอออนที่เพิ่มขึ้น

ในสภาวะที่เหมาะสมของการใช้อนุภาคทองนาโนเข้มข้น 1.83 นาโนโมลาร์ โครเมียมไอออนเข้มข้น 4.81 ไมโครโมลาร์ และสารละลายฟอสเฟตบัฟเฟอร์ (พีเอช 6.5) เข้มข้น 10 มิลลิโมลาร์ และใช้เวลา 10 นาทีในการทำปฏิกิริยา ทำให้ได้กราฟมาตรฐานโบรไมด์ไอออนจากการเปลี่ยนแปลงสีในช่วง 0.31 - 3.75 ไมโครโมลาร์ ( $y = 3.4803x - 0.6065$ ,  $R^2 = 0.9970$ ) ขีดจำกัดการตรวจวัดและขีดการตรวจวัดเชิงปริมาณเท่ากับ 0.04 และ 0.13 ไมโครโมลาร์ ตามลำดับ ร้อยละการได้กลับคืนอยู่ในช่วง 79.9 - 92.2 ค่าร้อยละเบี่ยงเบนมาตรฐานสัมพัทธ์ของความเที่ยงภายในวันและระหว่างวันดีกว่ำร้อยละ 7.12 อย่างไรก็ตามเนื่องจากผลของเมตริกซ์ทำให้ใช้กราฟการเติมสารมาตรฐานในการตรวจวัดเชิงปริมาณหาโบรไมด์ไอออนในข้าวสาร

การเตรียมตัวอย่างข้าวสารก่อนการตรวจวัดอาศัยการย่อยด้วยต่างและเผาให้เป็นเถ้าที่อุณหภูมิ 600 องศาเซลเซียส เป็นเวลา 4 ชั่วโมง ซึ่งสามารถกำจัดสารอินทรีย์และธาตุองค์ประกอบบางส่วนได้ จากการยืนยันผลโดยเทคนิคเอกซเรย์ฟลูออเรสเซนซ์สเปกโตรเมตรี พบว่าโบรไมด์ไอออนไม่สลายตัวเมื่อเผาตัวอย่างให้เป็นเถ้าที่อุณหภูมิสูง (600 องศาเซลเซียส) วิธีเซนเซอร์ที่พัฒนาขึ้นมีความจำเพาะมากกับโบรไมด์ไอออนเมื่อเทียบกับไอออนอื่นที่พบในข้าว นอกจากนี้ได้พัฒนาการตรวจวัดโบรไมด์ไอออนในข้าวสารขาว จำนวน 5 ยี่ห้อ พบปริมาณโบรไมด์ไอออนอยู่ในช่วง 3.12 - 5.21 มิลลิกรัมต่อกิโลกรัม โดยผลสอดคล้องกับการตรวจวัดด้วยเทคนิคไอออนโครมาโทกราฟีอย่างไม่แตกต่างอย่างมีนัยสำคัญ และมีค่าไม่เกินค่าปริมาณสารพิษตกค้างสูงสุดที่กำหนดโดยคณะกรรมการอาหารระหว่างประเทศ (โคเด็กซ์)

<b>Thesis Title</b>	Anti-aggregation of gold nanoparticles for inorganic bromide detection in rice sample
<b>Author</b>	Mr. Siwat Plaisen
<b>Major Program</b>	Chemistry (Analytical Chemistry)
<b>Academic Year</b>	2017

## ABSTRACT

A simple and highly sensitive colorimetric sensor for inorganic bromide ( $\text{Br}^-$ ) detection in rice samples was developed. The sensor is based on anti-aggregation of gold nanoparticle (AuNPs) *via* the adsorbed  $\text{Br}^-$  on AuNPs surface, leading to interruption of an AuNPs aggregation process based on coordination of chromium ion ( $\text{Cr}^{3+}$ ) and citrate capped AuNPs. Consequently, the solution color of aggregation state changed from blue to red color of anti-aggregation state with increasing the  $\text{Br}^-$  concentration.

Under the optimum condition of 1.83 nM AuNPs with 4.81  $\mu\text{M}$   $\text{Cr}^{3+}$  in 10 mM phosphate buffer (pH 6.5) and 10 min of reaction time, a linear calibration curve based on the color transition observed by naked eye was 0.31 - 3.75  $\mu\text{M}$   $\text{Br}^-$  ( $y = 3.4803x - 0.6065$ ,  $R^2 = 0.9970$ ). The limit of detection (LOD) and limit of quantification (LOQ) were 0.04 and 0.13  $\mu\text{M}$ , respectively. The recoveries were 79.9 - 92.2 % and intra- and inter-day precisions as % relative standard deviation were better than 7.12 %. However, due to matrix effect, a standard addition curve was applied for accurate determination of  $\text{Br}^-$  in rice samples.

The preparation of rice samples before colorimetric detection was carried out by alkaline digestion and dry ashing at 600 °C for 4 h that can remove organic compounds and the minor elements. The X-ray fluorescence spectrometry (XRF) results confirmed that  $\text{Br}^-$  did not evaporate after ashing at high temperature (600 °C). The developed sensor is very selective to  $\text{Br}^-$  compared to other ions which is found in rice samples. Moreover, it was successfully applied for determination of  $\text{Br}^-$  in five brands of white rice samples. The  $\text{Br}^-$  residues were detected ranging from 3.12 - 5.21  $\text{mg kg}^{-1}$  in all samples which was corresponded to the  $\text{Br}^-$  detected by ion chromatography with no significant difference and no over the maximum residue limit of 50  $\text{mg kg}^{-1}$  set by CODEX.

## Acknowledgements

The successful completion of this thesis would be quite impossible without the help of many people. I wish to express my gratitude to those who have contributed to the completion of this thesis:

I would like to thank my advisor, Dr. Thitima Rujiralai and my co-advisor, Assistant Professor Dr. Wilairat Cheewasedtham for giving me the opportunity to work on my interested field for their guidance, advice, encouragement, suggestions and support throughout the whole duration of this work.

I would like to thank the examining committee members, Assistant Professor Dr. Supaporn Sangsrichan and Assistant Professor Dr. Apon Numnuam, for their good comments and suggestions and their valuable time.

I would like to thank Professor Dr. Jens Christian Tjell for his great suggestion and guidance for thesis.

I would like to thank all instructors and all staff in the Department of Chemistry for my education and training throughout this graduate studies.

I would like to thank the Research Assistantship (Contract No. 1-2558-02-003), Faculty of Science, Prince of Songkla University, the Center of Excellence for Innovation in Chemistry (PERCH-CIC), Office of the Higher Education Commission, Ministry of Education (OHEC), and the Graduate School, Prince of Songkla University.

Thanks also go to the Department of Chemistry, Faculty of Science, Prince of Songkla University for the support of available facilities.

Many thanks go to all members in research room Ch315, members of graduate student and my best friends for continual care throughout this thesis.

Finally, and most importantly, I would like to thank my family for their loves, encouragement, understanding and support throughout my life.

Siwat Plaisen

## **The Relevance of the Research Work to Thailand**

The purpose of this Master of Science Thesis in Chemistry (Analytical chemistry) is to develop the colorimetric method for detection of inorganic bromide based on anti-aggregation of gold nanoparticles and application in rice samples.

The developed method is robust colorimetric sensor which is the facile, sensitive and selective detection of bromide ion in rice samples. This work can be applied to monitor the bromide contaminated in rice samples as the screening test for food safety.



## Contents

	<b>Page</b>
Table of Contents	ix
List of Table	xv
List of Figure	xvi
List of Abbreviations	xx
<b>CHAPTER 1 INTRODUCTION</b>	<b>1</b>
1.1 Background and rationale	1
1.2 Review of literature	4
1.2.1 Methyl bromide and bromide ion	4
1.2.1.1 Physical and chemical properties of methyl bromide	4
1.2.1.2 Physical and chemical properties of bromide ion	4
1.2.1.3 The toxicity of methyl bromide and bromide ion on human health	5
1.2.1.4 The use of methyl bromide as a pesticide	6
1.2.1.5 Environmental impact of methyl bromide	7
1.2.1.6 The use of methyl bromide in Thailand	7
1.2.2 Gold nanoparticles (AuNPs)	8
1.2.2.1 The introduction of AuNPs	8
1.2.2.2 The surface plasmon resonance phenomenon	9
1.2.2.3 The synthesis method of AuNPs	11
1.2.2.4 The application of colorimetric sensing based on aggregation and anti-aggregation	12
1.2.3 Analytical techniques	15
1.2.3.1 Ultraviolet-Visible spectrophotometry	15
1.2.3.2 Other techniques	16
1.2.4 Method validation	19

## Contents (continued)

	<b>Page</b>
1.2.4.1 Linearity	19
1.2.4.2 Limit of detection (LOD) and limit of quantification (LOQ)	20
1.2.4.3 Matrix effect	21
1.2.4.4 Accuracy	22
1.2.4.5 Precision	23
1.3 Objective	23
1.4 Benefit	23
<b>CHAPTER 2 EXPERIMENTAL</b>	<b>24</b>
2.1 Overall scope	24
2.2 Chemicals and reagents	25
2.3 Laboratory glassware	26
2.3.1 Glassware	26
2.3.2 Preparation and cleaning method of glassware	26
2.3.2.1 Cleaning method of general glassware	26
2.3.2.2 Cleaning method of specific glassware	26
2.4 Apparatus and materials	27
2.5 Instrument	28
2.5.1 UV-Visible spectrophotometer	28
2.5.2 Transmission electron microscopy	28
2.5.3 Zeta potential analyzer	28
2.5.4 Inductively coupled plasma optical emission spectrometer	28
2.5.5 X-Ray Fluorescence Spectrometer	29
2.5.6 Ion chromatography	29
2.6 Preparation of solution	29
2.6.1 Preparation of stock standard solution of 12.52 mM (1000 ppm) bromide ion	29
2.6.2 Preparation of 0.015% w/v Gold(III) chloride solution	29

**Contents (continued)**

	<b>Page</b>
2.6.3 Preparation of 1% w/v sodium citrate solution	29
2.6.4 Preparation of 19.23 mM (1000 ppm) chromium (III) solution	29
2.6.5 Preparation of 20 mM Sodium dihydrogen phosphate solution	30
2.6.6 Preparation of 20 mM Di-sodium hydrogen phosphate solution	30
2.6.7 Preparation of working standard solution of 0.1252 mM (10 ppm) bromide ion	30
2.6.8 Preparation of working concentration range of bromide ion	30
2.6.9 Preparation of 0.1154 mM (6 ppm) chromium (III) solution	31
2.6.10 Preparation of working concentration range of chromium (III) ion	31
2.6.11 Preparation of 0.01 M sodium phosphate buffer solution	32
2.6.12 Preparation of 1% (w/v) potassium hydroxide in 50% ethanol	32
2.6.13 Preparation of interference ion solution for study of selectivity	32
2.7 The synthesis and characterization of gold nanoparticles	33
2.7.1 The synthesis of gold nanoparticles solution	33
2.7.2 Characterization of AuNPs particles	34
2.7.2.1 The surface plasmon resonance (SPR) measurement	34
2.7.2.2 The morphology of AuNPs	34
2.7.2.3 Zeta-potential measurements	35
2.7.2.4 Size distribution measurements	35
2.7.2.5 The stability of AuNPs solution	35
2.8 Optimization of parameters affecting the bromide ion sensor	35
2.8.1 Concentrations of chromium ( $\text{Cr}^{3+}$ )	36
2.8.2 pH of phosphate buffer solution	36

## Contents (continued)

	<b>Page</b>
2.8.3 Concentration of phosphate buffer solution	36
2.8.3.1 The aggregation of AuNPs	37
2.8.3.2 The anti-aggregation of AuNPs	37
2.8.4 Concentration of AuNPs	37
2.8.5 Reaction time	37
2.9 Overall colorimetric detection method for bromide ion (Br <sup>-</sup> )	38
2.10 Method validation	39
2.10.1 Linearity	39
2.10.2 Limit of detection (LOD) and limit of quantification (LOQ)	39
2.10.3 Matrix effect	39
2.10.3.1 Sample preparation of composite samples	39
2.10.3.2 The standard addition method	40
2.10.4 Accuracy	40
2.10.5 Precision	40
2.11 Comparison of developed sample preparation with SPE method	41
2.11.1 The extraction of rice samples with water	41
2.11.2 Solid phase extraction for clean-up of the water extract of rice	41
2.11.3 The detection of the water extract of rice	42
2.12 Comparison of ashing time by inductively coupled plasma optical emission spectrometry (ICP-OES)	42
2.13 Selectivity	42
2.14 The investigation of the remained bromide in residues by X-ray fluorescence spectrometry (XRF)	42
2.15 Application of the developed sensor to rice samples	43
2.15.1 Sample collection	43
2.15.2 The determination of Br <sup>-</sup> in rice samples with developed sensor	43
2.15.2.1 Overall sample preparation	43
2.15.2.2 Colorimetric detection of Br <sup>-</sup> in samples	43

## Contents (continued)

	<b>Page</b>
2.15.3 Confirmation of Br <sup>-</sup> detected by developed sensor with ion chromatography	44
2.16 Statistics	44
<b>CHAPTER 3 RESULT AND DISCUSSION</b>	<b>45</b>
3.1 The synthesis of gold nanoparticles	45
3.2 Proposed sensing mechanism	47
3.3 Characterization of AuNPs particles	49
3.3.1 The surface plasmon resonance (SPR) of AuNPs	49
3.3.2 The morphology of AuNPs	50
3.3.3 Particles size distribution of AuNPs solution	51
3.3.4 Zeta potential of AuNPs	52
3.3.5 The stability of AuNPs	52
3.4 Optimization of parameters affecting the detection of bromide	53
3.4.1 Concentrations of Cr <sup>3+</sup>	53
3.4.2 pH of solution	55
3.4.3 Concentrations of phosphate buffer	57
3.4.4 Concentrations of AuNPs	57
3.4.5 Reaction time	58
3.5 Method validations	59
3.5.1 Linearity	59
3.5.2 Limit of detection (LOD) and limit of quantification (LOQ)	62
3.5.3 Matrix effect	62
3.5.4 Accuracy	63
3.5.5 Precision	64
3.6 Preliminary development of sample preparation with SPE method	65
3.7 Comparison of different digestion method by inductively coupled plasma optical emission spectrometry (ICP-OES)	66

**Contents (continued)**

	<b>Page</b>
3.8 Selectivity	67
3.9 Comparison of ashing time by inductively coupled plasma optical emission spectrometry (ICP-OES)	70
3.10 The investigation of the remained bromide in residues by X-ray fluorescence spectrometry (XRF)	70
3.11 Application of the developed sensor to rice samples	71
3.12 Comparison of developed sensor with other reported analytical methods	73
<b>CHAPTER 4 CONCLUSION</b>	<b>75</b>
4.1 The synthesis of gold nanoparticles	75
4.2 Proposed sensing mechanism	75
4.3 Characterization of AuNPs particles	75
4.4 Optimization of parameters affecting the detection of bromide	76
4.5 Method validations	77
4.6 Development of sample preparation	78
4.7 Selectivity	78
4.8 Application of the developed sensor to rice samples	79
4.9 Comparison of developed sensor with other reported analytical methods	79
Reference	80
Appendix A	90
Appendix B	97
Appendix C	99
VITAE	110

## List of Tables

<b>Table</b>	<b>Page</b>
<b>1.1</b> The properties of methyl bromide	4
<b>1.2</b> The properties of bromine	5
<b>1.3</b> The various techniques applied for Br <sup>-</sup> detection in different samples	17
<b>1.4</b> The spectrometric method applied for Br <sup>-</sup> detection in different samples.	18
<b>2.1</b> The chemicals used throughout experiment	25
<b>2.2</b> The apparatus and materials used throughout experiment	27
<b>2.3</b> The working concentration range of bromide solution	31
<b>2.4</b> Preparation of 0.01 M sodium phosphate buffer solution at different pH	32
<b>2.5</b> The amount of interested ions for preparation of interference solution	33
<b>3.1</b> Recoveries of spiked Br <sup>-</sup> in composite rice samples with relative standard deviation (RSD) values (n = 3)	64
<b>3.2</b> The intra-day and inter-day precisions	64
<b>3.3</b> Comparison of metals detected in rice samples which prepared by different digestion method followed by inductively coupled plasma-optical emission spectrometric detection (ICP-OES) (n = 3)	67
<b>3.4</b> The determination of Br <sup>-</sup> in rice samples by developed sensor (n = 3) and ion chromatography (n = 2)	68
<b>3.5</b> Comparison of the developed sensor with other method applied for Br <sup>-</sup> in different samples	74
<b>A1</b> The corresponding linear equation and coefficient of determination (R <sup>2</sup> ) obtained from the result of the effect of phosphate buffer pH (Figure A2)	92
<b>A2</b> The corresponding linear equation and correlation coefficient (R <sup>2</sup> ) obtained from the result of the effect of concentration of AuNPs (Figure A5)	94
<b>A3</b> The repeatability measurement of blank signal (n = 20)	95

## List of Figures

Figure	Page
1.1 Detection of methyl bromide residues in various brands of Thai rice samples (Thai-PAN, 2013).	7
1.2 Schematic illustration of the collective oscillation of free electrons in a metal nanosphere (Peiris et al., 2015).	10
1.3 TEM images, color solution and SPR band of gold spheres and gold nanorods which appears in different color based on size and shape (Alkilany & Murphy, 2010).	10
1.4 Schematic of the refined nanoparticle growth mechanism of the Turkevich method (Polte, 2015).	11
1.5 The AuNPs was capped with citrate (Guo et al., 2014)	11
1.6 The platform of colorimetric sensing involved with (A) aggregation state of AuNPs and (B) anti-aggregation state of AuNPs.	13
1.7 The schematic of colorimetric sensor based on the aggregation of AuNPs for $\text{Fe}^{3+}$ detection with a <i>p</i> -amino salicylic acid dithiocarbamate functionalized AuNPs (Mehta et al., 2014).	14
1.8 The schematic of colorimetric sensor based on the anti-aggregation of AuNPs for $\text{Ag}^+$ detection with tris- (hydroxymethyl) aminomethane as aggregation inducer (Safavi et al., 2017).	14
1.9 The summery of $\text{Br}^-$ determination method.	16
1.10 The correlation plot between the measured signal and analyte concentration with the linear range response and non-linear range response.	20
1.11 The plots of standard addition and standard calibration curves.	22
2.1 Scope of method development for the AuNPs colorimetric sensor of bromide ion in rice samples.	24
2.2 The procedure of gold nanoparticles synthesis.	34
2.3 The colorimetric detection procedure for determination of $\text{Br}^-$ .	38
3.1 The illustration representing the process of AuNPs synthesis: (a) boiling gold(III) chloride solution, (b) gold(III) chloride solution after addition of tri-sodium citrate, (c - e) the color transition of reaction and (f) synthesized AuNPs.	46
3.2 The UV-Vis adsorption spectrum of the surface plasmon resonance phenomena of successfully synthesized AuNPs.	46



## List of Figures (continued)

Figure	Page
<b>3.3</b> (a) The TEM image of AuNPs with the scale bars of 100 nm. (b) The histograms of 100 particles size.	47
<b>3.4</b> The illustration of proposed mechanism for the colorimetric sensor of Br <sup>-</sup> detection based on the anti-aggregation of AuNPs.	48
<b>3.5</b> UV-Vis absorption spectra of (a) AuNPs, (b) aggregation of AuNPs in the presence of 4.80 μM Cr <sup>3+</sup> and (c) anti-aggregation of AuNPs in the presence of 3.13 μM Br <sup>-</sup> and 4.80 μM Cr <sup>3+</sup> . Photograph of A, B and C correspond a,b and c, respectively.	49
<b>3.6</b> The TEM image of (a) AuNPs, (b) the aggregation of AuNPs in the presence of Cr <sup>3+</sup> and (c) the anti-aggregation of AuNPs in the presence of Br <sup>-</sup> and Cr <sup>3+</sup> .	50
<b>3.7</b> Lognormal distribution diagram of (a) AuNPs, (b) the aggregation of AuNPs in the presence of Cr <sup>3+</sup> and (c) the anti-aggregation of AuNPs in the presence of Br <sup>-</sup> and Cr <sup>3+</sup> .	51
<b>3.8</b> The zeta potential value at pH 6.5 of AuNPs without Br <sup>-</sup> and after addition of 0.63, 2.50 and 4.38 μM Br <sup>-</sup> .	52
<b>3.9</b> (a) The absorbance intensity at 519 nm of pure AuNPs solution for each week at interval of 2 weeks. (b) The absorbance ratio (A <sub>519</sub> /A <sub>673</sub> ) of 2.50 μM Br <sup>-</sup> after using the synthesized AuNPs suspension stored in the dark at 4 °C in 4 months.	53
<b>3.10</b> The absorbance ratio of A <sub>519</sub> /A <sub>673</sub> on the various concentration of Cr <sup>3+</sup> . Condition: 500 μL of 5.52 nM AuNPs, 500 μL of 10 mM phosphate buffer (pH 7.0), 100 μL of Cr <sup>3+</sup> , total volume of 1200 μL and 10 min of reaction time. Inset shows color solution of AuNPs depending on the concentration of Cr <sup>3+</sup> . The bars showing different letter are significantly different at $p > 0.05$ .	55
<b>3.11</b> The effect of phosphate buffer pH on the sensitivity of Br <sup>-</sup> concentration ranged from 0.63 - 5.01 μM. Condition: 500 μL of 5.52 nM AuNPs, 500 μL of 10 mM phosphate buffer, 100 μL of Br <sup>-</sup> , 100 μL of 57.70 μM Cr <sup>3+</sup> and 10 min of reaction time. The bars showing different letter are significantly different at $p > 0.05$ .	56
<b>3.12</b> The influence of concentrations of phosphate buffer (pH 6.5) on the aggregation and anti-aggregation of AuNPs. Condition: 500 μL of 5.52 nM AuNPs, 500 μL of phosphate buffer pH 6.5, 100 μL of 30.04 μM Br <sup>-</sup> for signal <sub>analyte</sub> or 100 μL of ultrapure water for signal <sub>blank</sub> , 100 μL of 57.70 μM Cr <sup>3+</sup> and 10 min for reaction time.	57

## List of Figures (continued)

Figure	Page
<b>3.13</b> The effect of AuNPs concentrations on the sensitivity of Br <sup>-</sup> concentration range from 0.63 - 2.50 μM. Condition: 300-700 μL of 5.52 nM AuNPs, 250 μL of 20 mM total volume of 1200 μL and 10 min of reaction time. The bars showing different letter are significantly different at $p > 0.05$ .	58
<b>3.14</b> The reaction time of (a) blank (without Br <sup>-</sup> ), (b) 1.25 μM Br <sup>-</sup> , (c) 2.50 μM Br <sup>-</sup> and (d) 5.01 μM Br <sup>-</sup> . Condition: 400 μL of 5.52 nM AuNPs, 500 μL of 10 mM phosphate buffer, 100 μL of Br <sup>-</sup> , 100 μL of 57.70 μM Cr <sup>3+</sup> , total of 1200 μL and 2 - 30 min of reaction time.	59
<b>3.15</b> (a) Color solution of AuNPs depends on the concentration of Br <sup>-</sup> under the optimum condition of 400 μL of 5.52 nM AuNPs, 250 μL of 20 mM phosphate buffer, 100 μL of Br <sup>-</sup> , 100 μL of 57.70 μM Cr <sup>3+</sup> and 10 min of reaction time. (b) UV-Vis absorption spectra of AuNPs relating to the different concentration of Br <sup>-</sup> .	60
<b>3.16</b> The correlation plot between the absorption intensity ratio of A <sub>519</sub> /A <sub>673</sub> and various concentration of Br <sup>-</sup> (a) with the linear response of developed sensor in the range of 0.13 - 6.26 μM Br <sup>-</sup> (n = 3) and (b) with the linear calibration curve in the range of 0.31 - 3.75 μM Br <sup>-</sup> (k = 3, n = 3).	61
<b>3.17</b> Curves of (a) the standard addition curve and (b) the standard calibration curve for Br <sup>-</sup> concentration ranging of 0.31 - 3.75 μM.	61
<b>3.18</b> The detected color solution using this developed sensor under the optimum condition: Ultrapure water used as (a) standard blank, (b) SPE blank, (c) 0.34 mg L <sup>-1</sup> standard Br <sup>-</sup> , (d) 0.34 mg L <sup>-1</sup> standard Br <sup>-</sup> passed through SPE. Rice sample extracts with (e) sample blank, (f) sample blank passed through SPE (g) spiked sample and (f) spiked sample passed through SPE (n = 3).	65
<b>3.19</b> Selectivity of the Br <sup>-</sup> detection. (a) Absorbance ratio response (A <sub>519</sub> /A <sub>673</sub> ) of the proposed sensor for 5 μM Br <sup>-</sup> (red bar) was plotted against the 5000 μM of ion interferences <i>i.e.</i> , K <sup>+</sup> , Mg <sup>2+</sup> , Ca <sup>+</sup> , Al <sup>3+</sup> , NO <sub>2</sub> <sup>-</sup> , NO <sub>3</sub> <sup>-</sup> , PO <sub>4</sub> <sup>3-</sup> , SO <sub>4</sub> <sup>2-</sup> , F <sup>-</sup> and Cl <sup>-</sup> (blue bar) and the mixture of Br <sup>-</sup> and other ions including 5000 μM of NO <sub>2</sub> <sup>-</sup> , NO <sub>3</sub> <sup>-</sup> , PO <sub>4</sub> <sup>3-</sup> , SO <sub>4</sub> <sup>2-</sup> , F <sup>-</sup> , 3000 μM of K <sup>+</sup> , 500 μM of Cl <sup>-</sup> , 25 μM Mg <sup>2+</sup> , Ca <sup>+</sup> , Al <sup>3+</sup> (violet bar). All signals were corresponding to blank. (b) The photograph is examples of the corresponding detection sensor .	65

## List of Figures (continued)

<b>Figure</b>	<b>Page</b>
<b>3.20</b> Effect of 5 mg L <sup>-1</sup> of I <sup>-</sup> and SCN <sup>-</sup> on selectivity of the detection of 5 mg L <sup>-1</sup> Br <sup>-</sup> .	70
<b>3.21</b> Correlation between Br <sup>-</sup> standard and Br <sup>-</sup> detected by XRF in the composite rice sample solution.	71
<b>3.22</b> (a) The corresponding color of white rice sample 1- sample 5 (Table 3.4), respectively. (b) The color chart in the presence of Br <sup>-</sup> concentration of 0.00 - 50.00 mg kg <sup>-1</sup> .	72
<b>A1</b> The UV-Vis absorption spectra on the concentration of Cr <sup>3+</sup> ranged from 0.00-19.23 μM	86
<b>A2</b> The UV-Vis absorption spectra of (a) AuNPs, (b) AuNPs + 50 μM Cr <sup>3+</sup> , (c) AuNPs + 50 μM Fe <sup>3+</sup> and (d) AuNPs + 50 μM Al <sup>3+</sup> prepared in 10 mM phosphate buffer (pH 7.0). Inset is the corresponding photograph of a - d.	86
<b>A3</b> Effect of pH of phosphate buffer on aggregation of AuNPs in the presence of Cr <sup>3+</sup> , Fe <sup>3+</sup> and Al <sup>3+</sup> .	87
<b>A4</b> The effect of pH of phosphate buffer on the linearity curve of Br <sup>-</sup> concentration ranged from 0.63 - 5.01 μM.	87
<b>A5</b> The color of solution on the effect of pH of phosphate buffer corresponding to the linearity curve of Br <sup>-</sup> concentration ranged from 0.63 - 5.01 μM Br <sup>-</sup> (Figure A2).	88
<b>A6</b> The effect of phosphate buffer concentration (pH 6.5) (a) Analyte signal (0.25 μM Br <sup>-</sup> ) and (b) Blank signal (no Br <sup>-</sup> ).	89
<b>A7</b> The effect of concentration of AuNPs on the linearity curve of Br <sup>-</sup> concentration ranged from 0.63 - 2.50 μM.	89
<b>A8</b> The color of solution on the effect of concentration of AuNPs corresponding to the linearity curve of Br <sup>-</sup> concentration ranged from 0.63 - 2.50 μM Br <sup>-</sup> (Figure A5).	90
<b>A9</b> The XRF spectra of (a) 50, (b) 100, (c) 200 and (d) 400 mg L <sup>-1</sup> Br <sup>-</sup> spiked in the composite rice samples.	92
<b>B1</b> The UV-Vis adsorption spectrum of diluted AuNPs.	93

## List of Abbreviations

AuNPs	Gold nanoparticles
AgNPs	Silver nanoparticles
AOAC	Association of Official Analytical Chemists
COD	Chemical Oxygen Demand
CuNPs	Copper nanoparticles
FLD	Fluorescence detection
GC-ECD	Gas chromatography-electron capture detector
HLB	Hydrophilic-Lipophilic balance
HPLC	High performance liquid chromatography
IC	Ion chromatography
ICP-MS	Inductive coupled plasma-mass spectrometry
ICP-OES	Inductively coupled plasma optical emission spectrometer
LOD	limit of detection
LOQ	Limit of quantification
RSD	Relative standard deviation
SD	Standard deviation
SPE	Solid phase extraction
SPR	Surface plasmon resonance
TEM	Transmission electron microscopy
UV-Vis	Ultraviolet-Visible
XRF	X-Ray fluorescence spectrometer

# CHAPTER 1

## INTRODUCTION

### 1.1 Background and rationale

Methyl bromide ( $\text{CH}_3\text{Br}$ ) is a fumigant and particularly used for controlling a variety of pests such as insects, mites, moulds, nematodes, weeds, viruses and bacteria, soil disinfection and postharvest treatment of stored and dried foodstuffs including rice, tobacco, fresh fruits and vegetables (Norman, 2000; Sungwaranond et al., 1998; Wittayanan & Jongmevasna, 2015). Its toxic effects on human health are, for short-term exposure, headache, dizziness, nausea, vomiting, blurred vision, slurred speech and convulsions. High concentrations of methyl bromide may cause unconsciousness and death. Prolonged exposure to methyl bromide may cause injury of the central nervous system (U.S. Department of Health and Human Services, 1978). Furthermore, it can highly destroy the ozone layer through emission from agricultural pesticide uses, from the burning of biomass and leaded gasoline, and from the ocean (The Federal Register, 1999; Thomas, 1996). Thus, the use of methyl bromide was controlled by many organizations and already being phased out in January 1, 2005. For example, USA stopped methyl bromide, with emergency and critical use exemptions (FAO, 1999; The Federal Register, 1999; Thomas, 1996). China terminated the agricultural use of methyl bromide at the end of 2018 (CCM, 2017). The application of methyl bromide in European Union has been forbidden since 2010, but exception are made especially with regard to the International Standards for Phytosanitary Measures 15 (Baur et al., 2015).

After food commodities are fumigated, methylated products and inorganic bromide are formed as a result of reaction chemically with some constituents of treated foodstuffs or breakdown product of methyl bromide (Cova et al., 1986; Miyahara & Saito, 1994; Norman, 2000; Sungwaranond et al., 1998; Wittayanan & Jongmevasna, 2015). Inorganic bromide has been detected in rice and glutinous rice in the range of 0.13 - 11.93  $\text{mg kg}^{-1}$  and 0.20 - 1.37  $\text{mg kg}^{-1}$ , respectively, which were within the Codex maximum residue limit value of 50  $\text{mg kg}^{-1}$  (Sungwaranond et al., 1998). Methyl bromide residues can persist in nuts and seeds for 10 weeks and in dried fruit for 4 weeks (Norman, 2000). Cova et al. reported the higher concentrations of bromide ion detected in fumigated pastas with eggs, pastas with eggs and spinach and rice compared to unfumigated samples (Cova et al., 1986).

Thailand, is the world's leading rice production and also one of the largest rice consumers, imported an average of 357.69 and 103.85 tons per year of methyl bromide and a mixture between methyl bromide and chloropicrin, respectively to

eliminate undesired pests before commercializing during 2007 - 2012 (Sungwaranond et al., 1998). Due to its toxic, under the agreement of Montreal Protocol, Thailand agreed to gradually reduce and to phase out the use of methyl bromide by the year 2015 (The Montreal Protocol on Substances that Deplete the Ozone Layer, 1987). The Thai Ministry of Public Health notifies the maximum residue limit (MRL) of methyl bromide in rice of  $0.01 \text{ mg kg}^{-1}$  and of bromide ion in rice of  $50 \text{ mg kg}^{-1}$  (Notification of the Ministry of Public Health, 2013). In 2013, methyl bromide was not detected in any rice samples ( $n = 13$ ), however bromide ion in one sample was detected at  $77.2 \text{ mg kg}^{-1}$  and after 4 days, its concentration decreased to  $20.9 \text{ mg kg}^{-1}$  (Pimpun, 2013).

According to food globalization, rice consuming is increasing around the world. The determination of methyl bromide and inorganic bromide contamination in rice is, therefore, required as a guarantee method for consumer's safety. In most cases, bromide ion contaminations in rice have been found when food commodities are fumigated with either low or high concentration of methyl bromide and are particularly overdose or multiple fumigated with methyl bromide (Cova et al., 1986; Mahmoud et al., 2014; Norman, 2000; Pimpun, 2013; Sungwaranond et al., 1998; Wittayanan & Jongmevasna, 2015). Many studies have focused on inorganic bromide in food in order to assess the daily intake of bromide ion from food and water into human body (Chiu & Eubanks, 1989; Miyahara & Saito, 1994; Nguyen & Ludwig, 2014). Therefore, bromide ion is the main target analyte for this work, whether from the accumulation of bromide ion from the environment or the transformation of methyl bromide.

Prior to detection step, bromide ion in foodstuffs has been treated by different procedures e.g., low energy microwave digestion (Nguyen & Ludwig, 2014), high temperature heating  $\sim 850 \text{ }^\circ\text{C}$  (Baso-Cejas et al., 2007), hydrolysis with alkaline and ashing at  $550 \text{ }^\circ\text{C}$  (Sungwaranond et al., 1998), and suspension in 6 N sulfuric acid and propylene oxide followed by extraction with ethyl acetate (Mahmoud et al., 2014). Subsequently, the pre-treated samples are determined by sophisticated instrumentation such as inductively coupled plasma-mass spectrometry (Nguyen & Ludwig, 2014), gas chromatography-electron capture detector (Mahmoud et al., 2014; Sungwaranond et al., 1998), ion-exchange chromatography with visible light detection (Yu et al., 2011). However, these mentioned instrumentations require not only complex sample preparation and long analysis time but also complicated and expensive instruments are needed.

Nowadays, the gold nanoparticles (AuNPs) based colorimetric sensor has drawn increasing attention due to its low cost, rapid, selective as well as reliable detection (Hormozi-Nezhad & Abbasi-Moayed, 2014; Li et al., 2011; Liu et al., 2011; Zhou et al., 2014). In general, AuNPs change from dispersion to aggregation state and their color changes from ruby red to purple or blue (Hormozi-Nezhad & Abbasi-

Moayed, 2014; Li et al., 2011; Liu et al., 2011; Zhou et al., 2014). Its absorption band in the visible range with high extinction coefficient (e.g.,  $2.70 \times 10^8 \text{ M}^{-1} \text{ cm}^{-1}$ ) (Liu et al., 2011) appears when the incident photon frequency is in resonance with the excitation of the conduction electrons. This phenomenon is named as the surface plasmon resonance (SPR) (Hormozi-Nezhad & Abbasi-Moayed, 2014; Li et al., 2011; Liu et al., 2011; Zhou et al., 2014). According to these advantages, AuNPs can be used as a powerful tool for real-time monitoring *via* naked-eye detection, rather than using any advanced instruments.

AuNPs has also been applied for the detection of metal ions (Hormozi-Nezhad & Abbasi-Moayed, 2014; Li et al., 2011; Zhou et al., 2014), anions (Zhang et al., 2011), and organic residues (Kang et al., 2016; Kong et al., 2016) such as  $\text{Hg}^{2+}$ ,  $\text{Cu}^{2+}$ , clenbuterol, aflatoxins, tetracycline, amoxicillin and pazufloxacinmesilate, in which mostly it depends on the aggregation. It was reported that the AuNPs aggregation is not selective and can provide false positive results due to effects of many other external factors in real applications. Thus, the anti-aggregation or re-dispersion of AuNPs has become a good option in order to improve selectivity (Hormozi-Nezhad & Abbasi-Moayed, 2014; Li et al., 2011).

So far, the colorimetric probe based on AuNPs anti-aggregation process has not been found for bromide ion determination in rice samples. In this work, the AuNPs colorimetric sensor was developed for the facile, sensitive and selective detection of bromide ion in rice samples. The sensor is based on that bromide ion prevented aggregation of AuNPs. The addition of chromium ( $\text{Cr}^{3+}$ ) into a AuNPs solution resulted in the aggregation of AuNPs with a red-to-blue color change. In the presence of  $\text{Br}^-$ , the aggregation of AuNPs was interrupted and the corresponding color of solution changed from blue to red. The concentration of bromide ion in real samples can be easily observed by naked eyes, and also quantitatively measured by UV-visible spectroscopy.

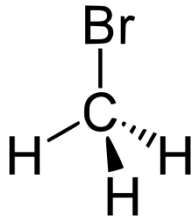
## 1.2 Review of literature

### 1.2.1 Methyl bromide and bromide ion

#### 1.2.1.1 Physical and chemical properties of methyl bromide

Methyl bromide or bromomethane is an organobromine compound with the properties as shown in Table 1.1 (NIOSH, 1996).

**Table 1.1** The properties of methyl bromide

Property	Status
Chemical formula	CH <sub>3</sub> Br
Molecular structure	
Molecular weight	94.94 g mol <sup>-1</sup>
Appearance	colorless gas
Odor	chloroform-like at high concentrations
Boiling point	4.0 °C
Melting point	-94.0 °C
Density	1.73 g mL <sup>-1</sup> at 0 °C
Vapor pressure	189.34 kPa (1420 mm Hg) at 20 °C
Flammability	non-flammable gas
Solubility in water	17.5 g L <sup>-1</sup>
Dissolvable	alcohol, chloroform, ether, benzene and carbon-tetrachloride

#### 1.2.1.2 Physical and chemical properties of bromide ion

Bromide (Br<sup>-</sup>) is the anion form of bromine element with the properties as shown in Table 1.2. It is classified as the common halogen element. Bromide and bromine have chemical similarities and are oxidizing agents. They form anions by accepting an electron (WHO, 2009).



**Table 1.2** The properties of bromine

<b>Property</b>	<b>Status</b>
Molecular weight	79.909 g mol <sup>-1</sup>
Appearance	dense mobile dark liquid
Boling point	58 °C
Melting point	-7 °C

### **1.2.1.3 The toxicity of methyl bromide and bromide ion on human health**

The toxic effects of methyl bromide on human health are: corrosive to both the skin and eyes, for short-term exposure, headache, dizziness, nausea, vomiting, blurred vision, slurred speech, lack of energy and convulsions. High concentrations of methyl bromide may cause unconsciousness and death. Prolonged exposure to methyl bromide may cause injury of the central nervous system. The signs of poisoning may be delayed only a few minutes to 48 h following methyl bromide exposure (NPIC, 2000; U.S. Department of Health and Human Services, 1978). Scientists predict that methyl bromide is toxic because it damages several sites in organism's cells and binds to DNA, fats, and proteins. The U.S. EPA classifies methyl bromide as a group D carcinogen that is not classifiable as to human carcinogenicity (U.S. EPA, 1997).

The intake of bromide above the acceptable dietary intake (1 mg kg<sup>-1</sup> body weight/day) has been described which was yielding a casual replacement of iodide by bromide during the biosynthesis of thyroid hormones and can affect the status of the thyroid gland (Baso-Cejas et al., 2007) and it has also been reported that bromide effects on endocrine system and reproduction in animals (van Leeuwen et al., 1983). Moreover, chronic toxicity from bromide can result in bromism, a syndrome with multiple neurological symptoms as the effect include: depression, lethargy, somnolence, loss of appetite and cachexia, nausea, chronic seizures, loss of neural sensitivity, paresis, delirium, confusion, abnormal speech, loss of concentration and memory, aggressiveness and psychosis and also relate to the nervous system, skin, glandular secretions and gastrointestinal tract (WHO, 2009).

#### 1.2.1.4 The use of methyl bromide as a pesticide

Methyl bromide was introduced as a pesticide in 1932, first registered in U. S. A. in 1961 and used as the fumigation substance in both of agriculture and industry by the filling air spaces in enclosed areas and penetrates cracks, crevices, and pores in soil, commodities, and structures (NPIC, 2000). It was particularly used for controlling a variety of pests such as insects, mites, moulds, nematodes, rodents, weeds, viruses and bacteria, soil disinfection and postharvest treatment of stored of agriculture product and dried foodstuffs including rice, tobacco, fresh fruits and vegetables (Norman, 2000; Sungwaranond et al., 1998; Wittayanan & Jongmevasna, 2015).

However, after food commodities are fumigated, methylated products and inorganic bromide are formed as a result of reaction chemically with some constituents of treated foodstuffs or breakdown product of methyl bromide (Cova et al., 1986; Miyahara & Saito, 1994; Norman, 2000; Sungwaranond et al., 1998; Wittayanan & Jongmevasna, 2015). Methyl bromide is easy to expose due to gaseous at 4 °C, thus it is possible that the over fumigating or the repeating fumigation process and the others non-following recommended application procedure lead to transformation of methyl bromide into inorganic bromide residue (Wittayanan et al., 2017). Inorganic bromide has been detected in rice and glutinous rice in the range of 0.13 - 11.93 mg kg<sup>-1</sup> and 0.20 - 1.37 mg kg<sup>-1</sup>, respectively, which were within the Codex maximum residue limit value of 50 mg kg<sup>-1</sup> (Sungwaranond et al., 1998). In addition, the Thailand Pesticide Alert Network (Thai-PAN) reported the detection of methyl bromide residues as inorganic bromide in 46 bands of rice samples. It was found that one band contaminated bromide higher than the Codex maximum residue limit value of 50 mg kg<sup>-1</sup> and 12 bands contaminated bromide with higher level of 5.4 - 4.0 mg kg<sup>-1</sup> as shown in Figure 1.1 (Thai-PAN, 2013). Methyl bromide residues can persist in nuts and seeds for 10 weeks and in dried fruit for 4 weeks (Norman, 2000). Cova et al. reported the higher concentrations of bromide ion detected in fumigated pastas with eggs, pastas with eggs and spinach and rice compared to unfumigated samples (Cova et al., 1986).

## ผลการตรวจเมทิลโบรไมด์ตกค้างในข้าวสารยี่ห้อต่างๆในท้องตลาด

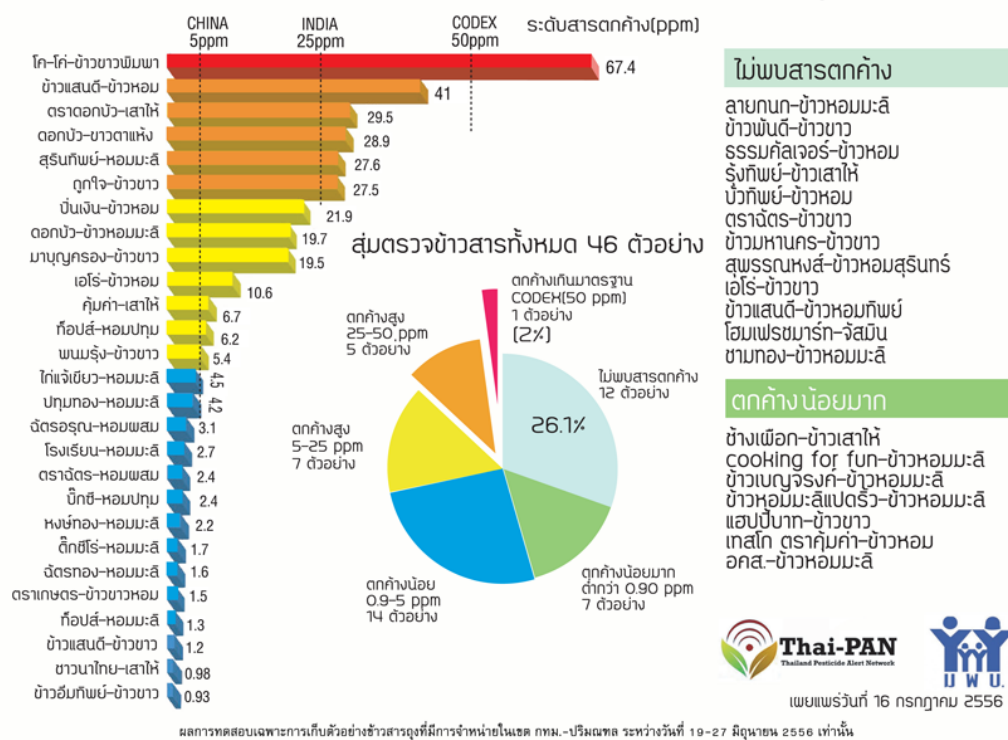


**Figure 1.1** Detection of methyl bromide residues in various brands of Thai rice samples (Thai-PAN, 2013).

### 1.2.1.5 Environmental impact of methyl bromide

Methyl bromide can highly destroy the ozone layer through emission from agricultural pesticide uses, from the burning of biomass and leaded gasoline, and from the ocean (The Federal Register, 1999; Thomas, 1996). Thus, many organizations controlled the use of methyl bromide and phased it out in January 1, 2005. For example, U.S.A stopped the production and use of methyl bromide, with emergency and critical use exemptions (FAO, 1999; The Federal Register, 1999; Thomas, 1996). The agricultural use of methyl bromide in China will also be terminated at the end of 2018 (CCM, 2017). The application of methyl bromide in European Union has been forbidden since 2010, but exception are made especially with regard to the International Standards for Phytosanitary Measures 15 (Baur et al., 2015).

### 1.2.1.6 The use of methyl bromide in Thailand

Thailand is the world's leading rice production with export up to 10.8 million tons of milled rice in 2014 (Sarigalaya, 2015) and also one of the largest rice

consumers. Usually, the international food safety standard is required for rice economy, thus to eliminate insects in rice grains, the fumigation of pesticide substances in Thailand is used in many steps of commodity conditions before trade (Wittayanan et al., 2017). Thailand imports an average of 357.69 and 103.85 tons per year of methyl bromide and a mixture between methyl bromide and chloropicrin, respectively to eliminate undesired pests before commercializing during 2007 - 2012 (Wittayanan & Jongmevasna, 2015).

Due to its toxic and the reduction of environmental impact, under the agreement of Montreal Protocol, Thailand agreed to gradually reduce and to phase out the use of methyl bromide by the year 2015 (The Montreal Protocol on Substances that Deplete the Ozone Layer, 1987).

## **1.2.2 Gold nanoparticles (AuNPs)**

### **1.2.2.1 The introduction of AuNPs**

Gold nanoparticles (AuNPs) are cluster of gold (Au) atom in the particles size range of 1-100 nm and have unique chemical, optical, electrical and magnetically properties, leading to their wide applications in sensing, catalysis, electronics and photonics. Its performances include tunable surface plasmon resonances, distance-dependent fluorescence quenching or enhancement, high electrical conductivity, and exceptional light-scattering properties (Amendola et al., 2014; Ghosh & Pal, 2007; Peixoto de Almeida et al., 2014). The other nanoparticles of noble metals such as copper (CuNPs) and silver (AgNPs) show similar characteristic properties that can be considered (Ghosh & Pal, 2007), however, AuNPs show other good performances such as

- 1) AuNPs has better photo-stability (Attia et al., 2015).
- 2) AuNPs is more stable than AgNPs which its absorbance was changed over time (Pinto et al., 2010). In addition, AuNPs is temperature stable (Pamies et al., 2016).
- 3) The color transition of AuNPs solution which was almost red to purple to blue or blue to red (Liu & Wang, 2013) provides greater sensitivity especially that can be easily detected by naked eyes compared with AgNPs which was light yellow to orange and to red (Bae et al., 2010; Kailasa et al., 2018). The color transition of CuNPs was red to orange to yellow (Soomro et al., 2014).

- 4) AgNPs is more toxic (Holder & Marr, 2013) but the toxicity of gold nanoparticles is supposed to be less (Alkilany & Murphy, 2010).
- 5) In this work, the colorimetric strategy depends on the coordination between citrate capped nanoparticle and  $\text{Cr}^{3+}$  induced the aggregation. It was found that AuNPs can be synthesized and stabilized with sodium citrate by one step directly while sodium borohydride was used for AgNPs synthesis and then adding citrate for stabilizing at cool condition (Bothra et al., 2015). The CuNPs synthesis is more complicate (Hatamie et al., 2014; Soomro et al., 2014).

### 1.2.2.2 The surface plasmon resonance phenomenon

The phenomenon of localized surface plasmon resonance (LSPR) or surface plasmon resonance (SPR) is characteristic of light absorption mechanism in any nano-size materials, which have an adequately high density of free electrons such as metals and heavily doped semiconductors. (Ghosh & Pal, 2007; Yang et al., 2015). When the light impinges on the nanoparticle, the free electrons surrounding the nanoparticle were inducing to oscillation with the frequency of electromagnetic field which was capable matching to the conduction band of the metal. The oscillation of the free electrons on the surface nanoparticle as electron cloud transition leads to a periodic charge separation and generates oscillating dipoles whose magnitude reaches a maximum at the nanoparticles surface while the atoms nuclei was still. The surface plasmon resonance depends on the size, shape and dielectric environment of nanoparticles (Ghosh & Pal, 2007; Toma et al., 2010; Yang et al., 2015). Figure 1.2 represented the illustration of phenomenon of SPR which is the unique property of noble metals nano-size materials.

Various colors of AuNPs particles will occur after dispersing in a solution due to their small size with a strong band in the UV-Vis range. Normally, the SPR bands of noble metal nanoparticles occur in the visible range, depending on size, shape, composition, crystalline nanoparticles, and spaces between nanoparticles. The example of different colors based on size and shape of nanoparticles is shown in Figure 1.3 (Hatamie et al., 2014; Toma et al., 2010).

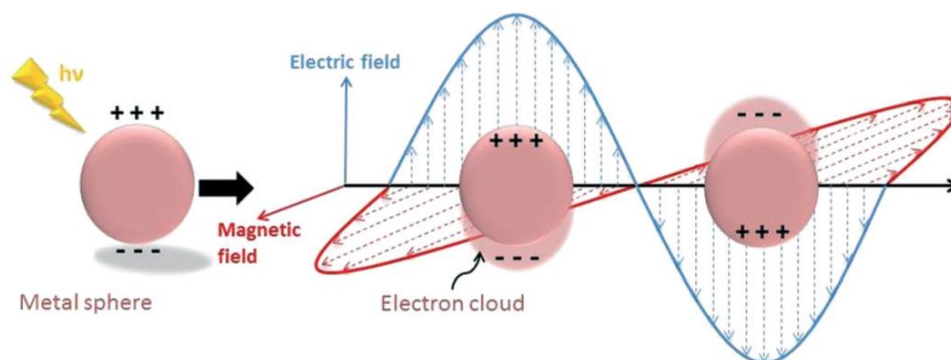


**Figure 1.2** Schematic illustration of the collective oscillation of free electrons in a metal nanosphere (Peiris et al., 2015).

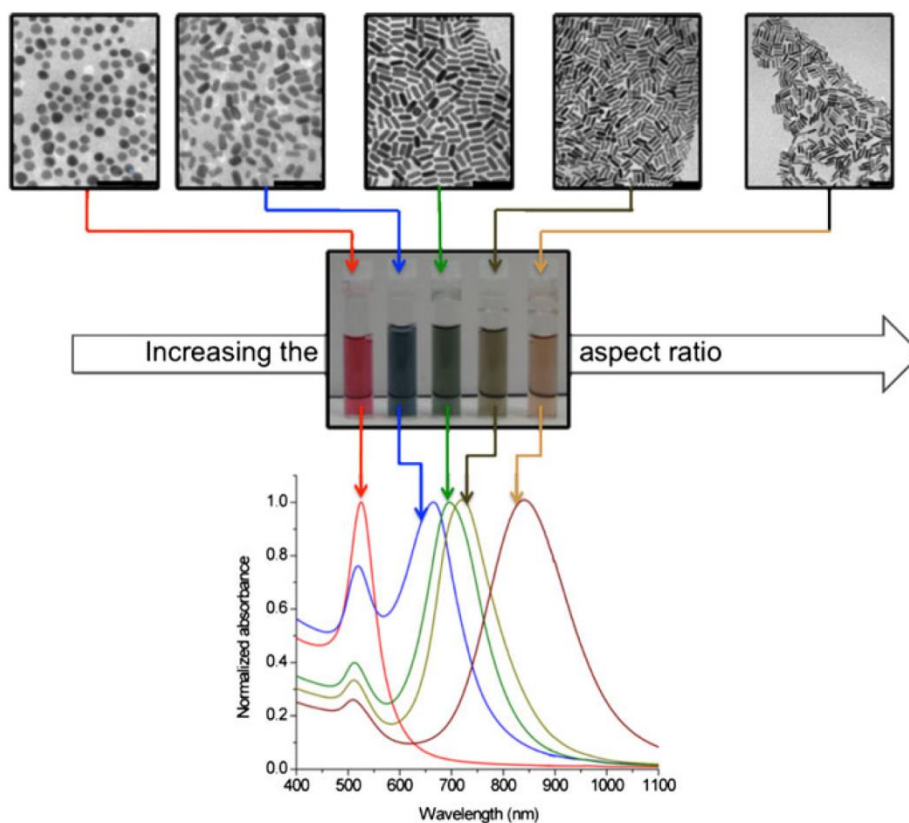


**Figure 1.3** TEM images, color solution and SPR band of gold spheres and gold nanorods which appears in different color based on size and shape (Alkilany & Murphy, 2010).

### 1.2.2.3 The synthesis method of AuNPs

The method as pioneered by Turkevich et al. in 1951 and refined by G. Frens in the 1970s is one of the most common synthetic for preparation of AuNPs which was performed by citrate reduction and stabilization. The reduction of a gold precursor ( $\text{HAuCl}_4$ ) was carried out by injecting sodium citrate ( $\text{Na}_3\text{C}_6\text{H}_5\text{O}_7$ ) in boiling aqueous solution.  $\text{Au}^{3+}$  is quickly reduced to  $\text{Au}^0$  atoms and forms to clusters, followed by their assembly into larger polycrystalline particles and completed by further aggregation with the metal-metal bonds (Figure 1.4) (Polte, 2015; Polte et al., 2010; Zhou et al., 2009). The resultant size of AuNPs can be controlled simply by changing the molar ratio of sodium citrate to  $\text{HAuCl}_4$  (Ji et al., 2007). It is known only that citrate anions coordinate to the metal surface by inner sphere complexation of the carboxylate groups to stabilized AuNPs (Cioran et al., 2014; Park & Shumaker-Parry, 2014). Citrate-capped AuNPs as shown in Figure 1.5 have electronegative charged surface, leading to dispersion from each other in water symmetrically by the electrostatic repulsion (Ling et al., 2008).

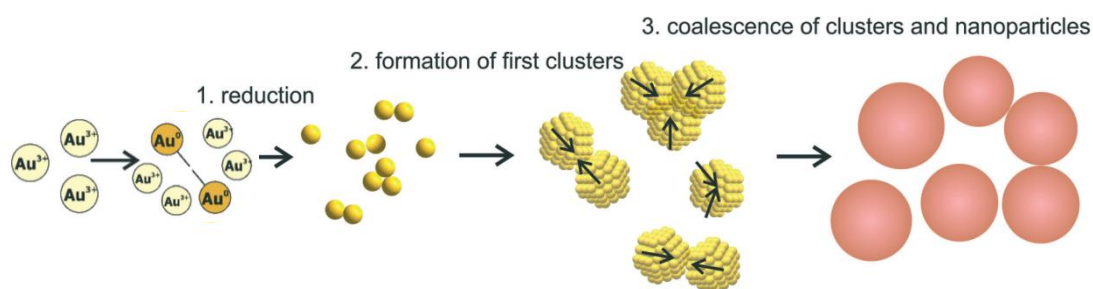


**Figure 1.4** Schematic of the refined nanoparticle growth mechanism of the Turkevich method (Polte, 2015).

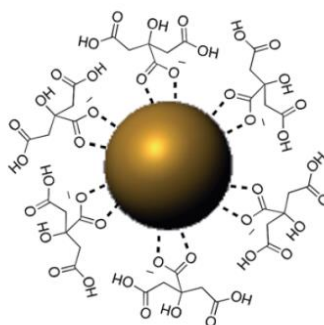


**Figure 1.5** The AuNPs was capped with citrate (Guo et al., 2014)

#### 1.2.2.4 The application to colorimetric sensing based on aggregation and anti-aggregation

Colorimetric sensing based on AuNPs has been considered due to the dominating optical feature of AuNPs. It is associated with the inter-particle plasmon coupling which can generate a significant absorption band shift in the visible region of the electromagnetic spectrum. The surface plasmon resonance (SPR) change of AuNPs is highly sensitive to the size, shape, capping agents and medium refractive index. According to these advantages, AuNPs can be applied as a powerful tool for real-time monitoring via naked-eye detection, demonstrating that no sophisticated instruments using advanced instruments are required (Liu et al., 2011; Yang et al., 2015).

Furthermore, the AuNPs based colorimetric sensor has drawn increasing attention due to its low cost, rapid, selective as well as reliable detection (Hormozi-Nezhad & Abbasi-Moayed, 2014; Li et al., 2011; Liu et al., 2011; Zhou et al., 2014). There are two mechanisms involved with AuNPs colorimetric sensing. The First mechanism is aggregation of AuNPs nanoparticles (Figure 1.6A), in which AuNPs change from dispersion to aggregation state because the analyte can induce and decrease the stability of AuNPs or specific binding with the surface functionalized AuNPs. It results in color changes from ruby red to purple or blue (Liu et al., 2011; Priyadarshini & Pradhan, 2017).

Figure 1.7 is an example of the schematic of colorimetric sensor based on the aggregation of AuNPs, in which a *p*-amino salicylic acid dithiocarbamate was added to functionalize AuNPs and then iron(III) ion ( $\text{Fe}^{3+}$ ) was binding to induce AuNPs aggregation (Mehta et al., 2014). Additionally, AuNPs has also been applied for the detection of metal ions (Hormozi-Nezhad & Abbasi-Moayed, 2014; Li et al., 2011; Zhou et al., 2014), anions (Zhang et al., 2011), and organic residues (Kang et al., 2016; Kong et al., 2016) such as  $\text{Hg}^{2+}$ ,  $\text{Cu}^{2+}$ , clenbuterol, aflatoxins, tetracycline, amoxicillin and pazufloxacinmesilate, in which mostly it depends on the aggregation.

The second mechanism is based on the anti-aggregation of AuNPs (Figure 1.6B) which the analyte reacts to inhibit the aggregated AuNPs, resulting in disaggregation of aggregated AuNPs or re-dispersed AuNPs state by disrupting the crosslink between nanoparticles (Safavi et al., 2017) or block the ability of binding ligand as aggregation inducer of AuNPs (Hormozi-Nezhad & Abbasi-Moayed, 2014). This mechanism results in a color change from blue to red. Figure 1.8 is an example mechanism of colorimetric sensor based on the anti-aggregation of AuNPs, in which the competitive interaction of AuNPs and silver(I) ion ( $\text{Ag}^+$ ) with tris-(hydroxymethyl) aminomethane as the aggregation inducer (Safavi et al., 2017).



The high extinction coefficients of AuNPs such as  $2.7 \times 10^8 \text{ M}^{-1} \text{ cm}^{-1}$  for AuNPs size of 13 nm (Liu et al., 2011) and  $3 \times 10^{11} \text{ M}^{-1} \text{ cm}^{-1}$  (Hormozi-Nezhad & Abbasi-Moayed, 2014) is higher than 1,000 times when compared with organic dyes. Therefore, the limit of detection (LOD) for AuNP-based colorimetric assays can be as low as nM level which can make this colorimetric sensor widely used for diagnosis of diseases and monitoring environmental contamination and food safety (Liu et al., 2011).

However, it was reported that the AuNPs aggregation is not selective and can provide false positive results due to effects of many other external factors in real applications. Thus, the anti-aggregation or re-dispersion of AuNPs has become a good option in order to improve selectivity (Hormozi-Nezhad & Abbasi-Moayed, 2014; Li et al., 2011).

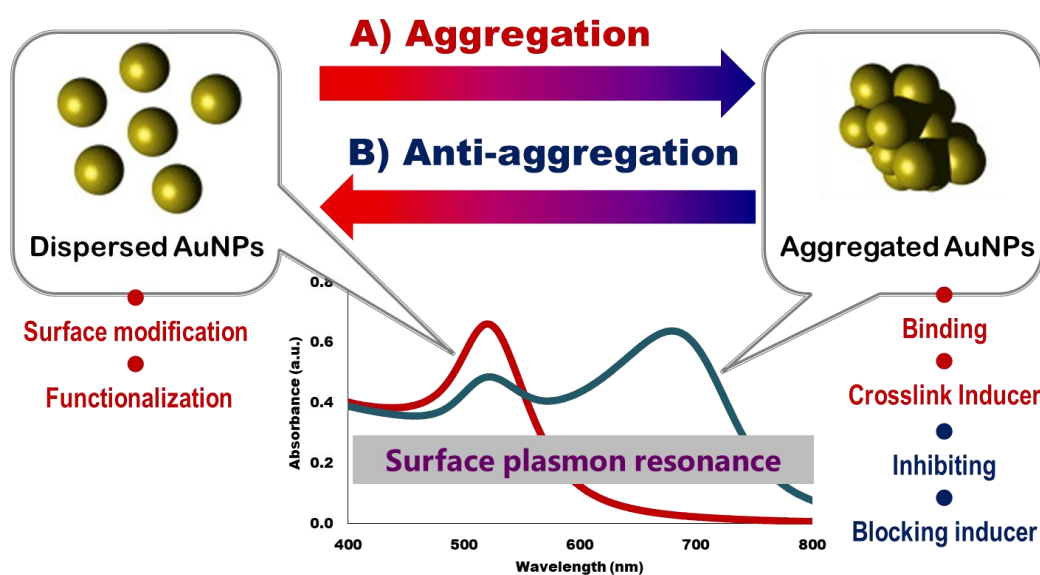


**Figure 1.6** The platform of colorimetric sensing involved with (A) aggregation state of AuNPs and (B) anti-aggregation state of AuNPs.

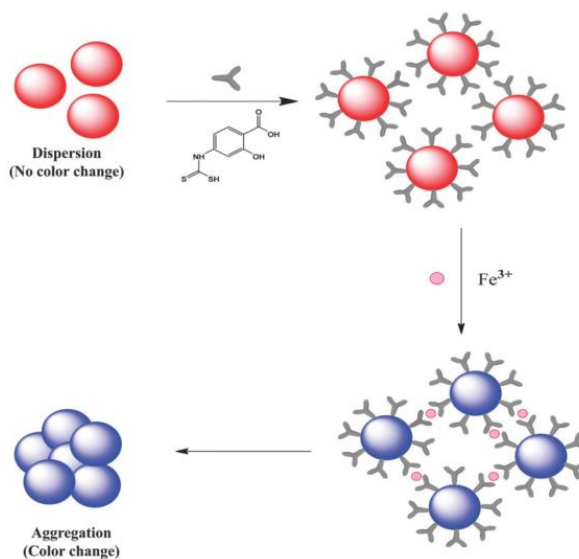


**Figure 1.7** The schematic of colorimetric sensor based on the aggregation of AuNPs for Fe<sup>3+</sup> detection with a *p*-amino salicylic acid dithiocarbamate functionalized AuNPs (Mehta et al., 2014).

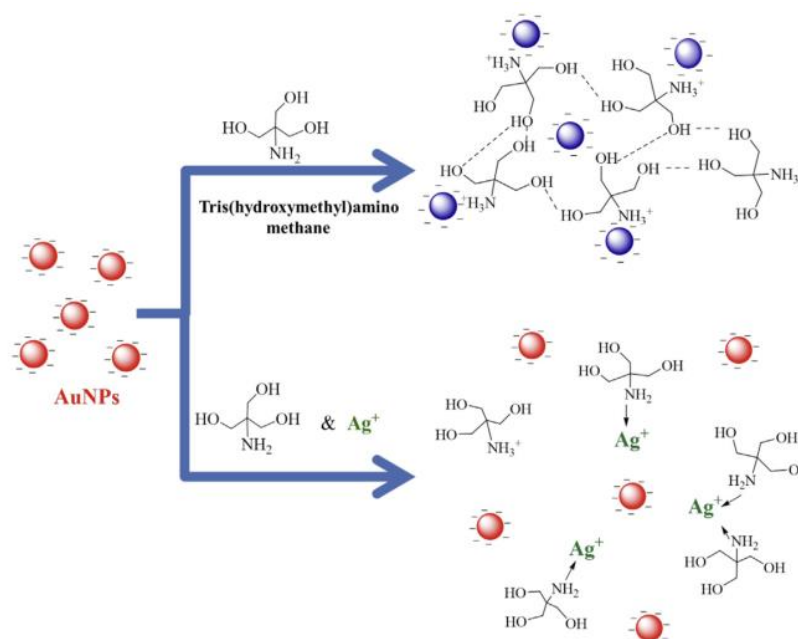


**Figure 1.8** The schematic of colorimetric sensor based on the anti-aggregation of AuNPs for Ag<sup>+</sup> detection with tris-(hydroxymethyl) aminomethane as aggregation inducer (Safavi et al., 2017).

### 1.2.3 Analytical techniques

#### 1.2.3.1 Ultraviolet-Visible spectrophotometry

The ultraviolet-visible-near-infrared radiation is applied in nanomaterial technology due to the rich information about the properties of gold nanoparticles. For spectrophotometric method, ultraviolet (UV) and visible (Vis) are in the range of 190 to 350 nm and 350 to 800 nm, respectively. The near infrared (NIR) spectrum is 800 to 2500 nm. The commercial spectrophotometer component is designed depending on the electromagnetic wavelength.

Normally, the spectrophotometer composes of four important parts. Firstly, it is the light source that can provide radiations over the electromagnetic wavelength. Secondly, it is a wavelength selector where the beams from the light source is passed through, resulting in limited bands of wavelength. Thirdly, the beam exiting the wavelength selector is passed through the sample cell and finally it is concentrated to a detector where all radiations is changed to electrical signals (Brown, 2005).

The spectroscopic technique is principally based on the Beer-Lambert law involving the linear relationship between absorption of light and the concentration of the analyte in a sample solution. One of the Beer-Lambert law applications is the determination of the concentration of analyte in sample solution at a certain wavelength (Equation 1.1). However, the linearity is limited by chemical and instrumental factors.

$$A = \epsilon bC \quad (1.1)$$

Where  $A$ ,  $\epsilon$ ,  $b$  and  $C$  are the analyte absorbance, the molar absorptivity ( $\text{L cm}^{-1} \text{ mole}^{-1}$ ), the cell pathlength and the concentration of analyte ( $\text{mol L}^{-1}$ ), respectively. Pathlength of the commercial cell is normally equal to 1 cm.

Based on the Beer's law, when the concentration of analyte increases, the light transmitted through a colored solution decreases exponentially (Skoog & Leary, 1992).

### 1.2.3.2 Other techniques

Bromide in samples can be detected by various techniques as shown in Table 1.3 and 1.4. The summary of Br<sup>-</sup> determination method is shown in Figure 1.9.

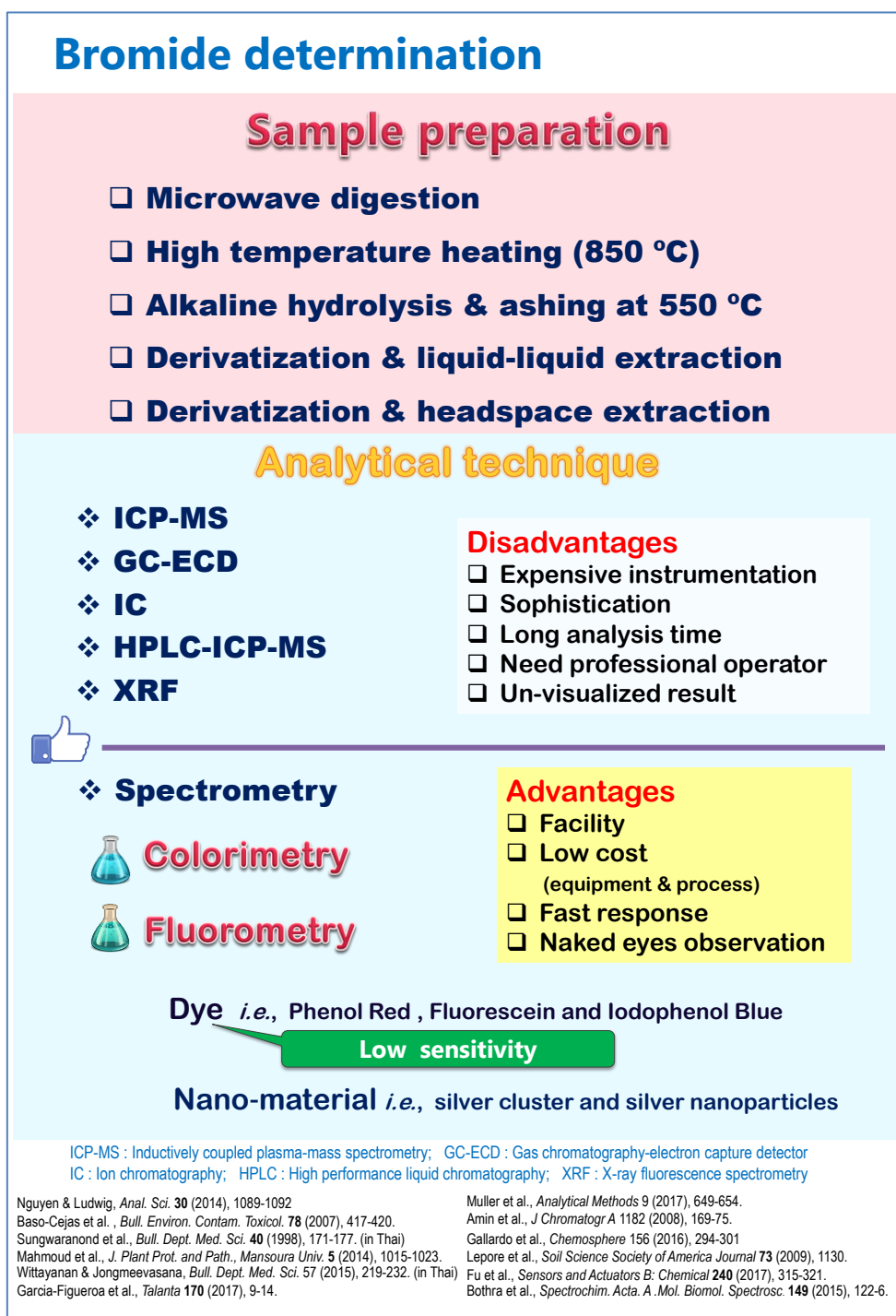


**Figure 1.9** The summary of Br<sup>-</sup> determination method.

**Table 1.3** The various techniques applied for Br<sup>-</sup> detection in different samples

Method <sup>a</sup>	Sample	Sample amount	Linear range	LOD	Detection time (min)	Reference
Microwave digestion/IC	Food	50 g	0.1 - 0.5 µg	-	4	(Miyahara & Saito, 1994)
Dry ashing and liquid-liquid extraction-derivatization/GC-ECD	Rice	2 g	0.01 - 0.1 mg kg <sup>-1</sup>	0.01 mg kg <sup>-1</sup>	-	(Sungwaranond et al., 1998)
Ion-selective PVC membrane	Water	-	32 - 100,000 µM	20 µM	-	(Shamsipur et al., 2000)
HPLC-ICP-MS	Water	50 µL	1 - 50 ug L <sup>-1</sup>	1 ug L <sup>-1</sup>	-	(Perrone et al., 2005)
Low pressure-IEC-visible light detection	Foodstuffs	25 g	0.03 - 0.5 mg L <sup>-1</sup>	0.002 mg L <sup>-1</sup>	7.5	(Yu et al., 2011)
Switching of cation and anion exchange columns-IC	River water	20 µL	-	1.81 mg L <sup>-1</sup>	> 6	(Amin et al., 2008)
Headspace solid-phase microextraction/GC-MS	Soil	1.5 g	-	-	> 15	(Yassaa et al., 2009)
Instrumental neutron activation analysis	Rice	0.1 g	-	0.16 mg kg <sup>-1</sup>	-	(Parengam et al., 2010)
Microwave digestion/ICP-MS	Food	1–2 g	0.002 - 0.1 mg kg <sup>-1</sup>	0.00068 mg kg <sup>-1</sup>	-	(Nguyen & Ludwig, 2014)
Liquid-liquid extraction-derivatization/GC-micro-ECD	Rice	2 g	5 - 75 mg kg <sup>-1</sup>	2 mg kg <sup>-1</sup>	20	(Wittayanan & Jongmevasna, 2015)
Total reflection X-ray fluorescence spectrometry	Soil and plant	1 g	1.25 - 12.5 mg kg <sup>-1</sup>	0.25 mg kg <sup>-1</sup>	25	(Gallardo et al., 2016)
microwave-wet digestion/ICP-MS	Honey	0.5 g	-	0.03 mg kg <sup>-1</sup>	20	(Muller et al., 2017)

**Table 1.4** The spectrometric method applied for Br<sup>-</sup> detection in different samples

Method <sup>a</sup>	Sample	Sample amount	Linear range (μM)	LOD (μM)	Detection time (min)	Reference
Heating/Phenol red spectrophotometry	Vegetables	5 g	6.26 - 56.32	3.13	5	(Baso-Cejas et al., 2007)
Phenol red and chloramine-T Colorimetry	Environmental samples	20-300 μL	0.00 - 375.45	1.38	5	(Lepore & Barak, 2009)
Aggregation and anti-aggregation of AgNPs	Water	-	0.99 - 5.66	1.67	-	(Bothra et al., 2015)
Dry ashing/Fluorescent Ag nanocluster detection	Dried kelp	1 g	0.10 - 50.00	-	60	(Fu et al., 2017)
Headspace single-drop microextraction/microvolume-FLD	Water	10 mL	62.50 - 312.88	16.27	10	(Garcia-Figueroa et al., 2017)

<sup>a</sup> IC, Ion chromatography; GC-ECD, Gas chromatography-electron capture detector; ICP-MS, Inductive coupled plasma-mass spectrometry; HPLC, High performance liquid chromatography; FLD, fluorescence detection

## 1.2.4 Method validation

### 1.2.4.1 Linearity

The linear calibration curve is a relationship between the measured signal of analyte and the series of different standard analyte concentration under the same conditions and covered the analyte concentration range which used in real samples. The evaluation of linear curve is performed by using the regression line which is constructed by plotting the concentration of standard of analyte on the horizontal (x) axis and response signal of analyte on the vertical (y) axis as seen in Figure 1.10. The linear equation as described in Equation 1.2 which was obtained from the regression line and the unknown concentration can be estimated from linear regression analysis which is often called a “least squares analysis”. The coefficient of determination as  $R^2$  is get closer to 1 or 100 % (Miller & Miller, 2015).

$$y = mx + c \quad (1.2)$$

Where y is measured absorbance

x is analyte concentration

m is slope of calibration curve (sensitivity)

c is intercept

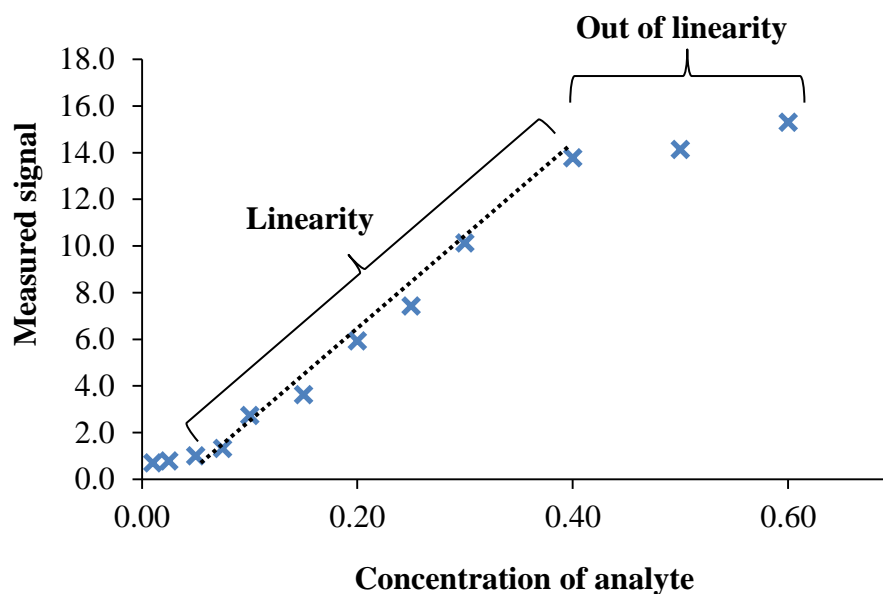


**Figure 1.10** The correlation plot between the measured signal and standard analyte concentration with the linear range response and non-linear range response.

#### 1.2.4.2 Limit of detection (LOD) and limit of quantification (LOQ)

Detection limit demonstrate the capable of detecting and determining trace and ultra-trace quantities of analytes. Limit of detection (LOD) is the concentration of analyte which gives an instrument signal (y) significantly different from the blank or background signal. The limit of quantification (LOQ) is the lowest concentration of analyte in the sample that can be quantitatively determined with defined precision under the optimum experimental conditions. It is a parameter of quantitative assays for low level of compounds in sample matrices (Miller & Miller, 2015). LOD and LOQ are analyte concentrations that gave a signal equal to the blank signal (S/N) plus three and ten standard deviations of the blank, respectively. These signals were calculated from the linear least squares line procedure as shown in Equation 1.3 for LOD and Equation 1.4 for LOQ (Miller & Miller, 2015).



$$\text{LOD Signal} = y_B + 3S_b \quad (1.3)$$

$$\text{LOQ Signal} = y_B + 10S_b \quad (1.4)$$

Where  $y_B$  is the blank signal

$S_B$  is the standard deviation of the blank

$y_B$  and  $S_B$  can be obtained from the blank experiment of 20 to 30 measurements (Skoog & Leary, 1992). The blank should have similar composition of analyte but no contain analyte (Miller & Miller, 2015).

#### 1.2.4.3 Matrix effect

The standard addition technique is widely applied to spectrophotometric, chromatographic and electrochemical analytical methods in order to overcome matrix effect.

The method of standard addition is carried out by spiking aliquots of a standard analyte to the sample. Equal volumes of the sample solution are taken and all samples but one are separately added with different concentration of analyte. All are then diluted to the same levels. The spiking standard sample was analyzed under the same condition of standard curve. The standard addition technique is shown in Figure 1.8B. The negative intercept on the x-axis corresponds to the concentration of analyte in sample.

The evaluation of matrix effect in term of relation of standard curve and standard addition curve was constructed by plotting the different concentrations of analyte from standard curve on a x-axis and the different concentrations of analyte from standard addition curve on a y-axis. If there is an identical result for both method, the slope and intercept value of the regression line will be close to 1 and 0, respectively. This implies that there is no matrix effect and the calibration curve can be used for the analysis of analyte concentration in sample (Miller & Miller, 2015). Another way, the standard addition curve and standard curve were plotted in the same curve as shown in Figure 1.11. If the slopes of both curves are not significantly different based on statistical analysis, it refers that matrix did not affect the analysis (Skoog & Leary, 1992).

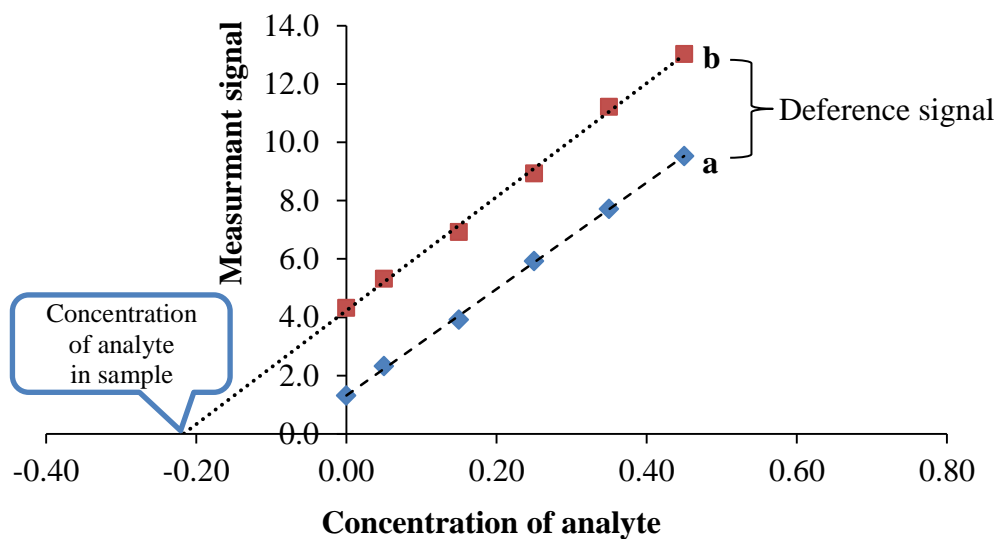


**Figure 1.11** The plots of standard addition and standard calibration curves.

#### 1.2.4.4 Accuracy

The accuracy is closeness of the “true” or accepted value. For the true value is usually obtained from the certified reference material (CRM) but sometimes the matrix of CRM is not suitable for real sample matrix or no CRM is available. Therefore, the fraction or percentage of the analyte, that is recovered when spiking known standard into the real sample, is analyzed using the entire method to evaluate the accuracy. The percentage of recovery is calculated as described in Equation 1.5 (AOAC, 2016)

$$\% \text{ Recovery} = \frac{C_F - C_U}{C_A} \times 100 \quad (1.5)$$

Where  $C_F$  is the concentration of spiked sample with standard analyte

$C_U$  is the concentration of un-spiked sample

$C_A$  is the concentration of standard added to sample

### 1.2.4.5 Precision

All measurements contain random error or noise that can be evaluated by repeating measurements of the same sample in 3 to 6 replicates and by calculating the standard deviation (SD) or relative standard deviation (RSD), as described in Equation 1.6 and 1.7, respectively (AOAC, 2016).

$$SD = \sqrt{\frac{\sum_{i=1}^n (X_i - \bar{X})^2}{n - 1}} \quad (1.6)$$

$$\% \text{ RSD} = \frac{SD}{\bar{X}} \times 100 \quad (1.7)$$

Where  $n$  is the total number of measurements

$\bar{X}$  is mean of measurement

$X_i$  is number of measurements

The repeatability describes the precision of within-run replicate or intra-day and reproducibility describes the precision of between-run replicate or inter-day.

## 1.3 Objective

**1.3.1** To develop the colorimetric probe based on AuNPs anti-aggregation process for bromide ion detection

**1.3.2** To apply the developed sensor for inorganic bromide determination in rice samples

## 1.4 Benefit

The developed colorimetric method based on the anti-aggregation of AuNPs was the facile, sensitive and selective detection of bromide ion in rice samples which can be easily observed by naked eyes, and also quantitatively measured by UV-visible spectroscopy.

## CHAPTER 2

### EXPERIMENTAL

#### 2.1 Overall scope

The development of the AuNPs colorimetric sensor for the facile, sensitive and selective detection of inorganic bromide (Bromide ion; Br<sup>-</sup>) in rice samples was followed these experiments. The experiment involved with the synthesis of AuNPs solution and characterization, the optimization of colorimetric detection conditions, method validation and sample preparation. The scope of this work was summarized in Figure 2.1.

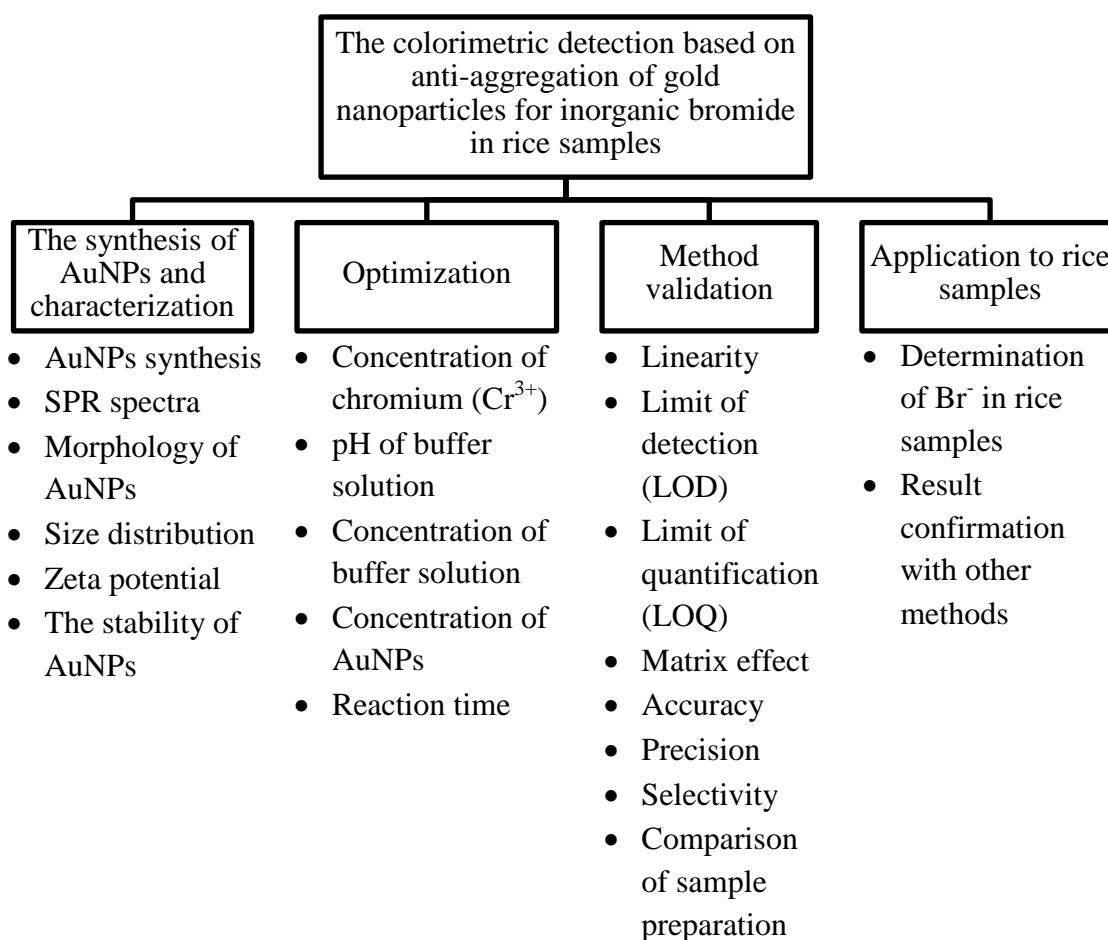


**Figure 2.1** Scope of method development for the AuNPs colorimetric sensor of inorganic bromide in rice samples.

## 2.2 Chemicals and reagents

All chemicals used in this work were of analytical grade as shown in Table 2.1 and the solutions were prepared using  $18 \text{ M}\Omega \text{ cm}^{-1}$  ultrapure water obtained from ELGA Maxima (England) for all experiments.

**Table 2.1** The chemicals used throughout experiment

<b>Chemicals</b>	<b>Brand</b>	<b>Country</b>
Aluminium nitrate nanohydrate	Anapure	-
Calcium chloride dihydrate	Merck	Germany
Chromium(III) nitrate nanohydrate	Alfa-Aesar	USA
Di-sodium hydrogen orthophosphate dodecahydrate	Ajax Finechem	Australia
Ethanol	RCI Labscan	Thailand
Gold(III) chloride trihydrate	Sigma-Aldrich	USA
Hydrochloric acid	RCI Labscan	Thailand
Magnesium sulfate heptahydrate	Ajax Finechem	Australia
Methanol	RCI Labscan	Thailand
Nitric acid	RCI Labscan	Thailand
Potassium bromide	Loba Chemi	India
Potassium chloride	Ajax Finechem	Australia
Potassium dihydrogen phosphate	Merck	Germany
Potassium fluoride	Ajax Finechem	Australia
Potassium hydroxide	RCI Labscan	Thailand
Potassium iodide	Ajax Finechem	Australia
Potassium nitrate	Ajax Finechem	Australia
Sodium dihydrogen orthophosphate dihydrate	Loba Chemi	India
Sodium nitrite	Ajax Finechem	Australia
Sodium sulfate anhydrous	RCI Labscan	Thailand
Tri-sodium citrate	Ajax Finechem	Australia

## **2.3 Laboratory glassware**

### **2.3.1 Glassware**

- 1) Amber bottle 100 mL
- 2) Beaker 25 mL, 50 mL, 150 mL, 250 mL and 1000 mL
- 3) Dropper
- 4) Duran bottle 250 mL
- 5) Glass bottle 25 mL
- 6) Glass funnel
- 7) Glass rod
- 8) Graduated cylinder 10 mL, 25 mL and 100 mL
- 9) Reagent bottle 250 mL
- 10) Screw cap test tube 50 mL
- 11) Vial with screw cap 2 mL
- 12) Vial with silicone septum cap 1.5 mL
- 13) Volumetric flask 25 mL, 100 mL and 250 mL
- 14) Watch glass

### **2.3.2 Preparation and cleaning method of glassware**

#### **2.3.2.1 Cleaning method of general glassware**

All glassware were cleaned with detergent solution (Tepol Pure, Thailand) and tap water for several times then rinsed with distilled water. After that it was immersed in 10% (v/v) nitric acid about 12 h, then washed well with distilled water and dried in the oven at 150 °C for 2 h, excepting that volumetric flask and cylinder were dried in the air.

#### **2.3.2.2 Cleaning method of specific glassware**

Glassware used for synthesis of AuNPs including Duran bottle, beaker, magnetic bar and volumetric flask were specially cleaned to avoid aggregation of gold colloids. After finishing from cleaning generally, they are rinsed with freshly prepared aqua regia solution as 3:1 (v/v) of HCl:HNO<sub>3</sub>, washed with ultrapure water for at least

2 times and then dried in the oven at 150 °C before use excepting that volumetric flask was washed with ultrapure water many times and dried in the air.

## 2.4 Apparatus and materials

All apparatus and materials are listed in Table 2.2.

**Table 2.2** The apparatus and materials used throughout experiment

<b>Chemicals</b>	<b>Brand</b>	<b>Country</b>
Analytical balance 0.0001 g	Mettler Toledo	Switzerland
Auto pipette 100 - 1000 $\mu$ L	Thermo Scientific	USA
Auto pipette 20 - 200 $\mu$ L	Thermo Scientific	USA
Auto pipette 5 - 50 $\mu$ L	CAPP Bravo	Denmark
Ball mill	Retsch MM400	Germany
Bench top pH meter	BANTE Instruments	China
Centrifuge machine	Hermie Labortechnik GmbH	Germany
Centrifuge tube 50 mL	Biologix	China
Digital camera, iPhone 6	Apple	USA
Disposable polystyrene cuvette	VWR We Enable Science	Germany
Freezer	UMA'C Scientific	China
HDPE bottle	Nalgene	USA
Hot air oven	Memmert	Germany
Hot plate	EGO	Germany
Hot plate and stirrer	IKA, C-MAGHS7	Germany
Magnetic bar	-	-
Microtube	Axygen	USA
Muffle furnace	Thermolyne	USA
Nickel crucible 50 mL, 1 mm thickness	Rotilabo	Germany
Nylon membrane filters 0.22 micron	Agela Technologies	USA
HLB extraction cartridge	OASIS, Waters Corporation	USA
Refrigerator	TOSHIBA	Japan
SPE Manifold	Aqlilent Technologies	USA

**Table 2.2** The apparatus and materials used throughout experiment (continued)

<b>Chemicals</b>	<b>Brand</b>	<b>Country</b>
Syringe	TERUMO	Philippines
Ultrasonic bath	Retsch	Germany
Vacuum pump	GAST	USA
Vortex mixer	LMS	Japan

## **2.5 Instrument**

### **2.5.1 UV-Visible spectrophotometer**

A UV-1800 spectrophotometer (Shimadzu, Japan) was used with a 1.5 mL disposable polystyrene cuvette to measure the surface plasmon resonance (SPR) spectra of AuNPs solution or its mixture solution in the absorption range of 400 - 800 nm.

### **2.5.2 Transmission electron microscopy**

A Transmission electron microscopy (TEM, JEM-2010, JEOL, Japan) was used to investigate the morphology including size, shape, dispersion state and aggregation state of AuNPs at a 200 kV acceleration voltage.

### **2.5.3 Zeta potential analyzer**

A zeta potential analyzer (ZetaPALS, Brookhaven, USA) was used for zeta-potential and size distribution measurements of AuNPs solution or its mixture solution.

### **2.5.4 Inductively coupled plasma optical emission spectrometer**

An inductively coupled plasma optical emission spectrometer (ICP-OES, AVIO 500, Perkin Elmer, USA) was used to analyze metals in composition of rice extracts.



### **2.5.5 X-Ray Fluorescence Spectrometer**

An X-Ray fluorescence spectrometer (XRF, PW2400, Philips, Netherlands) was used to analyze the bromine elements in sample solution prepared by our sample preparation method.

### **2.5.6 Ion chromatography**

A 940 Professional IC Vario (Metrohm, Switzerland) ion chromatograph was used for determination of bromide ion in sample solution prepared by our sample preparation method.

## **2.6 Preparation of solution**

### **2.6.1 Preparation of stock standard solution of 12.52 mM (1000 ppm) bromide ion**

Potassium bromide (0.1490 g) was dissolved in ultrapure water and adjusted volume to 100.00 mL in volumetric flask.

### **2.6.2 Preparation of 0.015% w/v gold(III) chloride solution**

Gold(III) chloride trihydrate (0.0435 g) was dissolved in 250 mL ultrapure water and kept in refrigerator before further synthesis.

### **2.6.3 Preparation of 1% w/v sodium citrate solution**

Trisodium citrate (0.2849 g) was freshly prepared by dissolving in ultrapure water and adjusted volume to 25.00 mL in volumetric flask.

### **2.6.4 Preparation of 19.23 mM (1000 ppm) chromium(III) solution**

Chromium(III) nitrate nanohydrate (0.1924 g) was dissolved in ultrapure water and adjusted volume to 25.00 mL in volumetric flask, then kept in HDPE bottle for further use.

### **2.6.5 Preparation of 20 mM sodium dihydrogen phosphate solution**

Sodium dihydrogen orthophosphate dihydrate (0.7800 g) was dissolved in ultrapure water and adjusted volume to 250.00 mL in volumetric flask.

### **2.6.6 Preparation of 20 mM di-sodium hydrogen phosphate solution**

Di-sodium hydrogen orthophosphate dodecahydrate (1.7910 g) was dissolved in ultrapure water and adjusted volume to 250.00 mL in volumetric flask.

### **2.6.7 Preparation of working standard solution of 0.1252 mM (10 ppm) bromide ion**

A 250  $\mu\text{L}$  of stock standard solution was pipetted into 25.00 mL volumetric flask and adjusted volume to the mark with ultrapure water.

### **2.6.8 Preparation of working concentration range of bromide ion**

The working concentration of bromide ion in the range of 0.06 - 10.01  $\mu\text{M}$  were freshly prepared for optimization and study of linearity by diluting of working standard solution with ultrapure water at the final volume of 2 mL as shown in the Table 2.3.

**Table 2.3** The working concentration range of bromide solution

<b>Initial concentration of Br<sup>-</sup> solution (μM)</b>	<b>Volume of 0.1252 mM working standard solution (μL)</b>	<b>Volume of ultrapure water (μL)</b>
0.75	12	1988
1.50	24	1976
3.75	60	1940
7.51	120	1880
11.26	180	1820
15.02	240	1760
22.53	360	1640
30.04	480	1520
37.55	600	1400
45.05	720	1280
52.56	840	1160
60.07	960	1040
75.09	1200	800
90.11	1440	560
120.14	1920	80

#### **2.6.9 Preparation of 0.1154 mM (6 ppm) chromium(III) solution**

A 300 μL of 19.23 mM chromium(III) solution was pipetted into 50 mL volumetric flask and adjusted volume to the mark with ultrapure water, then kept in HDPE bottle.

#### **2.6.10 Preparation of working concentration range of chromium(III) ion**

The concentration of chromium(III) solution at 11.54, 28.85, 57.70, 86.54, 115.39, 173.09 and 230.79 μM were prepared by pipetting 6.0, 15.0, 30.0, 45.0, 60.0, 90.0 and 120.0 μL of 19.23 mM chromium(III) stock solution, respectively into 10 mL volumetric flask and adjusted volume to the mark with ultrapure water.

### 2.6.11 Preparation of 0.01 M sodium phosphate buffer solution

Sodium phosphate buffer (0.01 M) in the pH range of 6.0 - 7.5 was prepared by mixing a volume of 0.02 M sodium dihydrogenphosphate and 0.02 M disodium hydrogenphosphate as shown in Table 2.4. The buffer was adjusted by either sodium dihydrogenphosphate or disodium hydrogenphosphate to obtain pH as required and made volume to 100 mL with ultrapure water in volumetric flask.

**Table 2.4** Preparation of 0.01 M sodium phosphate buffer solution at different pH

pH of buffer solution	Volume of 20 mM sodium dihydrogenphosphate (mL)	Volume of 20 mM disodium hydrogenphosphate (mL)
6.0	43.85	6.15
6.3	38.75	11.25
6.5	34.00	16.00
7.0	19.50	30.50
7.5	8.00	42.00

### 2.6.12 Preparation of 1% (w/v) potassium hydroxide in 50% ethanol

A 50 mL ethanol and 50 mL ultrapure water were mixed well together to obtain 50% (v/v) ethanol. Next, potassium hydroxide (1.0000 g) was dissolved in 50% (v/v) ethanol and the mixture was sonicated for 5 min and finally adjusted volume to 100 mL with volumetric flask.

### 2.6.13 Preparation of interference ion solution for study of selectivity

The ion solution of  $K^+$ ,  $Mg^{2+}$ ,  $Ca^{2+}$ ,  $Al^{3+}$ ,  $NO_2^-$ ,  $NO_3^-$ ,  $PO_4^{3-}$ ,  $SO_4^{2-}$ ,  $F^-$ ,  $Cl^-$  and  $I^-$  at the initial concentration of 60 mM was prepared for study of selectivity in this work by dissolving the ion standard with ultrapure water and adjusted volume to 25.00 mL in volumetric flask. The amount of ion compounds used are shown in Table 2.5.

**Table 2.5** The amount of interested ions for preparation of interference solution

<b>Ion</b>	<b>Compound</b>	<b>Weight (g)</b>
K <sup>+</sup>	KOH	0.0586
Mg <sup>2+</sup>	MgSO <sub>4</sub> .7H <sub>2</sub> O	0.3697
Ca <sup>2+</sup>	CaCl <sub>2</sub> .2H <sub>2</sub> O	0.2205
Al <sup>3+</sup>	Al(NO <sub>3</sub> ) <sub>3</sub> .9H <sub>2</sub> O	0.5627
NO <sub>2</sub> <sup>-</sup>	NaNO <sub>2</sub>	0.1035
NO <sub>3</sub> <sup>-</sup>	KNO <sub>3</sub>	0.1518
PO <sub>4</sub> <sup>3-</sup>	KH <sub>2</sub> PO <sub>4</sub>	0.2041
SO <sub>4</sub> <sup>2-</sup>	Na <sub>2</sub> SO <sub>4</sub>	0.2131
F <sup>-</sup>	KF	0.0872
Cl <sup>-</sup>	KCl	0.1118
I <sup>-</sup>	KI	0.2490

## 2.7 The synthesis and characterization of gold nanoparticles

### 2.7.1 The synthesis of gold nanoparticles solution

The synthesis of gold nanoparticles solution is shown in Figure 2.2. A volume of 250 mL of 0.015% (m/v) gold(III) chloride solution was added into a 500 mL Duran bottle and heated to boiling with vigorous stirring. Subsequently, after gold(III) chloride solution was vigorously boiled the 8.75 mL of 1% (w/v) tri-sodium citrate solution was added rapidly into the boiling solution, followed by stirring. The color of solution changed from pale yellow to wine red in a few minutes since Au<sup>3+</sup> was reduced to Au<sup>0</sup>, indicating the formation of citrate capped-gold nanoparticles (AuNPs). After that the AuNPs solution was continuously boiling for another 15 min to ensure the reaction was completed, allowed to cool down to room temperature under stirring. The AuNPs was transferred to 250 mL volumetric flask by glass funnel and adjusted volume with ultrapure water. The aliquot of resultant AuNPs solution was performed and stored in an amber glass bottle at 4 °C for further use. The concentration of synthesized gold nanoparticles solution from this method is 5.52 nM AuNPs.

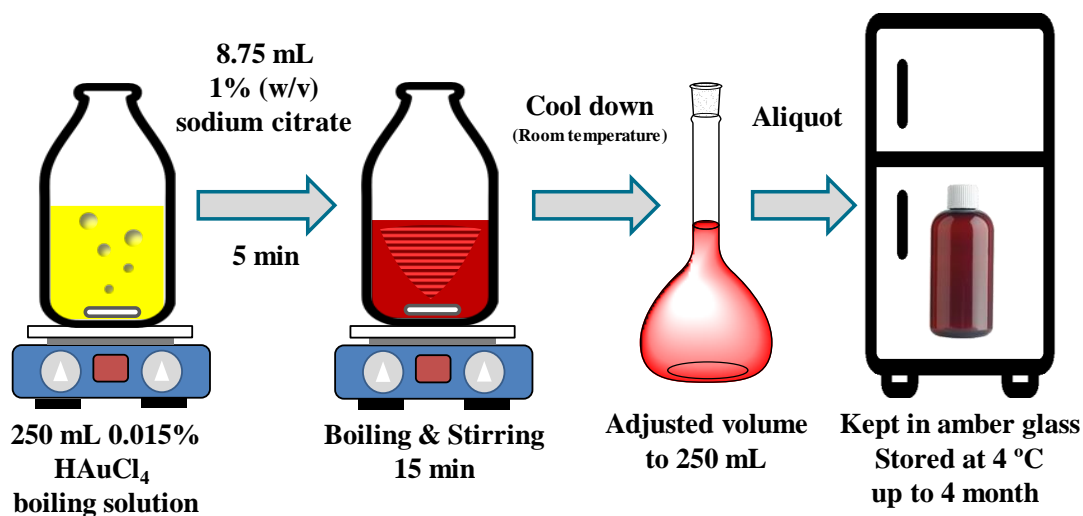


**Figure 2.2** The procedure of gold nanoparticles synthesis.

## 2.7.2 Characterization of AuNPs particles

### 2.7.2.1 The surface plasmon resonance (SPR) measurement

The surface plasmon resonance (SPR) spectra were measured by adding 1,200  $\mu\text{L}$  of AuNPs solution or its mixture solution into a 1.5 mL disposable polystyrene semi cuvette and ultrapure water was used as the reference sample with the conditions of UV-Visible spectrophotometer as follows

Wavelength range: 400 - 800 nm

Scan rate: Fast mode

Sampling interval: 1.0 nm

Slit width: 1.0 nm

### 2.7.2.2 The morphology of AuNPs

The morphology of AuNPs was measured by transmission electron with a 200 kV acceleration voltage. Before TEM measurements, the samples were 3 times diluted with ultrapure water and 5  $\mu\text{L}$  of diluted sample was deposited on the carbon coated copper grid and then evaporated at room temperature.

Sample 1: the diluted pure AuNPs solution was used to study size, shape and dispersion state of AuNPs.

Sample 2: the mixture of 1.8 nM AuNPs, 10 mM phosphate buffer and 4.80  $\mu\text{M Cr}^{3+}$  was prepared to study the aggregation state of AuNPs.

Sample 3: the mixture of 1.8 nM AuNPs, 10 mM phosphate buffer, 3.13  $\mu\text{M Br}^-$  and 4.80  $\mu\text{M Cr}^{3+}$  was prepared to study the anti-aggregation or re-dispersion state of AuNPs. The TEM size was calculated by software of ImageJ version 1.51k.

### **2.7.2.3 Zeta-potential measurements**

Zeta-potential measurements were performed on zeta potential analyzer with the software of ZetaPALS Potential Analyzer version 3.54. The solution of 1.8 nM AuNPs and 10 mM phosphate buffer was mixed with 0, 0.63, 2.50 and 4.38  $\mu\text{M Br}^-$  respectively for the study of charge value and stability on the surface of AuNPs.

### **2.7.2.4 Size distribution measurements**

Size distribution measurements were performed on zeta potential analyzer with the software of ZetaPALS Particle Sizing version 4.03. The samples 1, 2 and 3 from section 2.7.2.2 was measured by 2 times diluting with ultrapure water to study the size distribution of dispersed AuNPs, aggregated AuNPs and re-dispersed AuNPs.

### **2.7.2.5 The stability of AuNPs solution**

The stability of AuNPs solution was performed by measuring the SPR absorption of pure AuNPs solution from 1 day after synthesis until 4 months for every week and recorded a detection sensitivity of 2.50  $\mu\text{M Br}^-$  in total of 8 times during 4 months

## **2.8 Optimization of parameters affecting the bromide ion sensor**

To obtain the optimum analytical conditions for the detection of bromide ion, various parameters including concentration of  $\text{Cr}^{3+}$ , pH and concentration of phosphate buffer, concentration of AuNPs and reaction time were investigated. One parameter was varied whereas the other parameters were kept constant. All experiments were repeated three times with a report of mean and standard deviation (SD).

### 2.8.1 Concentrations of chromium ( $\text{Cr}^{3+}$ )

The effect of different concentrations of  $\text{Cr}^{3+}$  in the range of 1.0 - 19.2  $\mu\text{M}$  was investigated. It was performed by adding 500  $\mu\text{L}$  of 5.52 nM AuNPs, 500  $\mu\text{L}$  of 10 mM phosphate buffer (pH 7.0) and 100  $\mu\text{L}$  of  $\text{Cr}^{3+}$  solution into a microtube, respectively. Then the mixture was adjusted to the final volume of 1200  $\mu\text{L}$  with the addition of 100  $\mu\text{L}$  of ultrapure water. The mixture was immediately vortex mixed and left at room temperature for 10 min before measurement by UV-Visible spectrophotometry and the photograph was taken by digital camera. The initial concentration of  $\text{Cr}^{3+}$  solutions were 11.54, 28.85, 57.70, 86.54, 115.39, 173.09 and 230.79  $\mu\text{M}$  which were used for preparing of the final concentrations at 1.0, 2.4, 4.8, 7.2, 9.6, 14.4 and 19.2  $\mu\text{M}$  of  $\text{Cr}^{3+}$ .

### 2.8.2 pH of phosphate buffer solution

The effect of pH on anti-aggregated AuNPs via  $\text{Br}^-$  with different pH of phosphate buffer (6.0, 6.3, 6.5, 7.0 and 7.5) was investigated on the sensitivity of  $\text{Br}^-$  concentration ranged from 0.63 - 5.01  $\mu\text{M}$ . It was performed by adding 500  $\mu\text{L}$  of 5.52 nM AuNPs, 500  $\mu\text{L}$  of 10 mM phosphate buffer, 100  $\mu\text{L}$  of  $\text{Br}^-$  and 100  $\mu\text{L}$  of 57.70  $\mu\text{M}$   $\text{Cr}^{3+}$  solutions into a microtube, respectively. The mixture was immediately vortex mixed and left at room temperature for 10 min before measurement by UV-Visible spectrophotometry and the photograph was taken by digital camera. The different of  $\text{Br}^-$  concentration as initial concentration of  $\text{Br}^-$  solution at 7.51, 11.26, 15.02, 30.04 and 60.07  $\mu\text{M}$  were used to made final concentration range of 0.63, 0.94, 1.25, 2.50 and 5.01  $\mu\text{M}$  of  $\text{Br}^-$ , respectively.

### 2.8.3 Concentration of phosphate buffer solution

The effect of concentration of phosphate buffer pH 6.5 ranging from 2.5 - 25.0 mM was investigated on the aggregation and anti-aggregation of AuNPs. The aggregation of AuNPs as blank contained of 4.81  $\mu\text{M}$   $\text{Cr}^{3+}$  without  $\text{Br}^-$  in AuNPs. The anti-aggregation of AuNPs as analyte was in the presence of 4.81  $\mu\text{M}$   $\text{Cr}^{3+}$  and 2.50  $\mu\text{M}$   $\text{Br}^-$  in AuNPs. The different of phosphate buffer (pH 6.5) solution at the concentration of 1.0, 2.5, 5.0, 7.5, 10.0 and 25.0 mM was investigated.



### 2.8.3.1 The aggregation of AuNPs

It was performed by adding 500  $\mu\text{L}$  of 5.52 nM AuNPs, 500  $\mu\text{L}$  of phosphate buffer (pH 6.5) and 100  $\mu\text{L}$  of 57.70  $\mu\text{M}$   $\text{Cr}^{3+}$  solutions into a microtube, respectively. Then the mixture was adjusted to the final volume of 1200  $\mu\text{L}$  with the addition of 100  $\mu\text{L}$  of ultrapure water. The mixture was immediately vortex mixed and left at room temperature for 10 min before measurement by UV-Visible spectrophotometry and the photograph was taken by digital camera.

### 2.8.3.2 The anti-aggregation of AuNPs

It was performed by adding 500  $\mu\text{L}$  of 5.52 nM AuNPs, 500  $\mu\text{L}$  of phosphate buffer, 100  $\mu\text{L}$  of 30.04  $\mu\text{M}$   $\text{Br}^-$  and 100  $\mu\text{L}$  of 57.70  $\mu\text{M}$   $\text{Cr}^{3+}$  solutions into a microtube, respectively. The mixture was immediately vortex mixed and left at room temperature for 10 min before measurement by UV-Visible spectrophotometry and the photograph was taken by digital camera.

### 2.8.4 Concentration of AuNPs

The influences of amount of AuNPs with different concentration of 1.38, 1.83, 2.29, 2.75 and 3.21 nM were investigated on the sensitivity of  $\text{Br}^-$  concentration ranged from 0.63 - 2.50  $\mu\text{M}$ . It was performed by a volume of 5.52 nM AuNPs (300, 400, 500, 600 and 700  $\mu\text{L}$ ), 250  $\mu\text{L}$  of 20 mM phosphate buffer (pH 6.5), 100  $\mu\text{L}$  of  $\text{Br}^-$  and 100  $\mu\text{L}$  of 57.70  $\mu\text{M}$   $\text{Cr}^{3+}$  solutions were added into a microtube, respectively. Each mixture was added with ultrapure water at 450, 350, 250, 150 and 50  $\mu\text{L}$ , respectively to obtain total volume of 1200  $\mu\text{L}$ . The mixture was immediately vortex mixed and left at room temperature for 10 min before measurement by UV-Visible spectrophotometry and the photograph was taken by digital camera. The different of  $\text{Br}^-$  concentration as initial concentration of  $\text{Br}^-$  solution at 7.51, 11.26, 15.02 and 30.04  $\mu\text{M}$  were used to made final concentration range of 0.63, 0.94, 1.25 and 2.50  $\mu\text{M}$  of  $\text{Br}^-$ , respectively.

### 2.8.5 Reaction time

The influence of reaction time ranged from 0 - 30 min upon the interaction between AuNPs and  $\text{Br}^-$  in the range of 1.25, 2.50 and 5.01  $\mu\text{M}$  was investigated. It was performed by adding 400  $\mu\text{L}$  of 5.52 nM AuNPs, 500  $\mu\text{L}$  of 10 mM phosphate buffer, 100  $\mu\text{L}$  of  $\text{Br}^-$  and 100  $\mu\text{L}$  of 57.70  $\mu\text{M}$   $\text{Cr}^{3+}$  solutions into a microtube, respectively. Then the mixture was adjusted to the final volume of 1200  $\mu\text{L}$  with the

addition of 100  $\mu\text{L}$  of ultrapure water. The mixture was immediately vortex mixed and measurement by UV-Visible spectrophotometry of each reaction with measured every 2 min from 0 until 30 min. The different of  $\text{Br}^-$  concentration as initial concentration of  $\text{Br}^-$  solution at 15.02, 30.04 and 60.07  $\mu\text{M}$  were used to made final concentration range of 1.25, 2.50 and 5.01  $\mu\text{M}$  of  $\text{Br}^-$ , respectively.

## 2.9 Overall colorimetric detection method for bromide ion ( $\text{Br}^-$ )

The determination of bromide ion in this study is based on anti-aggregation of AuNPs as shown in Figure 2.3. A volume of 500  $\mu\text{L}$  of 5.52 nM AuNPs, 100  $\mu\text{L}$  ultrapure water, 500  $\mu\text{L}$  of 10 mM phosphate buffer (pH 6.5), 100  $\mu\text{L}$  of standard  $\text{Br}^-$  or sample and 100  $\mu\text{L}$  of 57.70  $\mu\text{M}$   $\text{Cr}^{3+}$  solutions were added into a microtube, respectively. The mixture was immediately vortex mixed and left at room temperature for 10 min before measurement by UV-Visible spectrophotometry and the photograph was taken by digital camera. Moreover, the color of solution was observed by naked eyes.

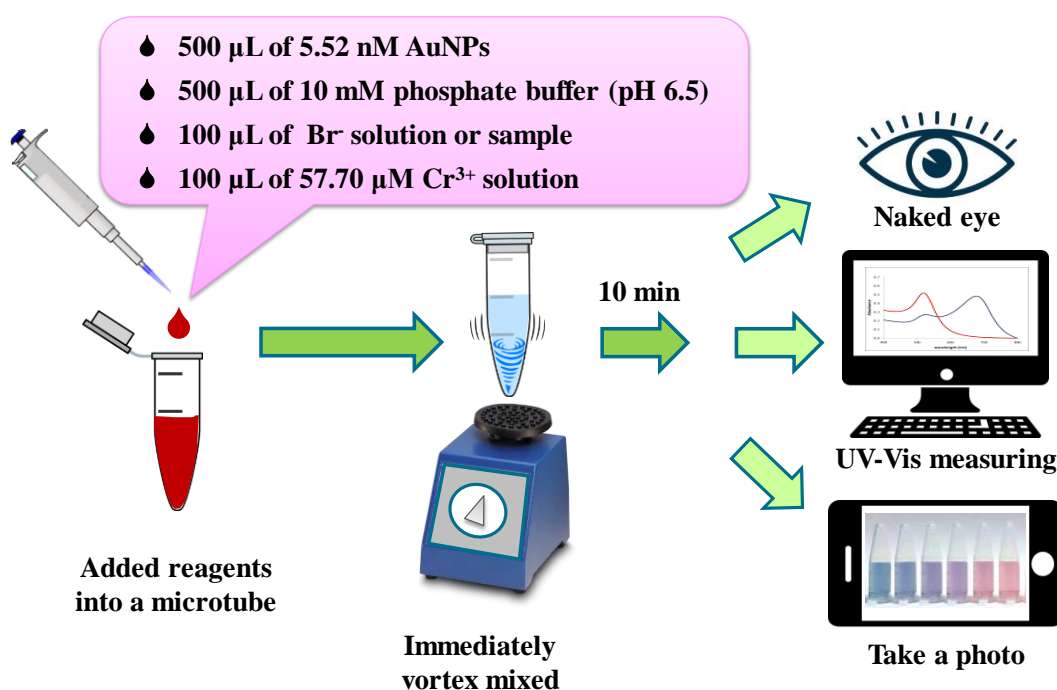


**Figure 2.3** The colorimetric detection procedure for determination of  $\text{Br}^-$ .

## 2.10 Method validation

Rice samples were collected randomly from the supermarket in Hat Yai, Songkhla province, Thailand. The ten brands of rice were mixed to obtain composite rice samples which were further used for recovery study and development of sample preparation method.

### 2.10.1 Linearity

The concentration of Br<sup>-</sup> in the range of 0.06 - 120.14 μM were investigated to study a linearity of developed sensor with the initial concentration including 0.75, 1.50, 3.75, 7.51, 11.26, 15.02, 22.53, 30.04, 37.55, 45.05, 52.56, 60.07, 75.09, 90.11 and 120.14 μM of Br<sup>-</sup> solution which was freshly prepared to obtain the final concentrations of 0.06, 0.13, 0.31, 0.63, 0.94, 1.25, 1.88, 2.50, 3.13, 3.75, 4.38, 5.01, 6.26, 7.51 and 10.01 μM Br<sup>-</sup>, respectively. The reaction procedure was performed as method in section 2.9. The linear regression was plotted between the absorbance ratio ( $A_{519}/A_{673}$ ) and concentration of Br<sup>-</sup>. The linear curve is assessed by linear equation and the coefficient of determination ( $R^2$ ) is close to 1.

### 2.10.2 Limit of detection (LOD) and limit of quantification (LOQ)

Limit of detection (LOD) and limit of quantification (LOQ) were calculated from equation 1.3 with the standard deviation ( $s_B$ ) of 20 times measurement of standard blank. The 20 sets of 57.70 μM Cr<sup>3+</sup> solution as standard blank was prepared as method mentioned in section 2.9 without adding Br<sup>-</sup> and the slope of calibration curve in the range of 0.31 - 3.75 μM Br<sup>-</sup> was used.

### 2.10.3 Matrix effect

#### 2.10.3.1 Sample preparation of composite samples

The rice samples of 10 band (100 g) were mixed to make the composite rice sample and ground by using Ball mill to obtain approximately ~5 μm powder sample and stored in a freezer at -22 °C when not in use. The digestion and dry ashing of rice samples was performed according to a report of Sungwaranond et al. (1998) with modifications.

Rice powder (2.0000 g) was weighted in a 50 mL nickel crucible and 5 mL of 1% potassium hydroxide in 50% ethanol was added. The sample was boiled on hotplate by gradually increasing heating rate to avoid the sample bumping until sample were dried and no smoke was observed.

Subsequently, the sample was heated in a muffle furnace at 600 °C for 4 h to eliminate some organic residues. After allowing the ash obtained to be cool down, it was added with 15 mL ultrapure water, boiled for 15 min on hotplate in order to dissolve inorganic bromide and filtered with 0.2 µm nylon membrane filter through a 25 mL volumetric flask. The ash residue in a nickel crucible was again boiled by adding other 10 mL of ultrapure water. This new solution was filtered through a previous volumetric flask and made volume to 25 mL with ultrapure water. The sample solution was then 1 fold diluted with ultrapure water before color reaction.

### **2.10.3.2 The standard addition method**

The matrix effect on developed sensor was investigated by using a standard addition curve spiked with Br<sup>-</sup> in the range of 0.31 - 3.75 µM into the rice sample extracts obtained from section 2.10.3.1. The slope of a standard addition curve was compared to that of a standard calibration curve at same concentration range.

The standard addition curve was performed by adding 400 µL of 5.52 nM AuNPs, 500 µL of 10 mM phosphate buffer (pH 6.5) into 100 µL of rice extracts followed by 100 µL of different concentration of standard Br<sup>-</sup> and 100 µL of 57.70 µM Cr<sup>3+</sup> solutions. The reaction was performed as the method in section 2.9. The initial concentration of Br<sup>-</sup> solution were 3.75, 7.51, 15.02, 30.04 and 45.05 µM to obtained final concentration range at 0.31, 0.63, 1.25, 2.50 and 3.75 µM Br<sup>-</sup>, respectively.

### **2.10.4 Accuracy**

The accuracy of developed method was investigated by recovery method (AOAC, 2016). Volumes of 25, 50, 100 and 125 µL of stock Br<sup>-</sup> solution were spiked into the composite rice samples to obtained final concentration of 12.0, 25.0, 50.0 and 60.0 mg kg<sup>-1</sup>, respectively with 3 replicates. All spiked and unspiked samples were carried out as the same method in section 2.10.3.1 and 2.10.3.2

### **2.10.5 Precision**

The study of precision for developed sensor was carried out by the inter-day and intra-day precisions. The inter-day precisions of the three concentration levels of Br<sup>-</sup> at 0.63, 1.25 and 3.75 µM were determined with the 3 measurements on 5 days. The intra-day precisions were obtained from the 5 measurements of each three concentration levels. Each measurement was prepared according to a method in

section 2.9. The standard calibration curve in the range of 0.31 - 3.75  $\mu\text{M}$   $\text{Br}^-$  was used. The initial concentration of  $\text{Br}^-$  solution were 7.51, 15.02 and 45.05  $\mu\text{M}$  to yield final concentration range at 0.63, 1.25 and 3.75  $\mu\text{M}$  of  $\text{Br}^-$ , respectively.

## **2.11 Comparison of developed sample preparation with SPE method**

Rice sample preparation in this work (section 2.10.3.1) was compared with SPE method involving with the extraction of rice sample with water, followed by clean-up method using solid phase extraction (SPE).

### **2.11.1 The extraction of rice samples with water**

The extraction of rice sample with water was performed according to Cheewasedtham and Jaffrezic-Renault (2016), with modification.

Rice powder (2.0000 g) was weighted into a 50 mL screw cap test tube and 25 mL of ultrapure water was added. Next, the sample was sonicated for 20 min to dissolve inorganic bromide ion from rice samples and transferred to centrifuge tube, followed by centrifugation at 6000 rpm for 30 min. The supernatant was filtered through 0.2  $\mu\text{m}$  nylon membrane filter. The water extract of rice was immediately kept in a refrigerator before clean-up by SPE. The composite rice sample spiked with a final concentration of 4.26  $\mu\text{M}$  (0.34  $\text{mg L}^{-1}$ )  $\text{Br}^-$  and unspiked sample were compared to investigate matrix effect. (Cheewasedtham & Jaffrezic-Renault, 2016)

### **2.11.2 Solid phase extraction for clean-up of the water extract of rice**

Solid phase extraction (SPE) for clean-up of the water extract of rice was performed according to a method of (Cheng et al., 1998), with modification.

The HLB cartridge for SPE was conditioned with 1 mL methanol and 1 mL ultrapure water, respectively and dried under air. After SPE conditioning, 5 mL of the water extract of rice from section 2.11.1 was loaded onto the dried HLB cartridge to eliminate polar organic compounds which was absorbed on the sorbent and then the eluate was kept in refrigerator for further experiment.

### 2.11.3 The detection of the water extract of rice

The water extract of rice samples were detected by developed sensor as mentioned in section 2.9 and the color of solution was observed by naked eyes.

### 2.12 Comparison of ashing time by inductively coupled plasma optical emission spectrometry (ICP-OES)

The composite rice sample was digested with acid and thermally decomposed to an ash in nickel crucible. The comparison of ashing time for 4 and 6 h was carried out, followed by the method as mentioned in section 2.10.3.1 to eliminate organic matters in samples. The residue solution was then measured by inductively coupled plasma optical emission spectrometry (ICP-OES).

### 2.13 Selectivity

The influence of other ions which can be found in rice samples was evaluated by selectivity of 5  $\mu\text{M}$   $\text{Br}^-$  towards 5  $\mu\text{M}$   $\text{I}^-$ , 250  $\mu\text{M}$  of  $\text{K}^+$ ,  $\text{NO}_2^-$ ,  $\text{NO}_3^-$ ,  $\text{PO}_4^{3-}$ ,  $\text{SO}_4^{2-}$ ,  $\text{F}^-$  and 25  $\mu\text{M}$  of  $\text{Mg}^{2+}$ ,  $\text{Ca}^+$ ,  $\text{Al}^{3+}$ ,  $\text{Cl}^-$  and the mixture of 5  $\mu\text{M}$   $\text{Br}^-$  with 250  $\mu\text{M}$  of  $\text{K}^+$ ,  $\text{NO}_2^-$ ,  $\text{NO}_3^-$ ,  $\text{PO}_4^{3-}$ ,  $\text{SO}_4^{2-}$ ,  $\text{F}^-$  and 25  $\mu\text{M}$  of  $\text{Mg}^{2+}$ ,  $\text{Ca}^{2+}$ ,  $\text{Al}^{3+}$ ,  $\text{Cl}^-$ .

The color detection was performed as method in section 2.9. The 100  $\mu\text{L}$  of each ion solution was used instead of  $\text{Br}^-$  solution with 3 replicates. The initial concentration at 60 mM of each ion solution was used to obtain final concentration at 5000  $\mu\text{M}$ . A solution of 60 mM  $\text{I}^-$  was 100 time diluted to obtain 5  $\mu\text{M}$   $\text{I}^-$ . Furthermore, 3000  $\mu\text{M}$  of  $\text{K}^+$ ,  $\text{NO}_2^-$ ,  $\text{NO}_3^-$ ,  $\text{PO}_4^{3-}$ ,  $\text{SO}_4^{2-}$ ,  $\text{F}^-$ , and 300  $\mu\text{M}$   $\text{Mg}^{2+}$ ,  $\text{Ca}^{2+}$ ,  $\text{Al}^{3+}$ ,  $\text{Cl}^-$  were 20 times and 200 times diluted, respectively to obtain 250  $\mu\text{M}$  of  $\text{K}^+$ ,  $\text{NO}_2^-$ ,  $\text{NO}_3^-$ ,  $\text{PO}_4^{3-}$ ,  $\text{SO}_4^{2-}$ ,  $\text{F}^-$  and 25  $\mu\text{M}$  of  $\text{Mg}^{2+}$ ,  $\text{Ca}^+$ ,  $\text{Al}^{3+}$ ,  $\text{Cl}^-$ .

### 2.14 The investigation of the remained bromide in residues by X-ray fluorescence spectrometry (XRF)

The composite rice sample (2.0000 g) was weighted in a nickel crucible and spiked with 100, 200, 400 and 800  $\mu\text{L}$  of 12,500  $\text{mg L}^{-1}$  standard  $\text{Br}^-$  solution to obtain the final  $\text{Br}^-$  concentrations of 50, 100, 200 and 400  $\text{mg L}^{-1}$  in sample solution. After that, these samples were digested and thermally decomposed to an ash as method in section 2.10.3.1. The ash samples were then dissolved with ultrapure water and adjusted pH to 8 with 1 M nitric acid. The resulting sample solution was analyzed by X-ray fluorescence spectrometry (XRF).

## **2.15 Application of the developed sensor to rice samples**

### **2.15.1 Sample collection**

Five brands of white rice samples were bought from the supermarket in Hat Yai, Songkhla province, Thailand and analyzed to quantify concentration of Br<sup>-</sup>.

### **2.15.2 The determination of Br<sup>-</sup> in rice samples with developed sensor**

#### **2.15.2.1 Overall sample preparation**

The rice sample (100 g) was ground by using Ball mill to obtain approximately ~5 μm powder sample and stored in a freezer at -22 °C when not in use

Rice powder (2.0000 g) was weighted in a 50 mL nickel crucible and 5 mL of 1% potassium hydroxide in 50% ethanol was added. The sample was boiled on hotplate by gradually increasing heating rate to avoid the sample bumping until sample were dried and no smoke was observed.

Subsequently, the sample was heated in a muffle furnace at 600 °C for 4 h to eliminate some organic residues. After allowing the ash obtained to be cool down, it was added with 15 mL ultrapure water, boiled for 15 min on hotplate in order to dissolve inorganic bromide and filtered with 0.2 μm nylon membrane filter through a 25 mL volumetric flask. The ash residue in a nickel crucible was again boiled by adding other 10 mL of ultrapure water. This new solution was filtered through a previous volumetric flask and made volume to 25 mL with ultrapure water. The sample solution was then 1 fold diluted with ultrapure water before color reaction.

#### **2.15.2.2 Colorimetric detection of Br<sup>-</sup> in samples**

The standard addition method was used for quantification of Br<sup>-</sup> in samples. The sample solution were added with Br<sup>-</sup> at 0.00, 0.05, 0.10 and 0.20 mg kg<sup>-1</sup> (equal to 0.00, 0.63, 1.25 and 2.50 μM Br<sup>-</sup>). A volume of 500 μL of 5.52 nM AuNPs, 100 μL ultrapure water, 500 μL of 10 mM phosphate buffer (pH 6.5), 100 μL of standard Br<sup>-</sup> or sample and 100 μL of 57.70 μM Cr<sup>3+</sup> solutions were added into a microtube, respectively. The mixture was immediately vortex mixed and left at room temperature for 10 min before measurement by UV-Visible spectrophotometry and the photograph was taken by digital camera. Moreover, the color of solution was observed by naked eyes.

The standard color chart was performed to screen the corresponding colorimetric results which by adding Br<sup>-</sup> standard ranged from 0.00, 6.25, 12.50, 18.75 and 50.00 mg kg<sup>-1</sup> in sample.

### **2.15.3 Confirmation of Br<sup>-</sup> detected by developed sensor with ion chromatography**

Bromine ion in the sample solutions prepared according to the method as mentioned in section 2.15.2.1 was determined with the conditions of ion chromatography as follows:

Column: Metrosep A Supp 5 - 100/4.0 mm.

Mobile phase: 4.6 mM Na<sub>2</sub>CO<sub>3</sub> + 1.3 mM NaHCO<sub>3</sub> + 5% Acetone

Flow rate: 0.80 mL min<sup>-1</sup>

Temperature: 30 °C

Pressure: 5.91 MPa

Detection: Conductivity detector

### **2.16 Statistics**

All the statistical analyses were performed using Microsoft Office Excel 2007. One-way ANOVA at the 95% confidence level was used for data analysis.



## CHAPTER 3

### RESULT AND DISCUSSION

The colorimetric sensor for facile, sensitive and selective detection of bromide ion in rice samples was developed and based on that bromide ion prevented aggregation of AuNPs which caused by the addition of  $\text{Cr}^{3+}$  to a AuNPs solution. The sensor promoted color of solution changed from blue-to-red corresponding to the concentration of bromide which can be easily observed by naked eyes, and also quantitatively measured by UV-visible spectroscopy.

#### 3.1 The synthesis of gold nanoparticles

The gold nanoparticles (AuNPs) were synthesized *via* the reduction of  $\text{Au}^{3+}$  to  $\text{Au}^0$  by using citrate as a reducing agent and stabilizer of AuNPs (Polte et al., 2010). The AuNPs synthesis was carried out as mentioned in section 2.7.1. The illustration of AuNPs synthesis is shown in Figure 3.1, which the pale clear yellow of gold(III) chloride solution (Figure 3.1a) became colorless (Figure 3.1b), dark blue and deep purple (Figures 3.1c - 3.1e), respectively in a few minute after tri-sodium citrate solution was rapidly injected into the boiling gold(III) chloride solution due to the redox reaction. Finally, it became wine red solution (Figure 3.1f), indicating the formation of citrate capped-gold nanoparticles (Zhou et al., 2014). The wine red solution of colloidal AuNPs demonstrated the surface plasmon resonance (SPR) absorption measured by UV-visible spectrophotometry with the maximum absorbance of SPR spectrum was 1.49 a.u. at the wavelength of 519 nm as shown in Figure 3.2.

The AuNPs concentration was calculated according to Beer's Law (Equation 1.1 in Chapter 1) with an extinction coefficient of  $2.70 \times 10^8 \text{ M}^{-1} \text{ cm}^{-1}$  at  $\sim 520 \text{ nm}$  for  $\sim 13 \text{ nm}$  AuNPs (Liu et al., 2011) (Detailed in Appendix B). The calculated AuNPs concentration was 5.52 nM. In addition, TEM image of AuNPs (Figure 3.3a) was recorded to investigate the size of individual particle by randomness of diameter measurements for 100 particles with ImageJ software to promote the histogram of size distribution of AuNPs (Figure 3.3b) shows the particle size of AuNPs was found to be 12 - 13 nm and the average of particles size was  $13.6 \pm 1.7 \text{ nm}$ . Therefore, all obtained result demonstrated that the synthesis of colloidal AuNPs was successful which was in good agreement to previous reports (Hormozi-Nezhad & Abbasi-Moayed, 2014; Li et al., 2011; Majzik et al., 2010; Zhou et al., 2014).

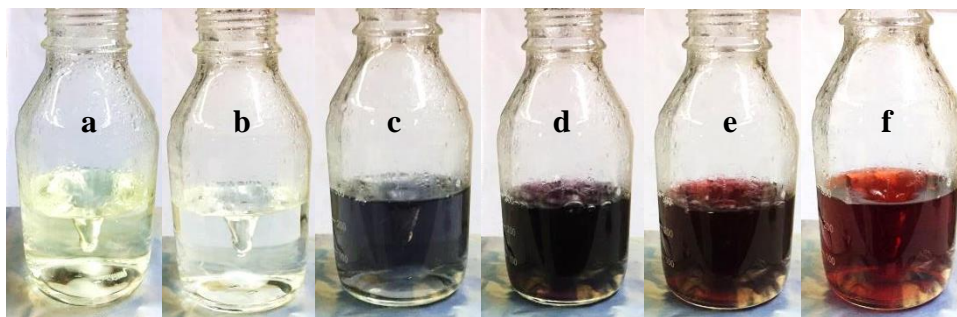


**Figure 3.1** The illustration representing the process of AuNPs synthesis: (a) boiling gold(III) chloride solution, (b) gold(III) chloride solution after addition of tri-sodium citrate, (c- e) the color transition of reaction and (f) synthesized AuNPs.

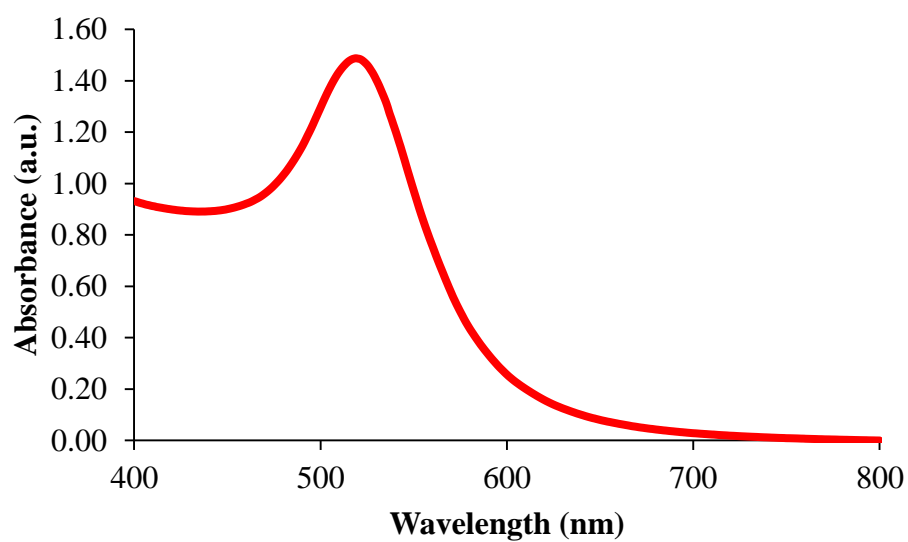


**Figure 3.2** The UV-Vis adsorption spectrum of the surface plasmon resonance phenomena of successfully synthesized AuNPs.

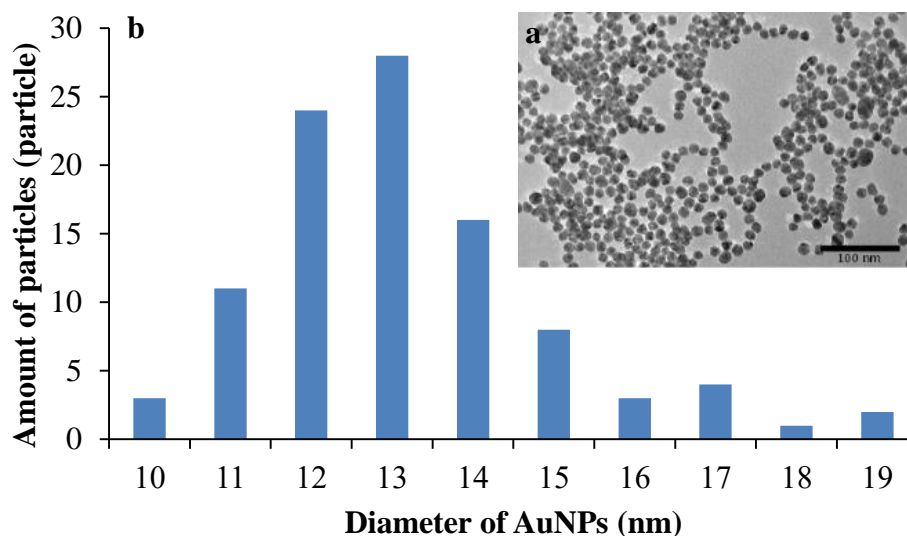


**Figure 3.3** (a) The TEM image of AuNPs with the scale bars of 100 nm. (b) The histograms of 100 particles size.

### 3.2 Proposed sensing mechanism

The illustration of proposed mechanism for the colorimetric sensor of bromide ion ( $\text{Br}^-$ ) detection based on the anti-aggregation of AuNPs is shown in Figure 3.4.

In this study, citrate ion can act as a reductant and a stabilizer of colloidal AuNPs. Thus, the wine red solution of colloidal AuNPs (Figure 3.4a) was relative stable due to the strong electrostatic repulsion between the negatively charged citrate ions on the surface of AuNPs via coordinating interaction of at least one carboxylate group with Au and remaining carboxylate group exposed to solution (Elavarasi et al., 2013; Park & Shumaker-Parry, 2014).

In addition, citrate can be used as the ligand for interaction with  $\text{Cr}^{3+}$  and  $\text{Cr}^{3+}$  can serve as cross linking agent between the pairs of citrate-coated AuNPs (Elavarasi et al., 2013; Wang et al., 2015). It was reported that  $\text{Cr}^{3+}$  could coordinate with citrate ions through carboxylate and hydroxyl groups in each citrate ion with the high formation constant of  $3.89 \times 10^{29}$  (Gabriel et al., 2007; Kornev & Mikryukova, 2004). Therefore, in the presence of  $\text{Cr}^{3+}$  in AuNPs solution,  $\text{Cr}^{3+}$  was able to induce the aggregation of AuNPs *via* the ligand-exchange process between  $\text{Cr}^{3+}$ -citrate complex, meaning that citrate had no longer influence in the stability of AuNPs. This ligand exchange is probably strong enough to overcome the electrostatic repulsion imposed by citrate-AuNPs, thus inducing aggregation of AuNPs (Figure 3.4a) and leading to the blue solution of aggregated AuNPs.

However, the AuNPs treated with  $\text{Br}^-$  followed by mixing with  $\text{Cr}^{3+}$  was still the red color solution. This was caused by the adsorption of  $\text{Br}^-$  on the AuNPs surface, leading to the prevention of aggregation driven by  $\text{Cr}^{3+}$ -citrate complex. This phenomena was called as an anti-aggregation of AuNPs (Figure 3.4b). Bromide ion is a chaotropic anion and can transfer its charge to the AuNPs surface and increase electrostatic stabilization (Pfeiffer et al., 2014).  $\text{Br}^-$  does not directly hinder the coordination between carboxylate group of citrate and  $\text{Cr}^{3+}$  but the adsorption of  $\text{Br}^-$  on surface of AuNPs may prevent the aggregation due to higher stability constant of  $\text{Au}(1+ \text{ or } 3+)-\text{Br}^-$  complex which is 12.3 and 32.8 for  $\text{Au}^+-$  and  $\text{Au}^{3+}-\text{Br}^-$  complex, respectively (Senanayake, 2004) compared to the lower stability constant of  $\text{Cr}^{3+}-\text{Br}^-$  complex (-2.66) (Vinokurov & Bondar, 2003). Therefore,  $\text{Br}^-$  could stabilize AuNPs and enhance the repulsion force between AuNPs that after addition of  $\text{Cr}^{3+}$ , it is difficult for  $\text{Cr}^{3+}$  to form chelation with citrate due to increased repulsion force of each AuNPs. A resultant solution showed the change of AuNPs from aggregation state (blue color) to dispersion state (red color).

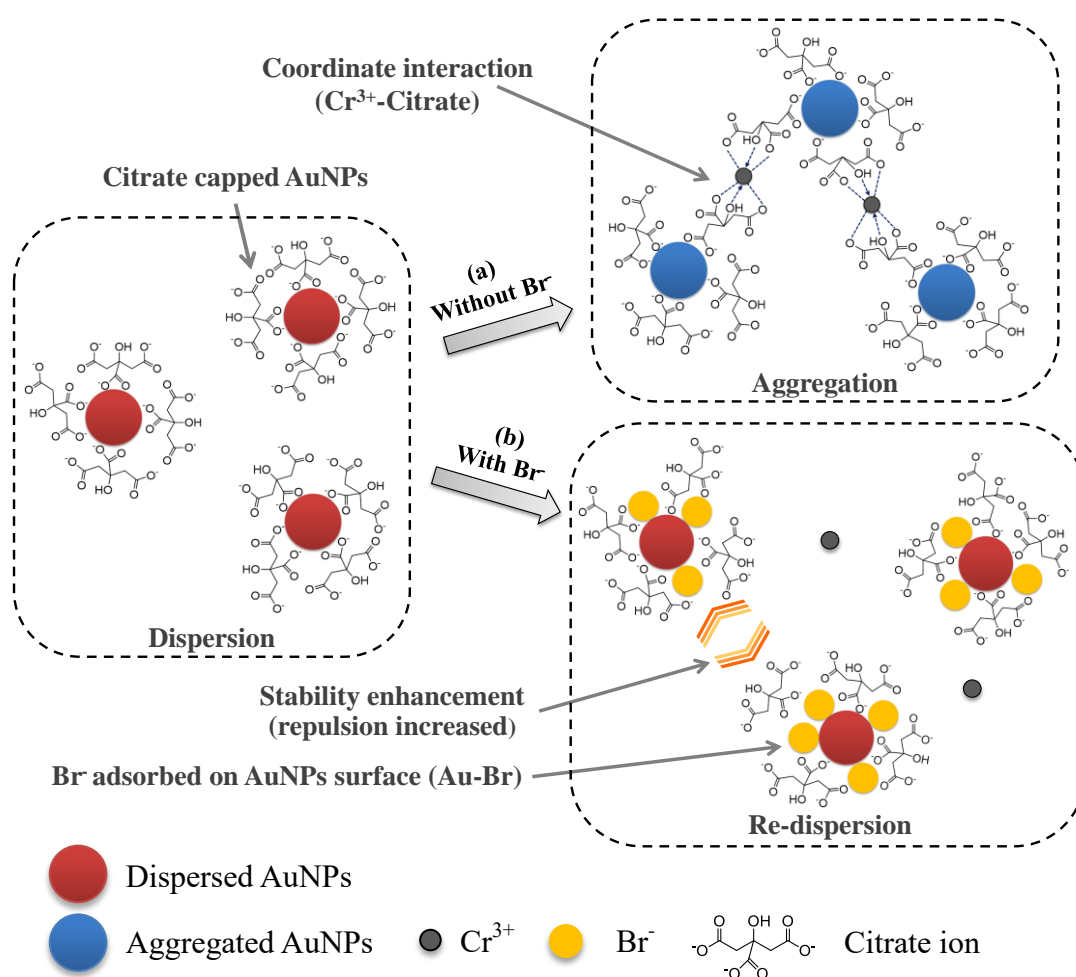


**Figure 3.4** The illustration of proposed mechanism for the colorimetric sensor of  $\text{Br}^-$  detection based on the anti-aggregation of AuNPs.

### 3.3 Characterization of AuNPs particles

#### 3.3.1 The surface plasmon resonance (SPR) of AuNPs

The SPR band of AuNPs, the aggregation of AuNPs and the anti-aggregation of AuNPs are shown in Figure 3.5. The diluted AuNPs solution in buffer demonstrated the maxima SPR absorption at 519 nm (Figure 3.5a) with a wine red color (Figure 3.5A), indicating that AuNPs are well dispersed and stable in this buffer.

Upon addition of  $\text{Cr}^{3+}$ , the intensity of SPR band of AuNPs at 519 nm decreased, and the new maxima absorption band appeared at 673 nm (Figure 3.5b) as a blue color (Figure 3.5B) since the AuNPs aggregation driven by  $\text{Cr}^{3+}$  caused the change of SPR, indicating the successful conjugation of  $\text{Cr}^{3+}$  with AuNPs. This caused red-to-blue color change which was in agreement of a report of Liu and Wang (2013). After addition of  $\text{Cr}^{3+}$ , the color of AuNPs did not change from wine red to blue (Figure 3.5C) because AuNPs was dispersion state which the decreased of SPR absorption band presented at 673 nm and increased band at 519 nm (Figure 3.5c).

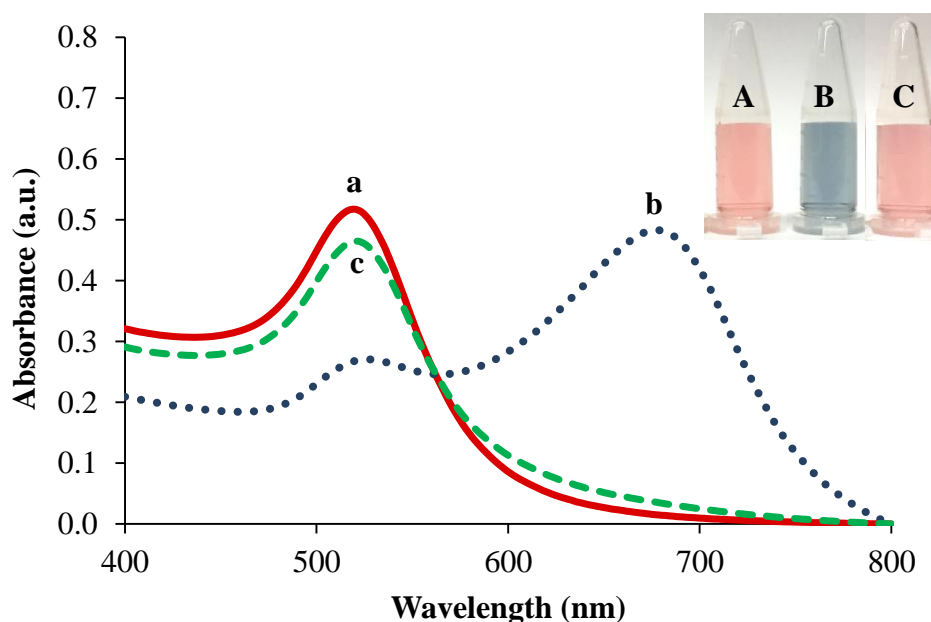


**Figure 3.5** UV-Vis absorption spectra of (a) AuNPs, (b) aggregation of AuNPs in the presence of  $4.80 \mu\text{M Cr}^{3+}$  and (c) anti-aggregation of AuNPs in the presence of  $3.13 \mu\text{M Br}^-$  and  $4.80 \mu\text{M Cr}^{3+}$ . Photographs of A, B and C correspond a, b and c, respectively.

### 3.3.2 The morphology of AuNPs

Figure 3.6 shows the TEM image of AuNPs, the aggregation of AuNPs and the anti-aggregation of AuNPs at the magnitude of 100,000 times. Based on the grid line of TEM pictures, the countable particles were found to be  $5.2 \pm 1.1$ ,  $21.8 \pm 6.2$  and  $9.6 \pm 2.3$  particles/cm<sup>2</sup> for Figure 3.6a, b and c, respectively. Each AuNPs particle before aggregation was spherical mono-disperse colloidal (Figure 3.6a). In the presence of Cr<sup>3+</sup> (Figure 3.6b), the heavy aggregations of AuNPs were observed in appearance of interconnected particles spread almost full area, confirming that Cr<sup>3+</sup> induced large-scaled aggregation of AuNPs through chelating reaction. While in presence of Br<sup>-</sup> and Cr<sup>3+</sup>, AuNPs remained dispersion with the decrease in the size of AuNPs compared to aggregation state (Figure 3.6c). Thus, it suggested the effective anti-aggregation induced by Br<sup>-</sup>.

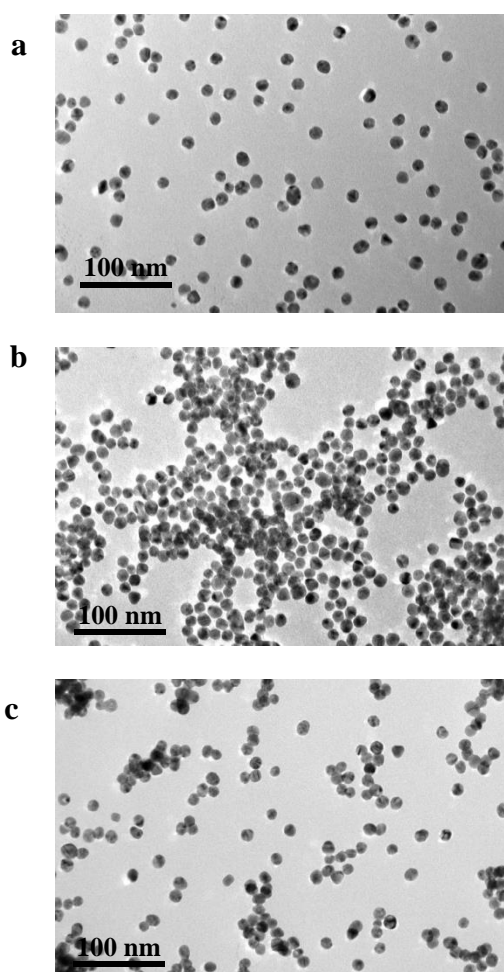


**Figure 3.6** The TEM image of (a) AuNPs, (b) the aggregation of AuNPs in the presence of Cr<sup>3+</sup> and (c) the anti-aggregation of AuNPs in the presence of Br<sup>-</sup> and Cr<sup>3+</sup>.

### 3.3.3 Particles size distribution of AuNPs solution

The particles size distribution of the solution of AuNPs, aggregated AuNPs and anti-aggregated AuNPs is shown in Figure 3.7. The lognormal distribution resultant of effective diameter (ED) of colloidal AuNPs solution demonstrated particles size distribution of  $16.43 \pm 0.81$  nm (Figure 3.7a), which was consistent with the histogram of particles size in section 3.1 at average particles size of  $13.6 \pm 1.7$  nm. This indicated that the successful synthesized of colloidal AuNPs. the AuNPs in the presence of  $\text{Cr}^{3+}$  demonstrated the clearly change of particles size distribution at  $262.30 \pm 4.07$  nm (Figure 3.7b) which was around 16 times of AuNPs without  $\text{Cr}^{3+}$ . Thus, the AuNPs was aggregated by  $\text{Cr}^{3+}$ , leading to the increased of particle size. However the anti-aggregation of AuNPs in the presence of  $\text{Br}^-$  and  $\text{Cr}^{3+}$  demonstrated particles size distribution of  $29.37 \pm 2.56$  nm (Figure 3.7c) which was close to particle size distribution of colloidal AuNPs solution. This demonstrated that the mixture were remained dispersed AuNPs, thus suggesting the effective anti-aggregation induced by  $\text{Br}^-$ .

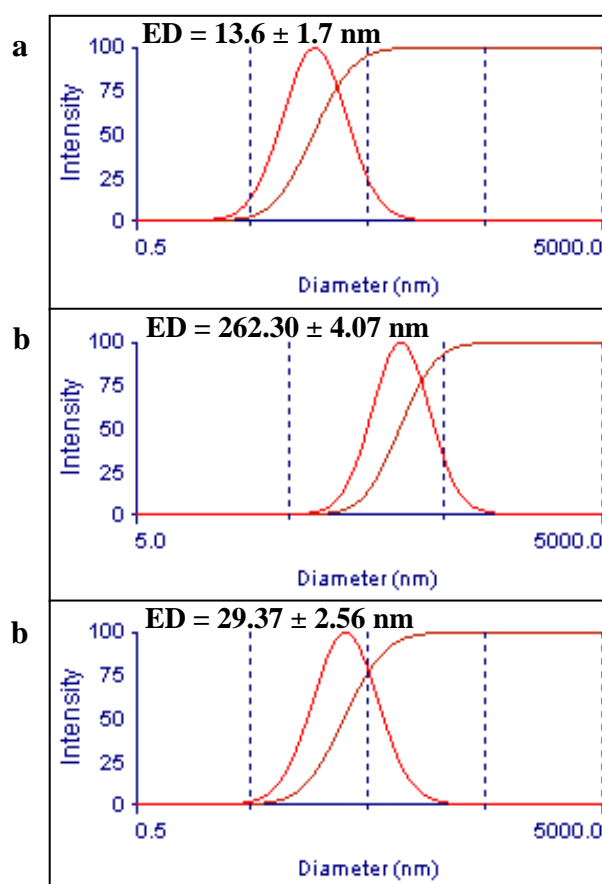


**Figure 3.7** Lognormal distribution diagram of effective diameter (ED) of (a) AuNPs, (b) the aggregation of AuNPs in the presence of  $\text{Cr}^{3+}$  and (c) the anti-aggregation of AuNPs in the presence of  $\text{Br}^-$  and  $\text{Cr}^{3+}$ .

### 3.3.4 Zeta potential of AuNPs

The colloids with high zeta potential (negative or positive) are electrically stabilized due to increased electrostatic repulsion that can inhibit agglomeration and settling, while colloids with low zeta potentials as close to 0 tend to coagulate or flocculate (Hanaor et al., 2012).

In this study, the bromide ion effect adsorbed on the AuNPs surface caused the increase electrostatic stabilization which could be proved by the zeta potential values of AuNPs without  $\text{Br}^-$  and after addition of 0.63, 2.50 and 4.38  $\mu\text{M}$   $\text{Br}^-$ . The results are shown in Figure 3.8. The zeta potential of AuNPs surface demonstrated negative value, indicating that citrate ion covered on the surface of AuNPs (Brewer et al., 2005). The zeta potential values in the presence of  $\text{Br}^-$  were found increased significantly when concentration of  $\text{Br}^-$  increased ( $p < 0.05$ ). This can also indicated that colloidal AuNPs has more electrical stability.

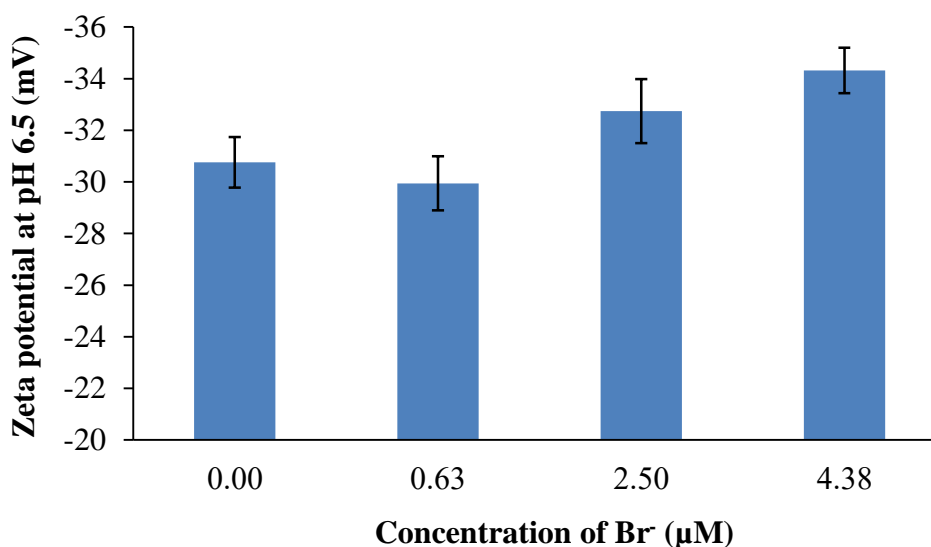


**Figure 3.8** The zeta potential value at pH 6.5 of AuNPs without  $\text{Br}^-$  and after addition of 0.63, 2.50 and 4.38  $\mu\text{M}$   $\text{Br}^-$ .

### 3.3.5 The stability of AuNPs

The stability of synthesized AuNPs was investigated by recording the SPR spectrum of pure AuNPs solution from 1 day after synthesis until 4 months for every week. Figure 3.9a shows the maximum absorbance at 519 nm of pure AuNPs solution with an average absorbance of  $1.49 \pm 0.01$ . It was found that no significant differences of measured absorbance during studied period were observed ( $p > 0.05$ ). This



demonstrated that the synthesized AuNPs can be kept in refrigerator up to 4 months without any loss of sensitivity.

In addition, the stability of stored AuNPs to detect of  $2.50 \mu\text{M Br}^-$  was investigated. The sensitivity of  $\text{Br}^-$  detection represented as the absorbance intensity ratio of  $A_{519}/A_{673}$  was recorded in total of 8 times during 4 months as shown in Figure 3.9b. It resulted that the sensitivity remained stable with no significant difference of the absorbance ratio between 8 measurements in 4 months ( $p > 0.05$ ). Thus, it was proved that the stability of AuNPs after several days for  $\text{Br}^-$  detection can be last at least 4 months.

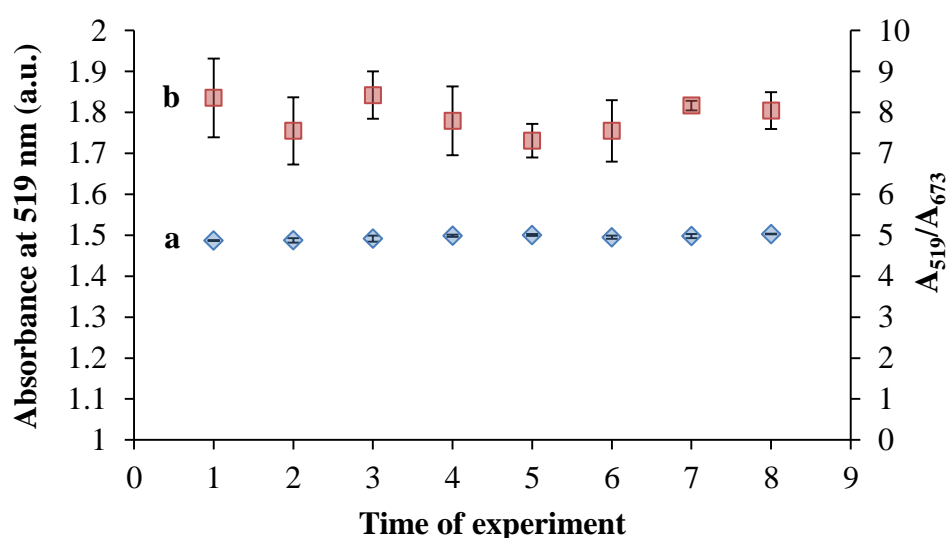


**Figure 3.9** (a) The absorbance intensity at 519 nm of pure AuNPs solution for each week at interval of 2 weeks. (b) The absorbance ratio ( $A_{519}/A_{673}$ ) of  $2.50 \mu\text{M Br}^-$  after using the synthesized AuNPs suspension stored in the dark at  $4^\circ\text{C}$  in 4 months.

### 3.4 Optimization of parameters affecting the detection of bromide

#### 3.4.1 Concentrations of $\text{Cr}^{3+}$

The effect of different concentrations of  $\text{Cr}^{3+}$  in the range of 0.96, 2.40, 4.81, 7.21, 9.62, 14.42 and  $19.23 \mu\text{M}$  was investigated to obtain the lowest amount of  $\text{Cr}^{3+}$  that can provide the completed AuNPs aggregation. When increasing concentration of  $\text{Cr}^{3+}$ , the color of the suspension gradually changed from wine red to purple and finally to blue (Figure 3.10, inset), corresponding to the UV-Vis absorption spectra (Figure A1) which the absorbance at 519 nm decreased and the absorbance at 673 nm

increased gradually. This indicated a disruption of stability of citrate capped AuNPs. Initially, at concentration of  $0.96 \mu\text{M Cr}^{3+}$ , the aggregation of AuNPs was negligible since the excess amounts of AuNPs provided a large number of binding sites and better affinity for citrate ion over  $\text{Cr}^{3+}$  (Liu & Wang, 2013). At concentration between  $2.40 - 4.81 \mu\text{M Cr}^{3+}$ , the aggregation was enhanced that can be seen from purple to blue solution. This may be attributed to that binding sites of citrate ion on the surface of AuNPs were occupied by  $\text{Cr}^{3+}$ , leading to aggregation. These results revealed the rapid decrease in the absorbance intensity ratio of  $A_{519}/A_{673}$  of  $0.96 - 4.81 \mu\text{M Cr}^{3+}$  as shown in Figure 3.10. At the concentration of  $\text{Cr}^{3+}$  higher than  $4.81 \mu\text{M}$ , the ratio became stable, indicating the maximum degree of aggregation. When considering to the lowest concentration of  $\text{Cr}^{3+}$  that provided the maximum degree of aggregation,  $4.81 \mu\text{M Cr}^{3+}$  was chosen for optimal concentration.

Although  $\text{Cr}^{3+}$  is a toxic substance, it is considered as an essential trace element and is less toxic than  $\text{Cr}^{6+}$  since  $\text{Cr}^{6+}$  has high solubility and mobility in biological systems (Shrivastava et al., 2016). The selected concentration of  $\text{Cr}^{3+}$  that is equal to  $4.81 \mu\text{M}$  or  $5.76 \text{ nmol Cr}^{3+}$  was very low when used in one test. Compared to the Chemical Oxygen Demand (COD) test using  $\text{K}_2\text{Cr}_2\text{O}_7$  ( $\text{Cr}^{6+}$ ) as a reagent and releasing  $\text{Cr}^{3+}$  as a product ( $240,268.32 \text{ nmol/test}$ ),  $\text{Cr}^{3+}$  used in our method was up to 40,000 times much lower than COD test (U.S. EPA, 1978), indicating that the use of  $\text{Cr}^{3+}$  for developed sensor was more environmental friendly.

Moreover, other non-toxic substances such as  $\text{Fe}^{3+}$  and  $\text{Al}^{3+}$  used as aggregation reagents was investigated as shown in Figure A2. It showed that at the same concentration of ions,  $\text{Cr}^{3+}$  provided heavy aggregation of citrate-stabilized gold nanoparticles but  $\text{Fe}^{3+}$  and  $\text{Al}^{3+}$  did not aggregate AuNPs. The optimization of pH of phosphate buffer ranging from 6.0 - 8.0 in the presence of  $\text{Cr}^{3+}$ ,  $\text{Fe}^{3+}$  and  $\text{Al}^{3+}$  was also carried out (Figure A3). Only  $\text{Cr}^{3+}$  gave response of the aggregation of AuNPs. These two investigations confirmed that  $\text{Cr}^{3+}$  is more specific for  $\text{Br}^-$  detection than other aggregation reagent ions ( $\text{Fe}^{3+}$  and  $\text{Al}^{3+}$ ).

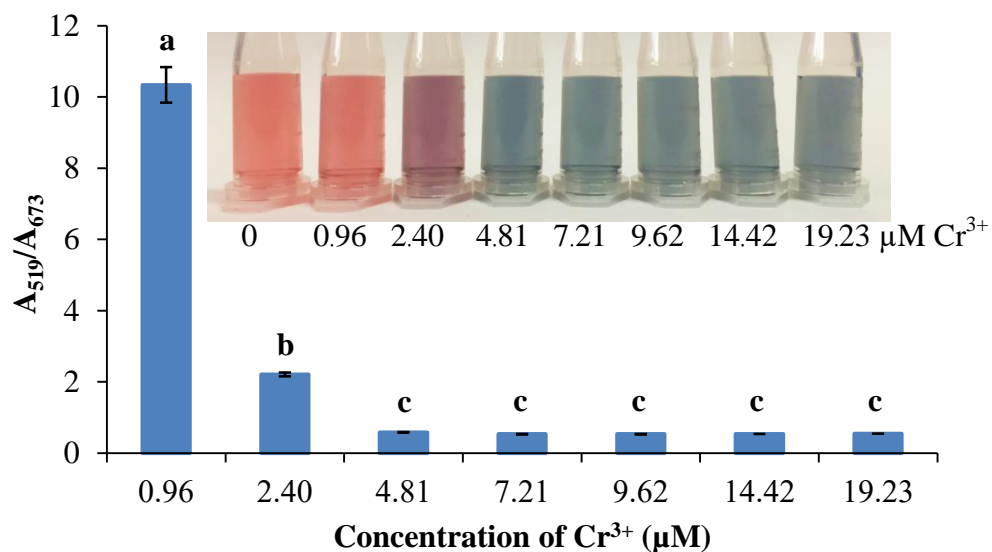


**Figure 3.10** The absorbance ratio of  $A_{519}/A_{673}$  on the various concentration of  $\text{Cr}^{3+}$ . Condition: 500  $\mu\text{L}$  of 5.52 nM AuNPs, 500  $\mu\text{L}$  of 10 mM phosphate buffer (pH 7.0), 100  $\mu\text{L}$  of  $\text{Cr}^{3+}$ , total volume of 1200  $\mu\text{L}$  and 10 min of reaction time. Inset shows color solution of AuNPs depending on the concentration of  $\text{Cr}^{3+}$ . The bars showing different letter are significantly different at  $p > 0.05$ .

### 3.4.2 pH of solution

The pH of solution could affect the anti-aggregation system between  $\text{Br}^-$  and AuNPs, thus, it influenced the  $A_{519}/A_{673}$  ratio. The phosphate buffer was chosen due to highly soluble in water and high buffering capacity in the studied range. The effect of phosphate buffer pH values (6.0, 6.3, 6.5, 7.0 and 7.5) onto the sensitivity of  $\text{Br}^-$  concentration ranged from 0.63 - 5.01  $\mu\text{M}$  was investigated (Figure 3.11). The sensitivity value obtained from the slope of linearity plotted from between  $A_{519}/A_{673}$  ratio (y axis) and  $\text{Br}^-$  concentration (x axis) as shown in Figure A4 are presented in Figure 3.11, with the summarized linear equation and the coefficient of determination ( $R^2$ ) of each pH in Table A1. The corresponding solution color affected by various pH was changed from blue to red as shown Figure A5.

The result presented that the sensitivity of bromide detection increased when pH of buffer increased from 6.0 to 6.5 (Figure 3.11). It is known that the  $\text{pK}_{a1}$ ,  $\text{pK}_{a2}$  and  $\text{pK}_{a3}$  values of citric acid are 3.2, 4.8 and 6.4, respectively (Chen et al., 2014; Kornev & Mikryukova, 2004). When pH value was lower than 6.4, citric acid group had high ability with  $\text{H}^+$ , resulting in the reduction of chelation interaction between

citrate ion and  $\text{Cr}^{3+}$ . This influenced the aggregation process, as a result, the decrease in sensitivity was observed.

In case of pH 6.5 (close to  $\text{pK}_{a3}$ ), citric acid was existed in trivalent anion which has the highest ability to chelate  $\text{Cr}^{3+}$  (Gabriel et al., 2007). This pH resulted the increase in affinity of chelation between citrate ion and  $\text{Cr}^{3+}$ . Therefore, high aggregation will lead to high anti-aggregation process in the studied concentration range of  $\text{Br}^-$  and then maximize sensitivity.

When pH increased from 7.0 - 7.5, the sensitivity was decreased because hydrolysis of  $\text{Cr}^{3+}$  is probably occurred, resulting in the formation of colloidal  $\text{Cr}(\text{OH})_3$  that could destroyed chelating reaction citrate capped-AuNPs with  $\text{Cr}^{3+}$  (Chen et al., 2014; Spiccia & Marty, 1986; Wang et al., 2015). Other possible reason was that interaction of Au-Br was broken down to form Au-OH (Pesic & Sergent, 1993) and  $\text{Br}^-$  was likely to be dispersed in the alkaline environment of solution rather than adsorption on the AuNPs surface. To obtain the maximum response of detection, a phosphate buffer of pH 6.5 was chosen.

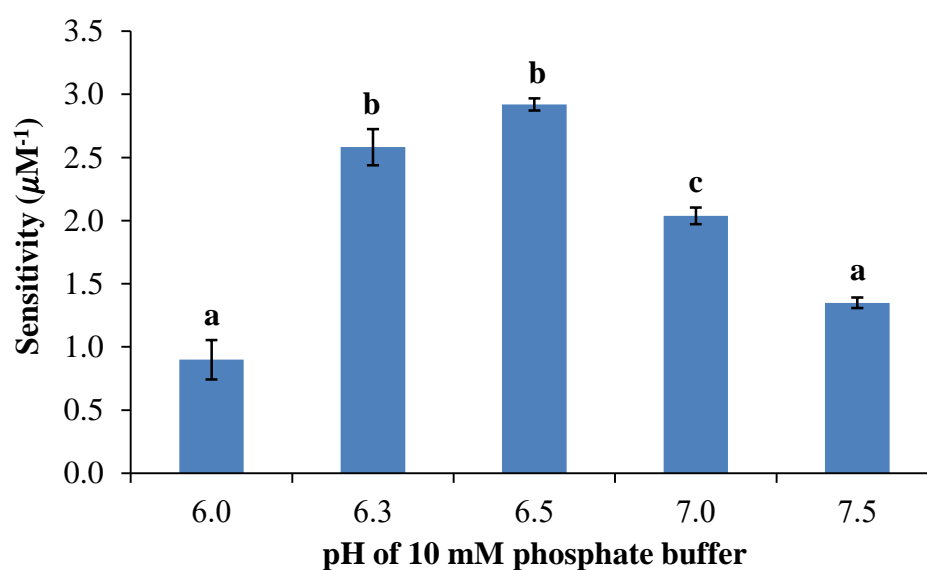


**Figure 3.11** The effect of phosphate buffer pH on the sensitivity of  $\text{Br}^-$  concentration ranged from 0.63 - 5.01  $\mu\text{M}$ . Condition: 500  $\mu\text{L}$  of 5.52 nM AuNPs, 500  $\mu\text{L}$  of 10 mM phosphate buffer, 100  $\mu\text{L}$  of  $\text{Br}^-$ , 100  $\mu\text{L}$  of 57.70  $\mu\text{M}$   $\text{Cr}^{3+}$  and 10 min of reaction time. The bars showing different letter are significantly different at  $p > 0.05$ .

### 3.4.3 Concentrations of phosphate buffer

The influence of concentrations of phosphate buffer (pH 6.5) including 2.5, 5.0, 7.5, 10.0 and 25.0 mM on the aggregation and anti-aggregation of AuNPs was performed by recording the change of intensity ratio of anti-aggregation signal by analyte and aggregation signal by  $\text{Cr}^{3+}$  as shown in Figure 3.12 with all signals obtained were demonstrated in Figure A6. Liu and Wang mentioned that citrate-capped AuNPs would aggregate in aqueous media with high ionic strength (Liu & Wang, 2013). In this study, the maximum tolerable ionic strength is found to be 10.0 mM since the maximum sensitivity was obtained. The result presented that a buffer concentration of 25.0 mM led to increase of much ionic strength which could disturb anti-aggregation to decrease and thus, the intensity ratio was decreased. Considering of the maximal ratio between signal of analyte and blank, thus, 10.0 mM phosphate buffer (pH 6.5) was chosen for next experiment.

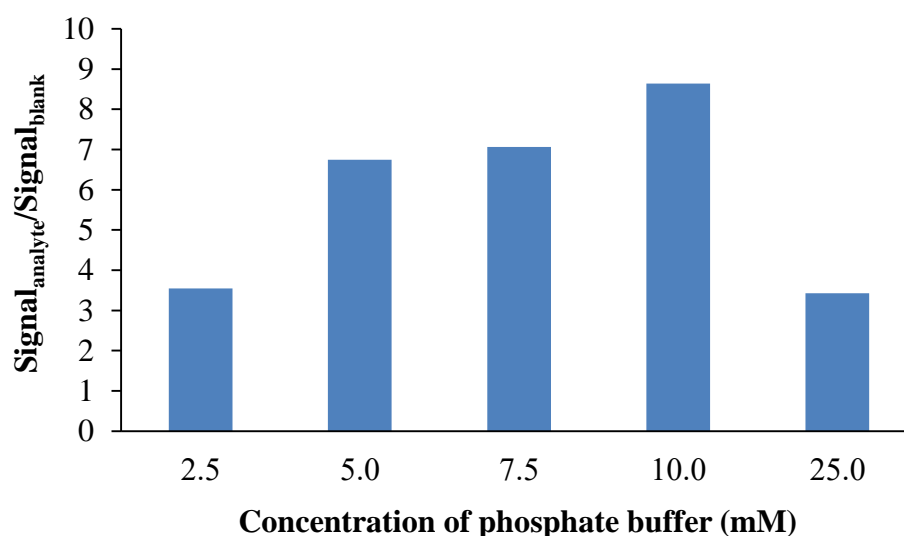


**Figure 3.12** The influence of concentrations of phosphate buffer (pH 6.5) on the aggregation and anti-aggregation of AuNPs. Condition: 500  $\mu\text{L}$  of 5.52 nM AuNPs, 500  $\mu\text{L}$  of phosphate buffer pH 6.5, 100  $\mu\text{L}$  of 30.04  $\mu\text{M}$   $\text{Br}^-$  for signal<sub>analyte</sub> or 100  $\mu\text{L}$  of ultrapure water for signal<sub>blank</sub>, 100  $\mu\text{L}$  of 57.70  $\mu\text{M}$   $\text{Cr}^{3+}$  and 10 min for reaction time.

### 3.4.4 Concentrations of AuNPs

The amount of AuNPs is relative to adsorption of bromide ion onto the AuNPs surface. If concentration of AuNPs increases, it is necessary to increase amount of  $\text{Br}^-$

to allow the anti-aggregation of AuNPs. Therefore, the different final concentrations of AuNPs including 1.38, 1.83, 2.29, 2.75 and 3.21 nM were performed to obtain the maximum sensitivity of  $\text{Br}^-$  concentration in the range of 0.63 - 2.50  $\mu\text{M}$  (Figure 3.13). The sensitivity value were the slope of linearity between the ratio of  $A_{519}/A_{673}$  and  $\text{Br}^-$  concentration and the summarize of these linear equations with the coefficient of determination ( $R^2$ ) are presented in Figure A7 and Table A2, respectively, together with the solution color corresponding to linearity in Figure A8. When AuNPs concentration was 1.38 nM, it was difficult to observe color of solution by naked eye due to its fade color. The sensitivity increased to be highest in case of 1.83 nM AuNPs and decreased when the concentrations above 1.8 nM because insufficient  $\text{Br}^-$  was adsorbed on high abundance of AuNPs, leading to low anti-aggregation. Therefore, 1.83 nM AuNPs was chosen.

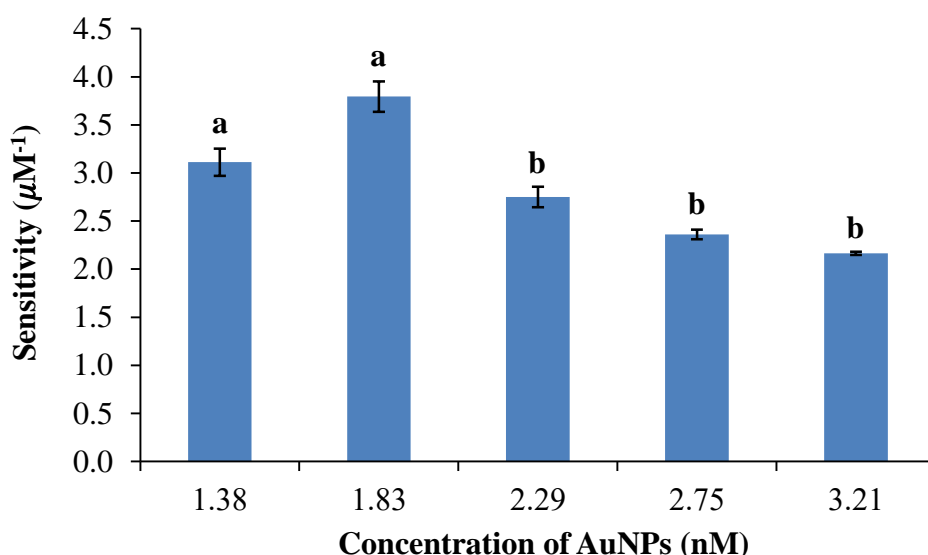


**Figure 3.13** The effect of AuNPs concentrations on the sensitivity of  $\text{Br}^-$  concentration range from 0.63 - 2.50  $\mu\text{M}$ . Condition: 300 - 700  $\mu\text{L}$  of 5.52 nM AuNPs, 250  $\mu\text{L}$  of 20 mM total volume of 1200  $\mu\text{L}$  and 10 min of reaction time. The bars showing different letter are significantly different at  $p > 0.05$ .

### 3.4.5 Reaction time

The influence of reaction time for anti-aggregation kinetics was investigated in range from 0 - 30 min at an interval of 2 min upon the interaction between AuNPs and  $\text{Br}^-$  concentration of 1.25, 2.50 and 5.01  $\mu\text{M}$  (Figure 3.14). It can be seen that the absorption intensity ratio ( $A_{519}/A_{673}$ ) of blank and low concentration of  $\text{Br}^-$  (1.25  $\mu\text{M}$ )

provided a low value due to rapid crosslink process of AuNPs by  $\text{Cr}^{3+}$ . In the presence of more concentration of  $\text{Br}^-$  ( $2.50 \mu\text{M}$ ), the ratio of  $A_{519}/A_{673}$  tended to decrease from 0 to 10 min and then was constant from 10 to 30 min, indicating that the anti-aggregation was complete at 10 min reaction time. This may be the interaction between  $\text{Br}^-$  and  $\text{Cr}^{3+}$  ion the surface and binding sites remaining of AuNPs. However, the ratio of  $A_{519}/A_{673}$  was stable from 2 min at the high amount of  $\text{Br}^-$  ( $5.01 \mu\text{M}$ ) due to the excess  $\text{Br}^-$  coated on AuNPs surface completely. Thus, the reaction of 10 min was chosen and all further sensor measurements can be carried out within 10 min.

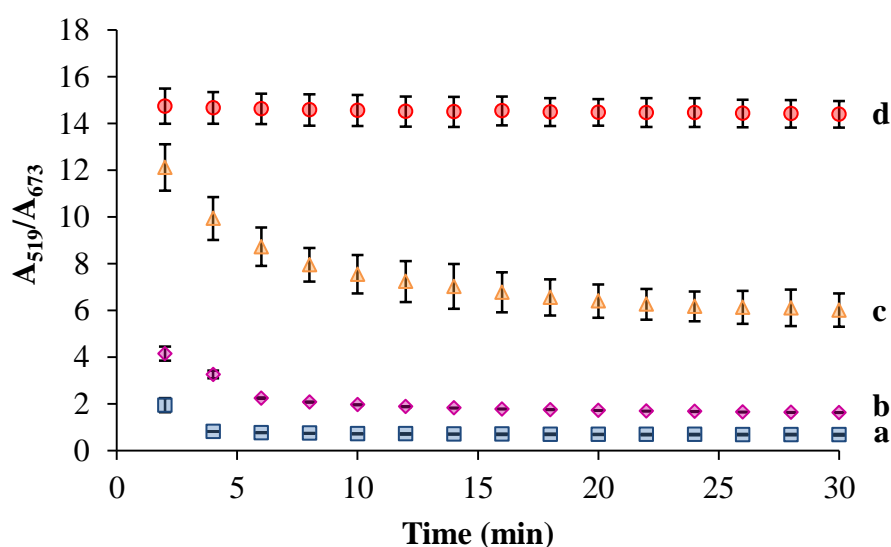


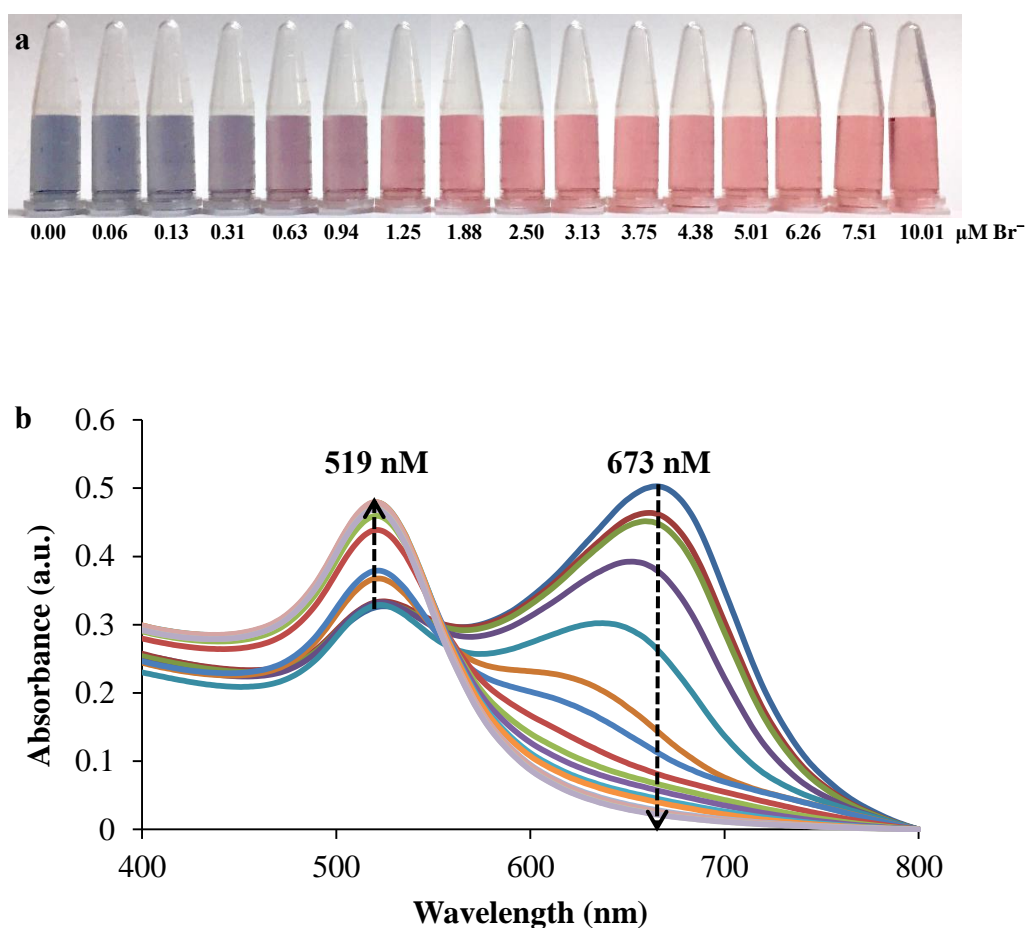
**Figure 3.14** The reaction time of (a) blank (without  $\text{Br}^-$ ), (b)  $1.25 \mu\text{M}$   $\text{Br}^-$ , (c)  $2.50 \mu\text{M}$   $\text{Br}^-$  and (d)  $5.01 \mu\text{M}$   $\text{Br}^-$ . Condition:  $400 \mu\text{L}$  of  $5.52 \text{ nM}$  AuNPs,  $500 \mu\text{L}$  of  $10 \text{ mM}$  phosphate buffer,  $100 \mu\text{L}$  of  $\text{Br}^-$ ,  $100 \mu\text{L}$  of  $57.70 \mu\text{M}$   $\text{Cr}^{3+}$ , total of  $1200 \mu\text{L}$  and 2-30 min of reaction time.

### 3.5 Method validations

#### 3.5.1 Linearity

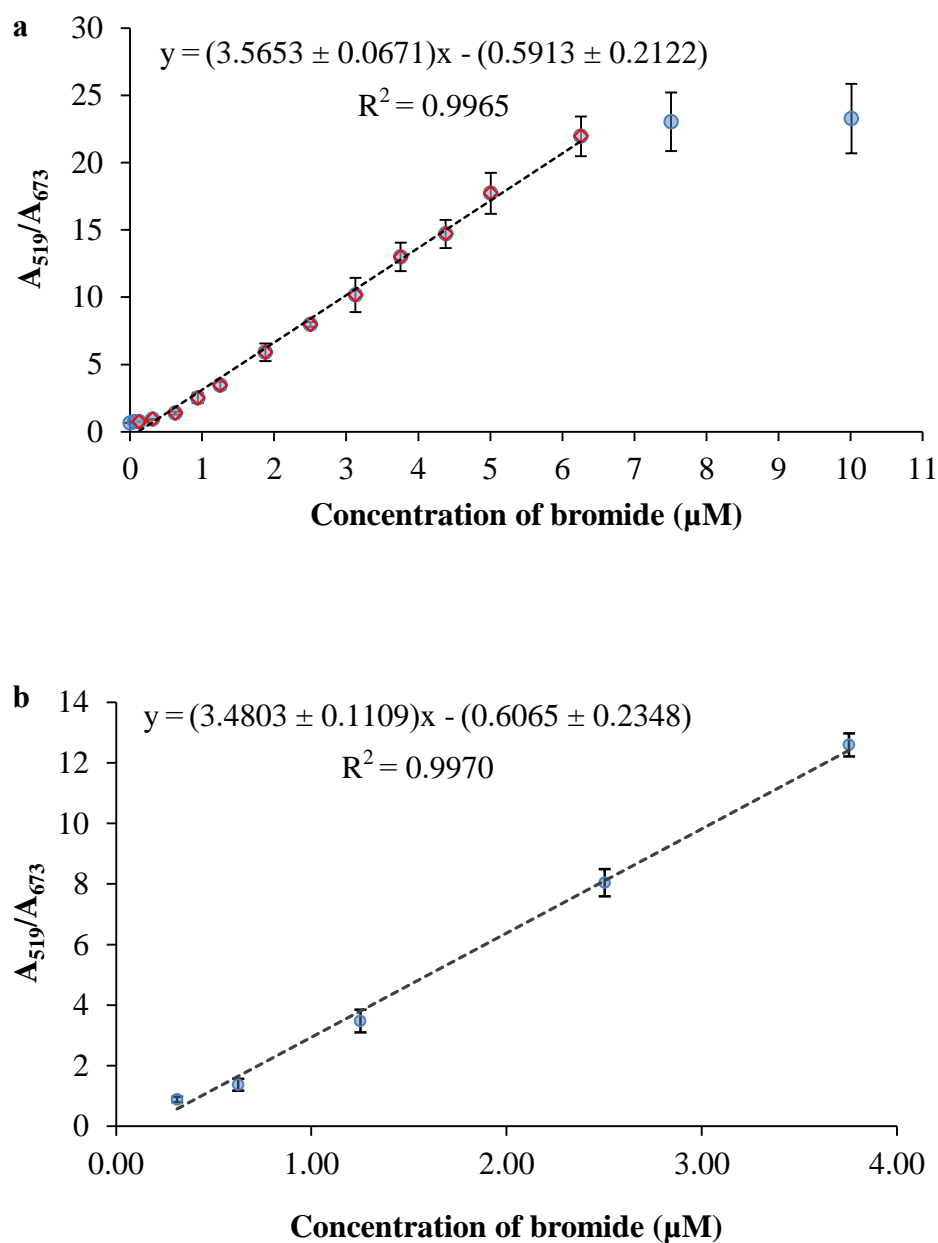
The concentration of  $\text{Br}^-$  ( $0.06, 0.13, 0.31, 0.63, 0.94, 1.25, 1.88, 2.50, 3.13, 3.75, 4.38, 5.01, 6.26, 7.51$  and  $10.01 \mu\text{M}$ ) were used to obtain the degree of anti-aggregation which the color of solutions changed gradually from blue to purple and to red depending on the increase of  $\text{Br}^-$  concentration (Figure 3.15a). The UV-visible absorption change corresponding to color changes is shown in Figure 3.15b, which the absorbance at  $673$  decreased and the peak at  $519 \text{ nm}$  increased due to anti-aggregation of AuNPs with increasing concentration of  $\text{Br}^-$ .

Figure 3.16a shows the correlation plot between the absorption intensity ratio of  $A_{519}/A_{673}$  and various concentration of  $\text{Br}^-$ . It was found that when  $\text{Br}^-$  increased, the absorption intensity ratio increase until the concentration of  $\text{Br}^-$  above  $6.26 \mu\text{M}$ , the ratio was constant. The linearity response of developed sensor based on UV-Vis measurement was in the range of  $0.13 - 6.26 \mu\text{M Br}^-$  ( $n = 3$ ) with a linear equation of  $y = (3.5653 \pm 0.0671)x - (0.5913 \pm 0.2122)$  and a coefficient of determination ( $R^2$ ) of  $0.9965 \pm 0.4463$ . Based on the color transition observed by naked eye from blank until constant color of solution, a good linearity of standard calibration curve was in the range of  $0.31 - 3.75 \mu\text{M Br}^-$  ( $k = 3, n = 3$ ) with a linear equation of  $y = (3.4803 \pm 0.1109)x - (0.6065 \pm 0.2348)$  and a coefficient of determination ( $R^2$ ) of  $0.9970 \pm 0.3165$  as shown in Figure 3.16b.



**Figure 3.15** (a) Color solution of AuNPs depends on the concentration of  $\text{Br}^-$  under the optimum condition of  $400 \mu\text{L}$  of  $5.52 \text{ nM AuNPs}$ ,  $250 \mu\text{L}$  of  $20 \text{ mM phosphate buffer}$ ,  $100 \mu\text{L}$  of  $\text{Br}^-$ ,  $100 \mu\text{L}$  of  $57.70 \mu\text{M Cr}^{3+}$  and  $10 \text{ min}$  of reaction time. (b) UV-Vis absorption spectra of AuNPs relating to the different concentration of  $\text{Br}^-$ .





**Figure 3.16** The correlation plot between the absorption intensity ratio of  $A_{519}/A_{673}$  and various concentration of  $\text{Br}^-$  (a) with the linear response of developed sensor in the range of 0.13 - 6.26  $\mu\text{M}$   $\text{Br}^-$  ( $n = 3$ ) and (b) with the linear calibration curve in the range of 0.31 - 3.75  $\mu\text{M}$   $\text{Br}^-$  ( $k = 3$ ,  $n = 3$ ).

### 3.5.2 Limit of detection (LOD) and limit of quantification (LOQ)

The limit of detection (LOD) and limit of quantification (LOQ) were the concentrations of  $\text{Br}^-$  that gave a signal equal to the blank signal (S/N) plus three and ten standard deviation of blank signal ( $n = 20$ ), respectively (Miller & Miller, 2015). The calculation of LOD and LOQ was performed according to equation 1.3 (chapter 1) with the mean and the standard deviation ( $n = 20$ ) of 0.6021 ( $y_B$ ) and 0.0446 ( $S_B$ ), respectively (Table A3). Under the linear equation of standard calibration curve of  $y = 3.5653x - 0.5913$ , LOD and LOQ was down to 0.04 and 0.13  $\mu\text{M}$ , respectively and limit of detection based on naked eye was found to be 0.31  $\mu\text{M}$ .

### 3.5.3 Matrix effect

In contrast to aqueous standard solution, trace quantification of analyte in real samples can suffer from the sample matrices which can cause a positive or negative response by increasing background noise or suppressing the signal response (Rujiralai et al., 2014). Hence, the matrix effect was investigated by using a standard addition curve (Figure 3.17a) in the range of 0.31 - 3.75  $\mu\text{M}$   $\text{Br}^-$  spiked into composite rice samples solution (final solution) compared to a standard calibration curve (Figure 3.17b).

As shown in Figure 3.17, the sensitivity of a standard addition curve (a) was significantly different from that of a standard curve (b) ( $p < 0.05$ ), indicating that the matrix had effect on the analysis of  $\text{Br}^-$  in rice samples. Therefore, the standard addition curve was used for accurate determination of  $\text{Br}^-$  in rice samples.

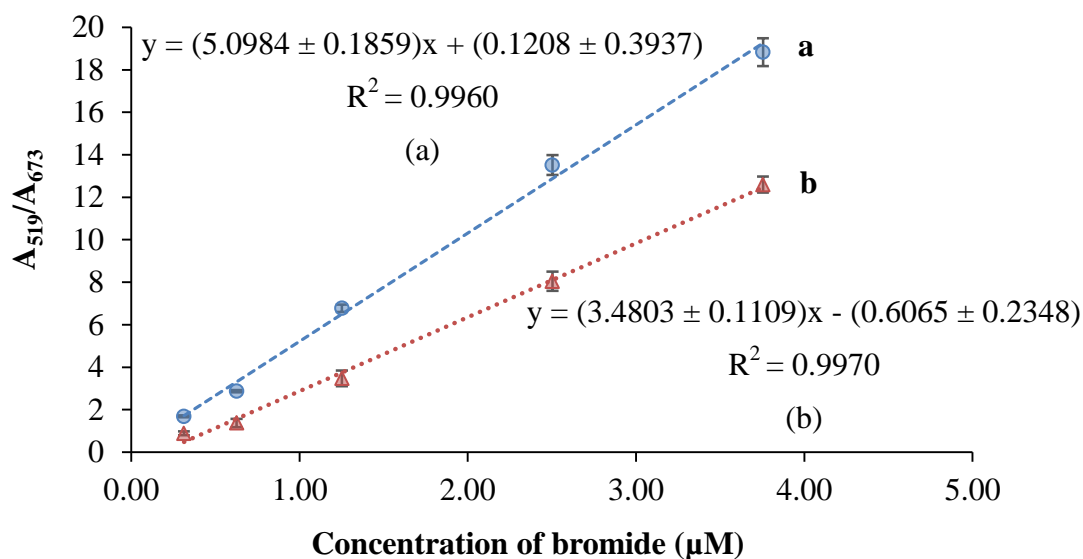


**Figure 3.17** Curves of (a) the standard addition curve and (b) the standard calibration curve for  $\text{Br}^-$  concentration ranging of 0.31 - 3.75  $\mu\text{M}$ .

### 3.5.4 Accuracy

The recovery was investigated by spiking the  $\text{Br}^-$  concentrations of 12, 25, 50 and 60  $\text{mg kg}^{-1}$  into composite rice samples and determining using our developed system. As seen in Table 3.1, good recoveries ranging from 79.9 - 92.2% was obtained with precisions (RSD) less than 4.0% ( $n = 3$ ). These recoveries were acceptable according to standard recovery of 80 - 110% reported by AOAC standard method for the analyte concentration range 100  $\mu\text{g kg}^{-1}$  to < 100  $\text{mg kg}^{-1}$  (AOAC, 2016). When the method detection limit (MDL) in rice samples was calculated *via* LOD and LOQ of the standard calibration curve, it was found to be 90 and 2.95  $\text{mg kg}^{-1}$ , respectively. Thus, the  $\text{Br}^-$  concentration detected in unspiked rice samples based on calculation from standard addition curve can be reported as lower than MDL (Table 3.1).

**Table 3.1** Recoveries of spiked Br<sup>-</sup> in composite rice samples with relative standard deviation (RSD) values (n = 3)

<b>Spiked concentration (mg kg<sup>-1</sup>)</b>	<b>Detected (mg kg<sup>-1</sup>) (Average ± SD)</b>	<b>%Recovery (Average ± SD)</b>	<b>%RSD</b>
0	2.19 ± 0.57*	-	-
12	11.78 ± 0.33	79.94 ± 2.76	2.81
25	23.52 ± 0.94	85.35 ± 3.74	3.98
50	48.28 ± 1.86	92.19 ± 3.71	3.85
60	50.42 ± 1.18	80.40 ± 1.97	2.35

\*based on calculation from standard addition curve

### 3.5.5 Precision

The inter-day precisions of the three concentration levels of Br<sup>-</sup> (0.63, 1.25 and 3.75 µM) determined on 5 days were between 3.07 - 7.12% (n = 45), whereas the intra-day precisions obtained from the 5 measurements of each three concentration levels on the same day ranged from 2.87 - 6.35% (n = 15) as shown in Table 3.2. These precisions were in the AOAC standard precision (repeatability) which is not more than 11% for 1 mg kg<sup>-1</sup> analyte concentration (AOAC, 2016).

**Table 3.2** The intra-day and inter-day precisions

<b>Spiked concentration (µM)</b>	<b>Intra-day (µM)</b>		<b>Inter-day (µM)</b>	
	<b>(Average ± SD)</b>	<b>%RSD</b>	<b>(Average ± SD)</b>	<b>%RSD</b>
0.63	0.63 ± 0.04	5.91	0.61 ± 0.04	7.12
1.25	1.22 ± 0.08	6.35	1.22 ± 0.08	6.91
3.75	3.73 ± 0.11	2.87	3.79 ± 0.12	3.07

### 3.6 Preliminary development of sample preparation with SPE method

To further evaluate the feasibility of developed sensor, First attempt to prepare rice sample was made by dissolving with water as a simple method and the water extract of rice was passed through a Oasis HLB solid phase sorbent which was carried out as in section 2.11.1 and 2.11.2, respectively and analyzed by developed colorimetric determination.

It appeared that no significant difference in color changes between unspiked sample (sample blank) and spiked sample with  $0.34 \text{ mg L}^{-1}$  (equal to  $50 \text{ mg kg}^{-1}$ ) was observed which both samples presented red solution as shown in Figure 3.18. This indicated that possible interferences especially organic substances as well as  $\text{Br}^-$  could dissolve in aqueous extracts. Srisawat et al. (2010) examined phenolic or flavonoid compounds in the rice water extracts. These compounds probably could interfere  $\text{Br}^-$  detection by: i) adsorbing on surface of AuNPs and hinder the ligand-exchange process between  $\text{Cr}^{3+}$ -citrate complex and ii) forming a complex with  $\text{Cr}^{3+}$  instead of citrate. Therefore, the sophisticated method for removal of organic interferences is required for further work and the remained organic interferences were further investigated for selectivity.

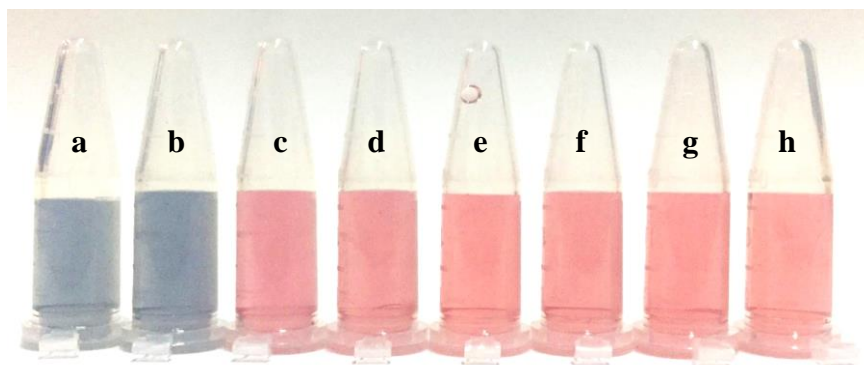


**Figure 3.18** The detected color solution using this developed sensor under the optimum condition: Ultrapure water used as (a) standard blank, (b) SPE blank, (c)  $0.34 \text{ mg L}^{-1}$  standard  $\text{Br}^-$ , (d)  $0.34 \text{ mg L}^{-1}$  standard  $\text{Br}^-$  passed through SPE. Rice sample extracts with (e) sample blank, (f) sample blank passed through SPE (g) spiked sample and (f) spiked sample passed through SPE ( $n = 3$ ).

### 3.7 Comparison of different digestion method by inductively coupled plasma optical emission spectrometry (ICP-OES)

The digestion and ashing method was selected for rice sample preparation according to Sungwaranond et al. (1998). The residue solutions of the composite rice sample which was digested with acid and thermally decomposed to ash were measured to analyze metals elements by inductively coupled plasma optical emission spectrometry (ICP-OES). The results is shown in Table 3.3 including (A) the rice sample (2.0 g) prepared by digesting with 1% potassium hydroxide in 50% ethanol and ashing for 4 h, (B) rice sample (2.0 g) prepared by digesting with 1% potassium hydroxide in 50% ethanol and ashing for 8 h and (C) rice sample (1.2 g) prepared by acidic digesting with hydrogen peroxide and hydrochloric acid.

It was shown that samples solution under the alkali digested and thermally decomposed consisted the major composition of high concentrations of K, Mg, Ca and P in the range of 6.66 - 13,544.17 mg kg<sup>-1</sup> whereas the minor composition of Al, Cr and Se were found in low concentration of 0.20 - 2.79 mg kg<sup>-1</sup>. In addition, it was found that Cu, Fe, Mn, Ni and Zn were not detected, however high concentration of these elements had been found when samples was prepared by acid digestion. The concentration of other cations such as Mg<sup>2+</sup>, Ca<sup>2+</sup>, Al<sup>3+</sup> obtained by our method was much lower than those obtained by acidic digestion excepting that higher amount of K<sup>+</sup> was detected. This was due to the addition of KOH for rice digestion, however, it has proved that K<sup>+</sup> residue did not interfere the colorimetric detection using AuNPs as shown in Figure 3.18. In addition, high recoveries of sample preparation and detection were obtained (Table 3.1). Thus, these results confirmed that our alkaline digestion and ashing method can remove some metals and organic interferences.

**Table 3.3** Comparison of metals detected in rice samples which prepared by different digestion method followed by inductively coupled plasma-optical emission spectrometric detection (ICP-OES) (n = 3)

Metal	Sample preparation method*		
	A (mg kg <sup>-1</sup> )	B (mg kg <sup>-1</sup> )	C (mg kg <sup>-1</sup> )
Al	0.0016 ± 0.0001	0.0028 ± 0.0000	1.0808 ± 0.0228
Ca	0.0068 ± 0.0001	0.0067 ± 0.0002	25.4417 ± 0.4185
Cr	0.0005 ± 0.0000	0.0003 ± 0.0000	0.0211 ± 0.0000
Cu	Not detected	Not detected	0.2564 ± 0.0077
Fe	Not detected	Not detected	0.6846 ± 0.0033
K	13.0542 ± 0.0520	13.5542 ± 0.0764	90.5528 ± 6.2761
Mg	0.0455 ± 0.00012	0.0547 ± 0.0007	24.9431 ± 0.3996
Mn	Not detected	Not detected	1.1388 ± 0.0203
Ni	Not detected	Not detected	0.0266 ± 0.0009
P	1.0049 ± 0.0147	0.9815 ± 0.0113	192.3577 ± 3.2884
Se	0.0002 ± 0.0000	0.0002 ± 0.0001	0.3111 ± 0.0156
Zn	Not detected	Not detected	2.3366 ± 0.0235

\*A: the rice sample (2.0 g) prepared by digesting with 1% potassium hydroxide in 50% ethanol and ashing for 4 h; B: rice sample (2.0 g) prepared by digesting with 1% potassium hydroxide in 50% ethanol and ashing for 8 h; C: rice sample (1.2 g) prepared by acidic digesting with hydrogen peroxide and hydrochloric acid.

### 3.8 Selectivity

Some other cations and anions in rice samples were investigated as they probably interfered the selectivity of Br<sup>-</sup>. It was reported that inorganic anions *i.e.*, F<sup>-</sup>, Cl<sup>-</sup>, NO<sub>2</sub><sup>-</sup>, NO<sub>3</sub><sup>-</sup> and SO<sub>4</sub><sup>2-</sup> were found in rice samples from four provinces in China by ion chromatography ranging from not detected to 20.90 mg kg<sup>-1</sup> (Sun et al., 2014). Some elements in rice extract prepared by our method using alkaline digestion and ashing method were determined by inductively coupled plasma-optical emission spectrometry (ICP-OES) as presented in Table 3.3.

It was shown that samples had high concentrations of K, Mg, Ca, and P whereas Al, Cr and Se were found in low concentration. The finding of K, Ca, Mg and Al was agreed with the data of other reports (Lu et al., 2013; Parengam et al., 2010). Thus, the 10 common ions including K<sup>+</sup>, Mg<sup>2+</sup>, Ca<sup>+</sup>, Al<sup>3+</sup>, NO<sub>2</sub><sup>-</sup>, NO<sub>3</sub><sup>-</sup>, PO<sub>4</sub><sup>3-</sup>,

$\text{SO}_4^{2-}$ ,  $\text{F}^-$ ,  $\text{Cl}^-$  were investigated toward  $\text{Br}^-$  under the same optimal conditions. In addition, Cu, Fe, Mn, Ni and Zn were not detected, thus they were not included as interferences.

The selectivity was evaluated by testing the absorbance intensity ratio ( $A_{519}/A_{673}$ ) of  $5\ \mu\text{M}$   $\text{Br}^-$  to  $5000\ \mu\text{M}$  of other ions including  $\text{K}^+$ ,  $\text{Mg}^{2+}$ ,  $\text{Ca}^+$ ,  $\text{Al}^{3+}$ ,  $\text{NO}_2^-$ ,  $\text{NO}_3^-$ ,  $\text{PO}_4^{3-}$ ,  $\text{SO}_4^{2-}$ ,  $\text{F}^-$  and  $\text{Cl}^-$ . As shown in Figure 3.19,  $\text{Br}^-$  (red bar) showed an instinct signal whereas in the absence of  $\text{Br}^-$ , the signal of other ions except  $\text{Cl}^-$  (blue bar) was almost identical to the blank even if they are 1000-folds of  $\text{Br}^-$ , suggesting no anti-aggregation of AuNPs by other ions.

Furthermore, the response of  $\text{Br}^-$  in the presence of the mixture of all ions including  $5000\ \mu\text{M}$  of  $\text{NO}_2^-$ ,  $\text{NO}_3^-$ ,  $\text{PO}_4^{3-}$ ,  $\text{SO}_4^{2-}$ ,  $\text{F}^-$ ,  $3000\ \mu\text{M}$  of  $\text{K}^+$ ,  $500\ \mu\text{M}$  of  $\text{Cl}^-$ ,  $25\ \mu\text{M}$   $\text{Mg}^{2+}$ ,  $\text{Ca}^+$ ,  $\text{Al}^{3+}$  (violet bar) increased to a level similar to that of  $\text{Br}^-$  alone (red bar). It can be explained by that  $\text{Br}^-$  is lightly hydrated and has higher polarizability which can be attractive close to AuNPs surface compared to  $\text{NO}_3^-$ ,  $\text{SO}_4^{2-}$ ,  $\text{F}^-$  and  $\text{Cl}^-$  while other negative ions are repelled from the surface of AuNPs (Merk et al., 2014).

Only the addition of  $5000\ \mu\text{M}$   $\text{Cl}^-$  can result in the anti-aggregation. However, considering that low abundance of  $\text{Cl}^-$  (about  $3.05\ \text{mg}\ \text{kg}^{-1}$ ) was detected in rice sample matrix and the concentration of  $\text{Cl}^-$  was five times higher than  $\text{Br}^-$ , the signal caused by  $\text{Cl}^-$  can be negligible. These results clearly revealed that the simultaneous presence of other competitive ions even at their very high concentration (may be high to  $5000\ \mu\text{M}$ ) did not interfere the determination of  $\text{Br}^-$ .

The other anions such as  $\text{I}^-$ ,  $\text{S}^{2-}$ ,  $\text{SO}_3^{2-}$ , and  $\text{SCN}^-$  could affect the detection of  $\text{Br}^-$ . Thus, the effect of  $\text{I}^-$  and  $\text{SCN}^-$  on selectivity of the detection was investigated as shown in Figure 3.20, which the responses of these ions were similar to that of  $\text{Br}^-$ . They strongly affected anti-aggregation of AuNPs, meaning that they interfered the anti-aggregation of AuNPs because  $\text{I}^-$  and  $\text{SCN}^-$  are the same a chaotropic anion as  $\text{Br}^-$  (Merk et al., 2014). However, concentration of  $\text{I}^-$  in white rice samples was found to be approximately 185 times lower than  $\text{Br}^-$  (Parengam, et al. 2010) while  $\text{S}^{2-}$ ,  $\text{SO}_3^{2-}$  and  $\text{SCN}^-$  have never been reported. Thus, our colorimetric sensor exhibited a high selectivity for  $\text{Br}^-$  over other ions in rice samples.

These results clearly revealed that the simultaneous presence of other competitive ions even at their very high concentration did not interfere the determination of  $\text{Br}^-$ . Thus, our colorimetric sensor exhibited a high selectivity for  $\text{Br}^-$  over other ions in rice samples.



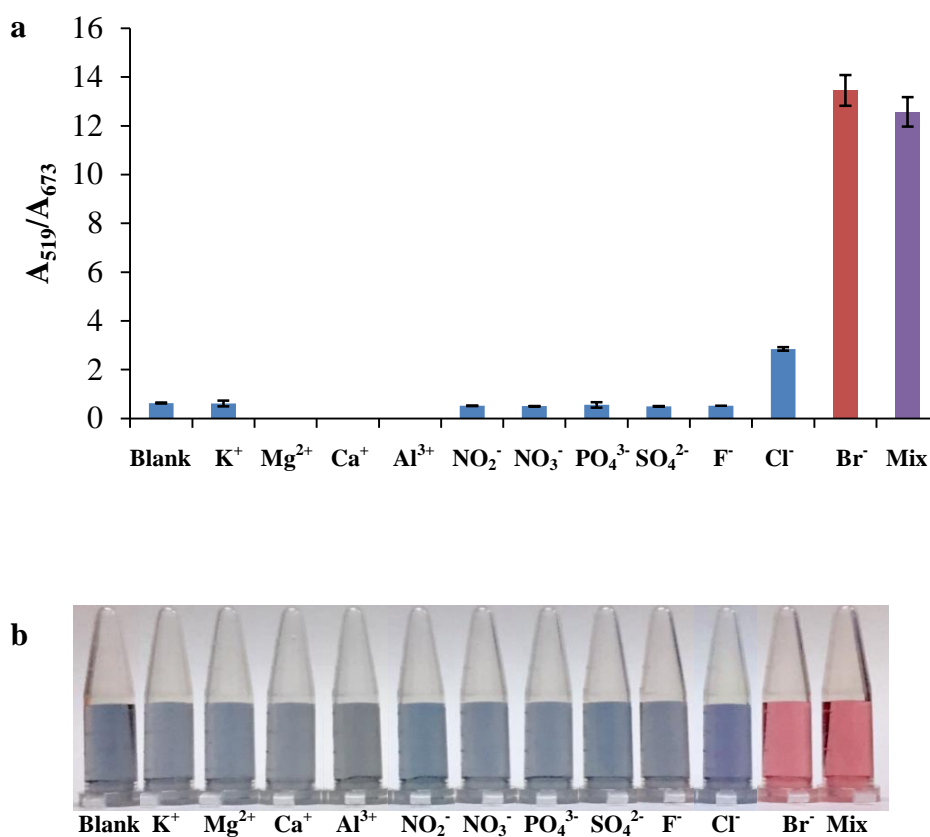


**Figure 3.19** Selectivity of the Br<sup>-</sup> detection. (a) Absorbance ratio response ( $A_{519}/A_{673}$ ) of the proposed sensor for 5  $\mu\text{M}$  Br<sup>-</sup> (red bar) was plotted against the 5000  $\mu\text{M}$  of ion interferences *i.e.*, K<sup>+</sup>, Mg<sup>2+</sup>, Ca<sup>+</sup>, Al<sup>3+</sup>, NO<sub>2</sub><sup>-</sup>, NO<sub>3</sub><sup>-</sup>, PO<sub>4</sub><sup>3-</sup>, SO<sub>4</sub><sup>2-</sup>, F<sup>-</sup> and Cl<sup>-</sup> (blue bar) and the mixture of Br<sup>-</sup> and other ions including 5000  $\mu\text{M}$  of NO<sub>2</sub><sup>-</sup>, NO<sub>3</sub><sup>-</sup>, PO<sub>4</sub><sup>3-</sup>, SO<sub>4</sub><sup>2-</sup>, F<sup>-</sup>, 3000  $\mu\text{M}$  of K<sup>+</sup>, 500  $\mu\text{M}$  of Cl<sup>-</sup>, 25  $\mu\text{M}$  Mg<sup>2+</sup>, Ca<sup>+</sup>, Al<sup>3+</sup> (violet bar). All signals were corresponding to blank. (b) The photograph is examples of the corresponding detection sensor.

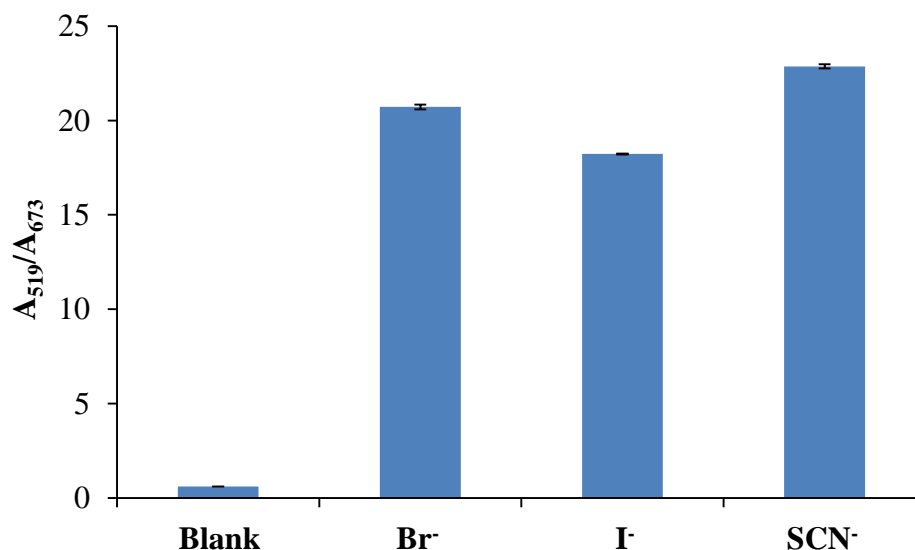


**Figure 3.20** Effect of  $5 \text{ mg L}^{-1}$  of  $\text{I}^-$  and  $\text{SCN}^-$  on selectivity of the detection of  $5 \text{ mg L}^{-1} \text{ Br}^-$ .

### 3.9 Comparison of ashing time by inductively coupled plasma optical emission spectrometry (ICP-OES)

In this work, ashing step for 8 h at temperature of  $550 \text{ }^\circ\text{C}$  was used and resulted in time consuming for sample preparation. Thus, it was further investigated at ashing time of 4 and 8 h with the temperature of  $600 \text{ }^\circ\text{C}$ .

The result showed that no significant differences by *t*-test with multiple sample ( $t < t_{\text{table}}$ ) in the concentrations of metal composition using the ashing step for 4 (method A) and 8 (method B) h were observed in all samples (Table 3.3). Therefore, in this work, rice samples were treated by alkaline digestion and ashing method of 4 h at  $600 \text{ }^\circ\text{C}$ .

### 3.10 The investigation of the remained bromide in residues by X-ray fluorescence spectrometry (XRF)

The residue of  $\text{Br}^-$  in ash was investigated to prove whether  $\text{Br}^-$  was lost by using high temperature of dry ashing method. The experiment was detected by X-ray fluorescence (XRF) technique. The composite rice samples were spiked with  $\text{Br}^-$  concentrations of 50, 100, 200 and  $400 \text{ mg kg}^{-1}$ . The XRF results are shown detected peak of  $\text{Br}^-$  (Figure A9), meaning that the inorganic bromide was remained after ashing step. When plotting between the concentration of  $\text{Br}^-$  standard and  $\text{Br}^-$  detected by XRF, it shows good linearity (Figure 3.21). Therefore, it is proved that  $\text{Br}^-$  is not

lost by high temperature. Overall, the dry ashing at 600 °C for 4 h were suitable method for Br<sup>-</sup> application of rice samples with our developed sensor.

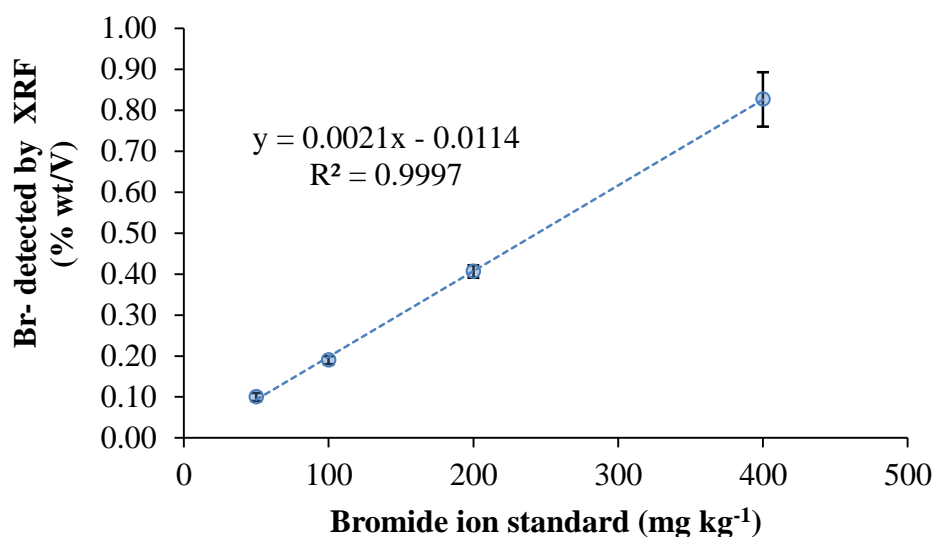


**Figure 3.21** Correlation between Br<sup>-</sup> standard and Br<sup>-</sup> detected by XRF in the composite rice sample solution.

### 3.11 Application of the developed sensor to rice samples

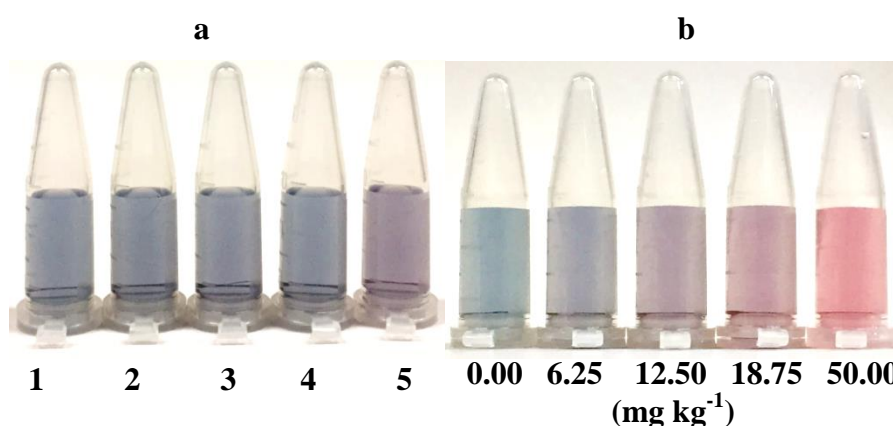
Five brands of white rice samples from the supermarket in Hat Yai, Songkhla province, Thailand was collected to determine the Br<sup>-</sup> contamination under the our developed method.

Table 3.4 shows the determination of Br<sup>-</sup> in rice samples by our sensor together with ion chromatographic (IC) results and the corresponding colorimetric results as shown in Figure 3.22a. The color chart added with Br<sup>-</sup> standard ranged from 6.25 - 50.00 mg kg<sup>-1</sup> in samples was made for naked eye detection (Figure 3.22b). The Br<sup>-</sup> residues were detected in all studied samples ranging from 3.12-5.21 mg kg<sup>-1</sup> (Wet weight) which were fallen in the range of 0.00 - 6.25 mg kg<sup>-1</sup> shown in color chart and higher than those detected by Parengam et al. (0.40 - 1.40 mg kg<sup>-1</sup>) (Parengam et al., 2010). However, the detectable concentrations of Br<sup>-</sup> did not exceed the MRL limit set by The Thai Ministry of Public Health (50 mg kg<sup>-1</sup>) (Notification of the Ministry of Public Health (No. 361) 013). Moreover, it showed that no interferences due to co-extracted compounds were found as seen in colorimetric result of samples (Figure 3.22a).

At present, there is no established standard method for detection of  $\text{Br}^-$  in rice samples. Our validated sensor with ion chromatographic (IC) technique was confirmed for the concentration of  $\text{Br}^-$  in rice samples (Table 3.4). It was found that the  $\text{Br}^-$  concentrations detected by sensor ( $3.12 - 5.21 \text{ mg kg}^{-1}$ ) were in agreement with those detected by IC ( $3.38 - 6.77 \text{ mg kg}^{-1}$ ) which there is no statistically significant differences by  $t$ -test with multiple samples ( $t < t_{\text{table}}$ ) from those detected by IC. These results confirmed that the developed sensor method can be applied for the analysis of  $\text{Br}^-$  in real complex samples.

**Table 3.4** The determination of  $\text{Br}^-$  in rice samples by developed sensor ( $n = 3$ ) and ion chromatography ( $n = 2$ )

Sample	Found ( $\text{mg kg}^{-1}$ , wet weight)	
	Developed sensor ( $n = 3$ )	Ion Chromatography ( $n = 2$ )
White rice 1	$3.12 \pm 0.83$	$3.41 \pm 1.61$
White rice 2	$4.23 \pm 1.10$	$6.25 \pm 0.80$
White rice 3	$4.07 \pm 1.70$	$3.41 \pm 2.41$
White rice 4	$4.16 \pm 0.48$	$4.00 \pm 2.41$
White rice 5	$5.21 \pm 0.91$	$6.82 \pm 4.82$



**Figure 3.22** (a) The corresponding color of white rice sample 1- sample 5 (Table 3.4), respectively. (b) The color chart in the presence of  $\text{Br}^-$  concentration of  $0.00 - 50.00 \text{ mg kg}^{-1}$ .

### **3.12 Comparison of developed sensor with other reported analytical methods**

To further demonstrate the advantages of the developed sensor, the performance of our sensor was compared with other previously reported methods. Table 3.5 lists the comparison results of our developed sensor with other methods that are sample amount, linear range, LOD and detection time. The LOD and linearity obtained by our sensor were clearly superior to the other work. In addition, our sensor has a short detection time compared with expensive methods (Fu et al., 2017; Gallardo et al., 2016; Wittayanan & Jongmevasna, 2015). Our sensor exhibited comparable sample amount used for detecting Br<sup>-</sup> in real samples to the methods mentioned in Table 3.5. Overall, these results confirmed that our method for Br<sup>-</sup> based on anti-aggregation of AuNPs was more efficient and sensitive.

**Table 3.5** Comparison of the developed sensor with other method applied for Br<sup>-</sup> in different samples.

Method <sup>a</sup>	Sample	Sample amount	Linear range (μM)	LOD (μM)	Detection time (min)	Reference
LLE-Deriv.- GC-μECD	Rice	2 g	62.58 - 938.63	25.03	20	(Wittayanan & Jongmevasna, 2015)
Microwave digestion-ICP-MS	Food	1 - 2 g	25.03 - 2503.00	8.51	1	(Nguyen & Ludwig, 2014)
Phenol red spectrophotometry	Vegetables	5 g	6.26 - 56.32	3.13	3	(Baso-Cejas et al., 2007)
LPIEC-visible light detection	Foodstuffs	25 g	0.38 - 62.58	0.03	7.5	(Yu et al., 2011)
Phenol red and chloramine-T colorimetry	Environmental samples	20 - 300 μL	0.00 - 375.45	1.38	5	(Lepore & Barak, 2009)
Aggregation and anti-aggregation of AgNPs	Water	-	0.99 - 5.66	1.67	-	(Bothra et al., 2015)
Total reflection X-ray fluorescence spectrometry	Soil	1 g	15.64 - 156.44	3.13	25	(Gallardo et al., 2016)
Fluorescent Ag nanocluster detection	Dried kelp	1 g	0.10 - 50.00	-	60	(Fu et al., 2017)
Anti-aggregation of AuNPs	Rice	2 g	0.31 - 3.75	0.04	< 10	This work

<sup>a</sup>LLE-Deriv.-GC-μECD: Liquid-liquid extraction-derivatization-gas chromatography-micro electron capture detector; ICP-MS: Inductive coupled plasma-mass spectrometry; LPIEC: Low pressure ion-exchange chromatography

## CHAPTER 4

### CONCLUSION

#### 4.1 The synthesis of gold nanoparticles

The gold nanoparticles (AuNPs) were successfully synthesized by the reduction of gold(III) chloride solution with tri-sodium citrate, resulting the formation of citrate capped-gold nanoparticles.

The wine red solution of colloidal AuNPs demonstrated the surface plasmon resonance (SPR) absorption with the maximum absorbance was 1.49 a.u. at the wavelength of 519 nm with the concentration of AuNPs of 5.52 nM, The average particles size was  $13.6 \pm 1.7$  nm in which was in good agreement with previous reports (Hormozi-Nezhad & Abbasi-Moayed, 2014; Li et al., 2011; Majzik et al., 2010; Zhou et al., 2014).

#### 4.2 Proposed sensing mechanism

The wine red solution of colloidal AuNPs was relatively stable due to the electrostatic repulsion of negatively charged of citrate ions on the surface of AuNPs (Elavarasi et al., 2013; Park & Shumaker-Parry, 2014).

In the presence of  $\text{Cr}^{3+}$ , AuNPs was aggregated by chelating of  $\text{Cr}^{3+}$ -citrate-AuNPs complex, resulting in blue solution. When the AuNPs was mixing with  $\text{Br}^-$  and  $\text{Cr}^{3+}$ , anti-aggregation of AuNPs was occurred due to the adsorption of  $\text{Br}^-$  on the AuNPs surface enhances AuNPs stability (Pfeiffer et al., 2014), presenting the change of AuNPs from aggregation state (blue color) to dispersion state (red color).

#### 4.3 Characterization of AuNPs particles

The colloidal AuNPs was demonstrated the SPR band of red solution of AuNPs at 519 nm, the TEM image of the spherical mono-disperse colloidal of individual particles and the effective diameter (ED) of size distribution was  $16.43 \pm 0.81$  nm

In the presence of AuNPs and  $\text{Cr}^{3+}$  lead to the aggregation of AuNPs which demonstrated the new maxima SPR band appeared at 673 nm while the SPR band at 519 nm was decreased, the TEM image showed interconnected particles of the heavy aggregations of AuNPs and the ED of size distribution increased to  $262.30 \pm 4.07$  nm.

When the presence of  $\text{Br}^-$  with AuNPs and  $\text{Cr}^{3+}$ , the anti-aggregation state was occurred which was strongly remained maxima SPR band at 519, the TEM image showed dispersion with the decrease in the size of AuNPs compared to aggregation state and the ED of size distribution decreased to  $29.37 \pm 2.56$  nm.

The zeta potential of AuNPs displayed negative value due to citrate ion covered on the surface of AuNPs (Brewer et al., 2005). After addition of 0.63, 2.50 and 4.38  $\mu\text{M}$   $\text{Br}^-$  into AuNPs, zeta potential value increased when the  $\text{Br}^-$  concentration increased, indicating that colloidal AuNPs has more electrical stability.

It was found that AuNPs can be kept in refrigerator up to 4 months with the average absorbance of  $1.49 \pm 0.01$  at 519 nm. In addition, the sensitivity of the detection of 2.50  $\mu\text{M}$   $\text{Br}^-$  resulting that remained stable with no significant difference of the absorbance ratio between 8 measurements in 4 months ( $p > 0.05$ ). The stability of AuNPs after several days for  $\text{Br}^-$  detection can be last at least 4 months.

#### 4.4 Optimization of parameters affecting the detection of bromide

The concentration of  $\text{Cr}^{3+}$  solution, pH and concentration of phosphate buffer, concentration of AuNPs and reaction time were optimized to obtain the best sensitivity of  $\text{Br}^-$  detection. The absorbance at 519 and 673 nm were directly related to the dispersed, aggregated and anti-aggregated state of AuNPs. Thus, the absorbance intensity ratio of  $A_{519}/A_{673}$  was used for the quantitative determination of  $\text{Br}^-$ .

The degree of AuNPs aggregation gradually increased when concentration of  $\text{Cr}^{3+}$  increased since the binding sites of citrate ion on the surface of AuNPs were coordinated with  $\text{Cr}^{3+}$ . The concentration of  $\text{Cr}^{3+}$  higher than 4.81  $\mu\text{M}$  showed stable intensity ratio with wine red to blue solution. Thus, 4.81  $\mu\text{M}$   $\text{Cr}^{3+}$  was chosen for optimal concentration.

The effect of phosphate buffer pH in the range of 6.0 - 7.5 was investigated. The sensitivity of  $\text{Br}^-$  increased when pH of buffer increased from 6.0 to 6.5. At pH value lower than 6.4, carboxylate group protonated to citric acid and lead to influence the aggregation capacity, resulting in low sensitivity of anti-aggregation. At pH 6.5 which was close to  $\text{pK}_{a3}$  of citric acid, citrate has the highest ability to chelate  $\text{Cr}^{3+}$  (Gabriel et al., 2007), leading to the high aggregation and thus, resulting in high capacity of anti-aggregation process with  $\text{Br}^-$ . When pH increased more than pH 6.5, the sensitivity decreased because of hydrolysis of  $\text{Cr}^{3+}$  that can destroy chelating reaction with citrate (Chen et al., 2014; Spiccia & Marty, 1986; Wang et al., 2015). In addition, the Au-Br form was broken down to form Au-OH (Pesic & Sargent, 1993) and were likely to disperse in the alkaline environment. Therefore a phosphate buffer pH 6.5 was chosen.



The investigation of buffer concentration resulting when concentration increased, the degree of aggregation increased while degree of anti-aggregation decreased due ionic strength. Upon the considering of the maximal ratio between the aggregation and anti-aggregation as blank and analyte, respectively, thus, 10.0 mM phosphate buffer (pH 6.5) was chosen.

When AuNPs concentration increased from 1.83 - 3.21 nM, the degree of anti-aggregation decreased due to more abundant AuNPs compared to limited bromide ion coated onto the AuNPs surface. However, AuNPs concentration lower than 1.83 nM was difficult to observe color of solution by naked eye and the sensitivity decreased too. Thus, 1.83 nM of AuNPs was chosen.

The anti-aggregation was found to be completed at 10 min reaction time.

#### 4.5 Method validations

The linearity response based on UV-Vis measurement ( $y = 3.5653x - 0.5913$ ,  $R^2 = 0.9965$ ) was in the range of 0.13 - 6.26  $\mu\text{M Br}^-$  ( $n = 3$ ). Based on the color transition observed by naked eye, a good linearity of standard calibration curve ( $y = 3.4803x - 0.6065$ ,  $R^2 = 0.9970$ ) was found to be in the range of 0.31 - 3.75  $\mu\text{M Br}^-$  ( $k = 3$ ,  $n = 3$ ). The limit of detection (LOD) and limit of quantification (LOQ) were 0.04 and 0.13  $\mu\text{M}$ , respectively. The recoveries of spiking  $\text{Br}^-$  concentrations was good ranging from 79.9 - 92.2% with precisions (RSD) less than 4.0% ( $n = 3$ ). The intra-day precisions obtained from the 5 measurements of three concentration levels of  $\text{Br}^-$  (0.63, 1.25, 3.75  $\mu\text{M}$ ) on the same day ranged from 2.87 - 6.35% ( $n = 15$ ), whereas the inter-day precisions of each three concentration levels determined on 5 days were fallen between 3.07 - 7.12% ( $n = 45$ ). These recoveries and precisions were acceptable within the range referred to in AOAC standard method.

The sensitivity of a standard addition curve was significantly different from that of a standard calibration curve ( $p < 0.05$ ) in the range of 0.31 - 3.75  $\mu\text{M Br}^-$ . This presented that the matrix had effect on the analysis of  $\text{Br}^-$  in rice samples. Therefore, the standard addition method was used for accurate determination of  $\text{Br}^-$  in rice samples.

#### 4.6 Development of sample preparation

In the beginning, the preparation of rice sample was made by dissolving with water as a simple method and the water extract of rice was passed through a solid phase sorbent cartridge then analyzed by colorimetric determination. The result appeared that there is no significant difference in color changes between unspiked and spiked sample, indicating that interferences especially organic substances could interfere the anti-aggregation of  $\text{Br}^-$ . In further, the sophisticated method need to removal of organic interferences and the remained organic interferences were further investigated for selectivity.

However, the sample preparation by digestion and ashing method was chosen due to the organic matrix was removed.

Alkaline and acid digestion methods were compared by inductively coupled plasma optical emission spectrometry (ICP-OES). The samples solution under the alkaline digestion with high temperature ashing consisted the high concentrations of major composition that is K, Mg, Ca and P whereas the minor composition of Al, Cr and Se but Cu, Fe, Mn, Ni and Zn were not detected. The concentration of other cations such as  $\text{Mg}^{2+}$ ,  $\text{Ca}^{2+}$ ,  $\text{Al}^{3+}$  obtained by our method was much lower than those obtained by acidic digestion. Therefore, alkaline digestion and ashing method was chosen since it removed some metals and organic interferences.

The ashing time for 4 and 8 h at temperature to 600 °C was compared. The result showed no significant difference in the concentrations of cations detected by two ashing time. Thus, in this work, rice samples were treated by alkaline digestion and ashing method for 4 h at 600 °C was selected.

To investigate the persistence of  $\text{Br}^-$  after ashing at high temperature, the sample was examined by X-ray fluorescence spectrometry (XRF). The XRF results showed detectable peak of  $\text{Br}^-$ . When plotting the concentration of  $\text{Br}^-$  standard with  $\text{Br}^-$  detected by XRF, the good linearity was obtained, thus it is proved that  $\text{Br}^-$  is not lost by high temperature.

#### 4.7 Selectivity

Ten common ions including  $\text{K}^+$ ,  $\text{Mg}^{2+}$ ,  $\text{Ca}^{2+}$ ,  $\text{Al}^{3+}$ ,  $\text{NO}_2^-$ ,  $\text{NO}_3^-$ ,  $\text{PO}_4^{3-}$ ,  $\text{SO}_4^{2-}$ ,  $\text{F}^-$ ,  $\text{Cl}^-$  were investigated for the selectivity effect

The selectivity was evaluated by testing the absorbance intensity ratio ( $A_{519}/A_{673}$ ) of 5  $\mu\text{M}$   $\text{Br}^-$  to 5000  $\mu\text{M}$  of other ions including  $\text{K}^+$ ,  $\text{Mg}^{2+}$ ,  $\text{Ca}^{2+}$ ,  $\text{Al}^{3+}$ ,  $\text{NO}_2^-$ ,  $\text{NO}_3^-$ ,  $\text{PO}_4^{3-}$ ,  $\text{SO}_4^{2-}$ ,  $\text{F}^-$  and  $\text{Cl}^-$ . The result showed no anti-aggregation of AuNPs by other ions. Moreover,  $\text{I}^-$  and  $\text{SCN}^-$  are strongly affected anti-aggregation of AuNPs

system and  $S^{2-}$  and  $SO_3^{2-}$  also. It was reported that concentration of  $I^-$  in white rice samples was found to be lower approximately 200 time than  $Br^-$  (Parengam, et al. 2010). Moreover,  $SCN^-$ ,  $S^{2-}$  and  $SO_3^{2-}$  have never been reported. Thus, other ions in rice samples are negligible for  $Br^-$  detection.

#### 4.8 Application of the developed sensor to rice samples

The  $Br^-$  residues of five brands of white rice were detected in all studied samples ranging from 3.12-5.21  $mg\ kg^{-1}$  which were fallen in the range of 0.00-6.25  $mg\ kg^{-1}$  shown in color chart by our sensor with naked eye detection. The detectable concentrations of  $Br^-$  did not exceed the MRL limit set by CODEX and The Thai Ministry of Public Health (50  $mg\ kg^{-1}$ ) (Notification of the Ministry of Public Health (No. 361)

In addition, the  $Br^-$  concentrations detected by sensor (3.12 - 5.21  $mg\ kg^{-1}$ ) were in agreement with those detected by IC (3.38 - 6.77  $mg\ kg^{-1}$ ) which there is no statistically significant differences by  $t$ -test with multiple samples ( $t < t_{table}$ ). These results confirmed that the developed sensor method can be applied for the analysis of  $Br^-$  in real complex samples.

#### 4.9 Comparison of developed sensor with other reported analytical methods

The comparison our developed sensor with other methods was performed. Our sensor had shorter detection time compared with expensive methods and exhibited comparable sample amount used for detecting  $Br^-$  in real sample.

However, to further improve of developed colorimetric sensor for application in rice sample was required the development of sample preparation method which makes detection was faster easier and low energy method.

In conclusion, robust colorimetric sensor for bromide ions by using citrate-capped AuNPs in the presence of  $Cr^{3+}$  was developed. The method was based on the anti-aggregation induced by  $Br^-$ , resulting in the color change from blue to red upon the addition of different concentrations of  $Br^-$ . It was also simple, highly sensitive and selective. The system presents low LOD and LOQ without any interfering effects of other ions in rice samples. Satisfying recoveries and precisions were achieved in our developed colorimetric sensor.

## References

- Alkilany, A. M., Murphy, C. J. 2010. Toxicity and cellular uptake of gold nanoparticles: what we have learned so far?. *Journal of Nanoparticle Research*, **12**(7), 2313-2333.
- Amendola, V., Meneghetti, M., Stener, M., Guo, Y., Chen, S., Crespo, P., García, M.A., Hernando, A., Pengo, P., Pasquato, L. 2014. Physico-chemical characteristics of gold nanoparticles. in: *Comprehensive Analytical Chemistry*, (Eds.) M. Valcárcel, Á. I. López-Lorente, Vol. 66, pp. 81-152.
- Amin, M., Lim, L. W., Takeuchi, T. 2008. Determination of common inorganic anions and cations by non-suppressed ion chromatography with column switching. *Journal of Chromatography A*, **1182**(2), 169-75.
- AOAC. 2016. Guidelines for Standard Method Performance Requirements. in: *Association of Official Analytical Chemists*.
- Attia, Y., Buceta, D., Requejo, F., Giovanetti, L., López-Quintela, M. 2015. Photostability of gold nanoparticles with different shapes: role of Ag clusters. *Nanoscale*, **7**, 11273-11279.
- Bae, D. R., Han, W. S., Lim, J. M., Kang, S., Lee, J. Y., Kang, D., Jung, J. H. 2010. Lysine-functionalized silver nanoparticles for visual detection and separation of histidine and histidine-tagged proteins. *Langmuir*, **26**(3), 2181-2185.
- Baso-Cejas, E., Brito, G., Díaz, C., Peña-Méndez, E. 2007. Determination of inorganic bromide content in several vegetable foods. *Bulletin of Environmental Contamination and Toxicology*, **78**, 417-420.
- Baur, X., Budnik, L. T., Zhao, Z., Bratveit, M., Djurhuus, R., Verschoor, L., Rubino, F.M., Colosio, C., Jepsen, J.R. 2015. Health risks in international container and bulk cargo transport due to volatile toxic compounds. *Journal of Occupational Medicine and Toxicology*, **10**, 1-18.
- Bothra, S., Kumar, R., Pati, R. K., Kuwar, A., Choi, H. J., Sahoo, S. K. 2015. Virgin silver nanoparticles as colorimetric nanoprobe for simultaneous detection of iodide and bromide ion in aqueous medium. *Spectrochimica Acta Part A: Molecular and Biomolecular Spectroscopy*, **149**, 122-126.

- Brewer, S. H., Glomm, W. R., Johnson, M. C., Knag, M. K., Franzen, S. 2005. Probing BSA binding to citrate-coated gold nanoparticles and surfaces. *Langmuir*, **21**(20), 9303-9307.
- CCM. 2017. China reveals a list of newly banned insecticides, CCM Data and business intelligence, <http://www.cnchemicals.com/Press/89543China%20reveals%20a%20list%20of%20newly%20banned%20insecticides.html>, accessed 18. 11. 2017.
- Cheewasedtham, W., Jaffrezic-Renualt, N. 2016. New rapid chemical and biosensor methods for determination of methyl bromide in rice sample. Reserch report, Prince of Songkla University.
- Chen, M., Cai, H. H., Yang, F., Lin, D., Yang, P. H., Cai, J. 2014. Highly sensitive detection of chromium(III) ions by resonance Rayleigh scattering enhanced by gold nanoparticles. *Spectrochimica Acta Part A: Molecular and Biomolecular Spectroscopy*, **118**, 776-781.
- Cheng, Y. F., Iraneta, P., Neue, U. D., Bouvier, E. S. P., Phillips, D. J. 1998. SPE with Oasis® HLB sorbent: simple procedures for superior sample preparation, Vol. 2017, Water Corporation.
- Chiu, G., Eubanks, R. D. 1989. Spectrophotometric determination of bromide. *Microchimica Acta*, **98**(4), 145-148.
- Cioran, A. M., Teixidor, F., Krpetic, Z., Brust, M., Vinas, C. 2014. Preparation and characterization of Au nanoparticles capped with mercaptocarboranyl clusters. *Dalton Transactions*, **43**(13), 5054-5061.
- Cova, D., Molinari, G.P., Rossini, L. 1986. Residues after fumigation with methyl bromide: Bromide ion and methyl bromide in middlings and final cereal foodstuffs. *Food Additives & Contaminants*, **3**(3), 235-240.
- Elavarasi, M., Rajeshwari, A., Chandrasekaran, N., Mukherjee, A. 2013. Simple colorimetric detection of Cr(III) in aqueous solutions by as synthesized citrate capped gold nanoparticles and development of a paper based assay. *Analytical Methods*, **5**(21), 6211-6218.
- Environmental Protection Agency. 1999. Protection of stratospheric ozone: Incorporation of montreal protocol adjustment for a 1999 interim reduction in class I, group VI controlled substances, *Federal Register*, **64**(104), 29240-29245.

- FAO. 1999. Codex maximum limits for pesticide residues, Codex Alimentarius Commission, FAO plant production and protection paper, Food Agriculture Organization-World Health Organization.
- Frens, G. 1973. Controlled nucleation for the regulation of the particle size in monodisperse gold suspensions. *Nature Physical Science*, **241**(105), 20-22.
- Fu, L., Li, C., Li, Y., Chen, S., Long, Y., Zeng, R. 2017. Simultaneous determination of iodide and bromide using a novel LSPR fluorescent Ag nanocluster probe. *Sensors and Actuators B: Chemical*, **240**, 315-321.
- Gabriel, C., Raptopoulou, C. P., Terzis, A., Tangoulis, V., Mateescu, C., Salifoglou, A. 2007. pH-specific synthesis and spectroscopic, structural, and magnetic studies of a chromium(III)-citrate species. Aqueous solution speciation of the binary chromium(III)-citrate system. *Inorganic Chemistry*, **46**(8), 2998-3009.
- Gallardo, H., Queralt, I., Tapias, J., Candela, L., Margui, E. 2016. Bromine and bromide content in soils: Analytical approach from total reflection X-ray fluorescence spectrometry. *Chemosphere*, **156**, 294-301.
- Garcia-Figueroa, A., Pena-Pereira, F., Lavilla, I., Bendicho, C. 2017. Headspace single-drop microextraction coupled with microvolume fluorospectrometry for highly sensitive determination of bromide. *Talanta*, **170**, 9-14.
- Ghosh, S. K., Pal, T. 2007. Interparticle coupling effect on the surface plasmon resonance of gold nanoparticles: From theory to applications. *Chemical Reviews*, **107**(11), 4797-4862.
- Guo, C., Hall, G., Addison, J. B., Yarger, J. 2014. Gold nanoparticle-doped silk films as biocompatible SERS substrate. *RSC Advances*, **5**, 1937-1942.
- Hanaor, D., Michelazzi, M., Leonelli, C., Sorrell, C. C. 2012. The effects of carboxylic acids on the aqueous dispersion and electrophoretic deposition of ZrO<sub>2</sub>. *Journal of the European Ceramic Society*, **32**(1), 235-244.
- Hatamie, A., Zargar, B., Jalali, A. 2014. Copper nanoparticles: a new colorimetric probe for quick, naked-eye detection of sulfide ions in water samples. *Talanta*, **121**, 234-238.
- Holder, A. L., Marr, L. C. 2013. Toxicity of silver nanoparticles at the air-liquid interface. *BioMed Research International*, **2013**, 1-11.

- Hormozi-Nezhad, M. R., Abbasi-Moayed, S. 2014. A sensitive and selective colorimetric method for detection of copper ions based on anti-aggregation of unmodified gold nanoparticles. *Talanta*, **129**, 227-232.
- Ji, X., Song, X., Li, J., Bai, Y., Yang, W., Peng, X. 2007. Size control of gold nanocrystals in citrate reduction: The third role of citrate. *Journal of the American Chemical Society*, **129**(45), 13939-13948.
- Kailasa, S. K., Chandel, M., Mehta, V. N., Park, T. J. 2018. Influence of ligand chemistry on silver nanoparticles for colorimetric detection of Cr<sup>3+</sup> and Hg<sup>2+</sup> ions. *Spectrochimica Acta Part A: Molecular and Biomolecular Spectroscopy*, **195**, 120-127.
- Kang, J., Zhang, Y., Li, X., Miao, L., Wu, A. 2016. A rapid colorimetric sensor of clenbuterol based on cysteamine-modified gold nanoparticles. *ACS Applied Materials & Interfaces*, **8**(1), 1-5.
- Kong, S., Liao, M., Gu, Y., Li, N., Wu, P., Zhang, T., He, H. 2016. Colorimetric recognition of pazufloxacin mesilate based on the aggregation of gold nanoparticles. *Spectrochimica Acta Part A: Molecular and Biomolecular Spectroscopy*, **157**, 244-250.
- Kornev, V. I., Mikryukova, G. A. 2004. Coordination compounds of chromium(III) with different complexones and citric acid in aqueous solutions. *Russian Journal of Coordination Chemistry*, **30**(12), 895-899.
- Lepore, B. J., Barak, P. 2009. A colorimetric microwell method for determining bromide concentrations. *Soil Science Society of America Journal*, **73**(4), 1130.
- Li, Y., Wu, P., Xu, H., Zhang, Z., Zhong, X. 2011. Highly selective and sensitive visualizable detection of Hg<sup>2+</sup> based on anti-aggregation of gold nanoparticles. *Talanta*, **84**(2), 508-12.
- Ling, J., Sang, Y., Huang, C. Z. 2008. Visual colorimetric detection of berberine hydrochloride with silver nanoparticles. *Journal of Pharmaceutical and Biomedical Analysis*, **47**(4), 860-864.
- Liu, D., Wang, Z., Jiang, X. 2011. Gold nanoparticles for the colorimetric and fluorescent detection of ions and small organic molecules. *Nanoscale*, **3**(4), 1421-1433.
- Liu, Y., Wang, X. 2013. Colorimetric speciation of Cr(III) and Cr(VI) with a gold nanoparticle probe. *Analytical Methods*, **5**(6), 1442-1448.

- Lu, L., Tian, S., Liao, H., Zhang, J., Yang, X., Labavitch, J.M., Chen, W. 2013. Analysis of metal element distributions in rice (*Oryza sativa* L.) seeds and relocation during germination based on X-ray fluorescence imaging of Zn, Fe, K, Ca, and Mn. *PLOS One*, **8**(2), 1-9.
- Mahmoud, A.A., Gouda, R., Ryad, L. 2014. Determination and validation of inorganic bromide by gas chromatograph in several foods. *Journal of Plant Protection and Pathology, Mansoura University*, **5**(11), 1015-1023.
- Majzik, A., Fulop, L., Csapo, E., Bogar, F., Martinek, T., Penke, B., Biro, G., Dekany, I. 2010. Functionalization of gold nanoparticles with amino acid, beta-amyloid peptides and fragment. *Colloids and Surfaces B: Biointerfaces*, **81**(1), 235-41.
- Mehta, V. N., Kailasa, S. K., Wu, H. F. 2014. Sensitive and selective colorimetric sensing of Fe<sup>3+</sup> ion by using p-amino salicylic acid dithiocarbamate functionalized gold nanoparticles. *New Journal of Chemistry*, **38**(4), 1503-1511.
- Merk, V., Rehbock, C., Becker, F., Hagemann, U., Nienhaus, H., Barcikowski, S. 2014. In situ non-DLVO stabilization of surfactant-free, plasmonic gold nanoparticles: effect of Hofmeister's anions. *Langmuir*, **30**(15), 4213-4222.
- Miller, J. N., Miller, J. C. 2015. *Statistics and Chemometrics for Analytical Chemistry. 6th ed.*, Pearson Education, UK.
- Miyahara, M., Saito, Y. 1994. Determination of bromide ions in food by unsuppressed ion chromatography with ultraviolet detection after microwave digestion in a sealed PTFE vessel. *Journal of Agricultural and Food Chemistry*, **42**(5), 1126-1131.
- Muller, E. I., Souza, J. P., Anschau, K. F., Enders, M. S. P., Muller, A. L. H., Mortari, S. R., Duarte, F. A. 2017. Determination of Br, Cl and I in honey using ICP-based techniques following microwave-assisted wet digestion with alkaline H<sub>2</sub>O<sub>2</sub> in a single reaction chamber. *Analytical Methods*, **9**(4), 649-654.
- Nguyen, T. K. D., Ludwig, R. 2014. Quantitative determination of bromine and iodine in food samples using ICP-MS. *Analytical Science*, **30**, 1089-1092.
- NIOSH. 1996. Methyl bromide. in: *NIOSH Pocket Guide to Chemical Hazards*, (Ed.) 4, Vol. 2018, National Institute for Occupational Safety and Health.
- Norman, K. N. T. 2000. The persistence of methyl bromide residues in rice, dried fruit, seeds and nuts following laboratory fumigation. *Pest Management Science*, **56**, 154-158.



- Notification of the Ministry of Public Health. 2013. Notification of the Ministry of Public Health (No. 361) B.E. 2556, The Government Gazette, pp. 5.
- NPIC. 2000. Methyl bromide. in: *Technical Fact Sheet*, (Ed.) National Pesticide Information Center, Oregon State University. Oregon.
- Pamies, R., Zhu, K., Kjøniksen, A. L., Nyström, B. 2016. Temperature effects on the stability of gold nanoparticles in the presence of a cationic thermoresponsive copolymer. *Journal of Nanoparticle Research*, **18**(11), 1-12.
- Parengam, M., Judprasong, K., Srianujata, S., Jittinandana, S., Laoharojanaphand, S., Busamongko, A. 2010. Study of nutrients and toxic minerals in rice and legumes by instrumental neutron activation analysis and graphite furnace atomic absorption spectrophotometry. *Journal of Food Composition and Analysis*, **23**(4), 340-345.
- Park, J. W., Shumaker-Parry, J. S. 2014. Structural study of citrate layers on gold nanoparticles: role of intermolecular interactions in stabilizing nanoparticles. *Journal of the American Chemical Society*, **136**(5), 1907-1921.
- Peiris, S., McMurtrie, J., Zhu, H. 2015. Metal nanoparticle photocatalysts: Emerging processes for green organic synthesis. *Catalysis Science & Technology*, **6**, 320-338.
- Peixoto de Almeida, M., Pereira, E., Baptista, P., Gomes, I., Figueiredo, S., Soares, L., Franco, R. 2014. Gold nanoparticles as (Bio)chemical sensors. in: *Comprehensive Analytical Chemistry*, (Eds.) M. Valcárcel, Á.I. López-Lorente, Vol. 66, Elsevier, pp. 529-567.
- Perrone, P.A., Reuter, W.M., Neubauer, K.R., Bosnak, C.P., Hall, G.A., Grosser, Z.A. 2005. Bromine speciation by HPLC/ICP-MS. PerkinElmer Life and Analytical Sciences, USA.
- Pesic, B., Sergent, R. H. 1993. Reaction mechanism of gold dissolution with bromine. *Metallurgical and Materials Transactions B*, **24**(3), 419-431.
- Pfeiffer, C., Rehbock, C., Huhn, D., Carrillo-Carrion, C., de Aberasturi, D. J., Merk, V., Barcikowski, S., Parak, W.J. 2014. Interaction of colloidal nanoparticles with their local environment: the (ionic) nanoenvironment around nanoparticles is different from bulk and determines the physico-chemical properties of the nanoparticles. *Journal of the Royal Society Interface*, **11**(96), 1-13.

- Pimpun, P. 2013. Methyl bromide and bromide ion, Department of Agriculture, Thailand. <http://www.thaipan.org/sites/default/files/file/4%20MB-Br%20Prapassara.pdf>, accessed 5. 8. 2016.
- Pinto, V.V., Ferreira, M.J., Silva, R., Santos, H.A., Silva, F., Pereira, C.M. 2010. Long time effect on the stability of silver nanoparticles in aqueous medium: Effect of the synthesis and storage conditions. *Colloids and Surfaces A: Physicochemical and Engineering Aspects*, **364**(1-3), 19-25.
- Polte, J. 2015. Fundamental growth principles of colloidal metal nanoparticles - a new perspective. *CrystEngComm*, **17**(36), 6809-6830.
- Polte, J., Ahner, T.T., Delissen, F., Sokolov, S., Emmerling, F., Thünemann, A.F., Kraehnert, R. 2010. Mechanism of gold nanoparticle formation in the classical citrate synthesis method derived from coupled in situ XANES and SAXS evaluation. *Journal of the American Chemical Society*, **132**(4), 1296-1301.
- Priyadarshini, E., Pradhan, N. 2017. Gold nanoparticles as efficient sensors in colorimetric detection of toxic metal ions: A review. *Sensors and Actuators B: Chemical*, **238**, 888-902.
- Rujiralai, T., Raekasin, N., Cheewasedtham, W., Cheewasedtham, C. 2014. Development of an effective extraction process for coenzyme Q<sub>10</sub> from Artemia. *Chemical Papers*, **68**(8), 1041-1048.
- Safavi, A., Ahmadi, R., Mohammadpour, Z. 2017. Colorimetric sensing of silver ion based on anti aggregation of gold nanoparticles. *Sensors and Actuators B: Chemical*, **242**, 609-615.
- Sarigalaya, C. 2015. Commerce Ministry: Rice exports for 2014 the highest in history Thai, Vol. 2018, ThaiPBS. <http://englishnews.thaipbs.or.th/commerce-ministry-rice-export-2014-highest-history/>, accessed 22. 1. 2018.
- Senanayake, G. 2004. Gold leaching in non-cyanide lixiviant systems: critical issues on fundamentals and applications. *Minerals Engineering*, **17**(6), 785-801.
- Shamsipur, M., Rouhani, S., Mohajeri, A., Ganjali, M.R., Rashidi-Ranjbar, P. 2000. A bromide ion-selective polymeric membrane electrode based on a benzo-derivative xanthenium bromide salt. *Analytica Chimica Acta*, **418**(2), 197-203.
- Shrivastava, K., Sahu, S., Patra, G. K., Jaiswal, N. K., Shankar, R. 2016. Localized surface plasmon resonance of silver nanoparticles for sensitive colorimetric detection of chromium in surface water, industrial waste water and vegetable samples. *Analytical Methods*, **8**(9), 2088-2096.

- Skoog, D.A., Leary, J.J. 1992. *Principles of instrumental analysis*, USA.
- Soomro, R. A., Nafady, A., Sirajuddin, Memon, N., Sherazi, T. H., Kalwar, N. H. 2014. L-cysteine protected copper nanoparticles as colorimetric sensor for mercuric ions. *Talanta*, **130**, 415-22.
- Spiccia, L., Marty, W. 1986. The fate of "active" chromium hydroxide,  $\text{Cr}(\text{OH})_3 \cdot 3\text{H}_2\text{O}$ , in aqueous suspension. Study of the chemical changes involved in its aging. *Inorganic Chemistry*, **25**(3), 266-271.
- Srisawat, U., Panunto, W., Kaendee, N., Tanuchit, S., Itharat, A., Lerdvuthisophon, N., Hansakul, P. 2010. Determination of phenolic compounds, flavonoids, and antioxidant activities in crude water extracts of Thai red and white rice cultivars. *Journal of the Medical Association of Thailand*, **76**(12), S82-S91.
- Sun, H., Xia, L., Liang, S., Shen, S. 2014. The correlation of inorganic anion contents in rice and its soils based on four geographical origin. *Food Analytical Methods*, **7**(9), 1791-1797.
- Sungwaranond, B., Jongmeevasana, P., Thoophom, G. 1998. Gas chromatographic determination of inorganic bromide in rice and glutinous rice. *The Bulletin of the Department of Medical Sciences, Thailand*, **40**(2), 171-177.
- Thai-PAN. 2013. The detection of methyl bromide residue in various brands in the market, Vol. 2016, Thailand Pesticide Alert Network (Thai-PAN).
- The Federal Register. 1999. Protection of stratospheric ozone: Incorporation of Montreal Protocol
- The Montreal Protocol on Substances that Deplete the Ozone Layer. 1987. The montreal protocol on substances that deplete the ozone layer/article 2H: Methyl bromide, <http://www.ozone.unep.org/en/handbook-montreal-protocol-substances-depleteozone-layer/16>, accessed 9. 04. 2018.
- Thomas, W. B. 1996. Methyl bromide: Effective pest management tool and environmental threat. *Journal of Nematology*, **28**(4S), 586-589.
- Toma, H. E., Zamarion, V. M., Toma, S. H., Araki, K. 2010. The coordination chemistry at gold nanoparticles. *Journal of the Brazilian Chemical Society*, **21**, 1158-1176.
- Turkevich, J., Stevenson, P.C., Hillier, J. 1951. A study of the nucleation and growth processes in the synthesis of colloidal gold. *Discussions of the Faraday Society*, **11**, 55-75.

- U.S. Department of Health and Human Services. 1978. *Occupational health guideline for methyl bromide*.
- U.S. EPA. 1978. Method 410.3: Chemical Oxygen Demand (Titrimetric, High Level for Saline Waters) by Titration, United States Environmental Protection Agency.
- U.S. EPA. 1997. Office of Pesticide Programs. in: *U.S. Government Printing Office*, United States Environmental Protection Agency. Washington, DC.
- van Leeuwen, F. X. R., den Tonkelaar, E. M., van Logten, M. J. 1983. Toxicity of sodium bromide in rats: Effects on endocrine system and reproduction. *Food and Chemical Toxicology*, **21**(4), 383-389.
- Vinokurov, E. G., Bondar, V. V. 2003. Prediction of stability constants for Cr(III) and Cr(II) complexes. *Russian Journal of Coordination Chemistry*, **29**(1), 66-72.
- Wang, X., Wei, Y., Wang, S., Chen, L. 2015. Red-to-blue colorimetric detection of chromium via Cr (III)-citrate chelating based on Tween 20-stabilized gold nanoparticles. *Colloids and Surfaces A: Physicochemical and Engineering Aspects*, **472**, 57-62.
- WHO. 2009. Bromide in drinking-water. in: *Background document for development of WHO Guidelines for Drinking-water Quality*, (Ed.) World Health Organization. Geneva, Switzerland.
- Wittayanan, W., Jongmevasna, W. 2015. Method development and removal of methyl bromide residue determined as total inorganic bromide in rice by gas chromatographic technique. *The Bulletin of the Department of Medical Sciences, Thailand*, **57**(3), 219-232.
- Wittayanan, W., Jongmevasna, W., Kaewklapanacharoen, L., Atisook, K. 2017. Method development and validation of hydrogen phosphide and inorganic bromide determined as fumigant residues in commercialized rice grains in Thailand. *International Food Research Journal*, **24**(3), 1204-1211.
- Yang, X., Yang, M., Pang, B., Vara, M., Xia, Y. 2015. Gold nanomaterials at work in biomedicine. *Chemical Reviews*, **115**(19), 10410-88.
- Yassaa, N., Wishkerman, A., Keppler, F., Williams, J. 2009. Fast determination of methyl chloride and methyl bromide emissions from dried plant matter and soil samples using HS-SPME and GC-MS: method and first results. *Environmental Chemistry*, **6**(4), 311-318.

- Yu, L., Zhang, X., Jin, J., Che, S., Yu, L. 2011. Simultaneous determination of chloride, bromide and iodide in foodstuffs by low pressure ion-exchange chromatography with visible light detection. *Czech Journal of Food Sciences*, **29**(6), 634-640.
- Zhang, M., Liu, Y.Q., Ye, B. C. 2011. Colorimetric assay for sulfate using positively-charged gold nanoparticles and its application for real-time monitoring of redox process. *Analyst*, **136**(21), 4558-4562.
- Zhou, J., Ralston, J., Sedev, R., Beattie, D. A. 2009. Functionalized gold nanoparticles: synthesis, structure and colloid stability. *Journal of Colloid and Interface Science*, **331**(2), 251-262.
- Zhou, Y., Dong, H., Liu, L., Li, M., Xiao, K., Xu, M. 2014. Selective and sensitive colorimetric sensor of mercury (II) based on gold nanoparticles and 4-mercaptophenylboronic acid. *Sensors and Actuators B: Chemical*, **196**, 106-111.

## Appendix A

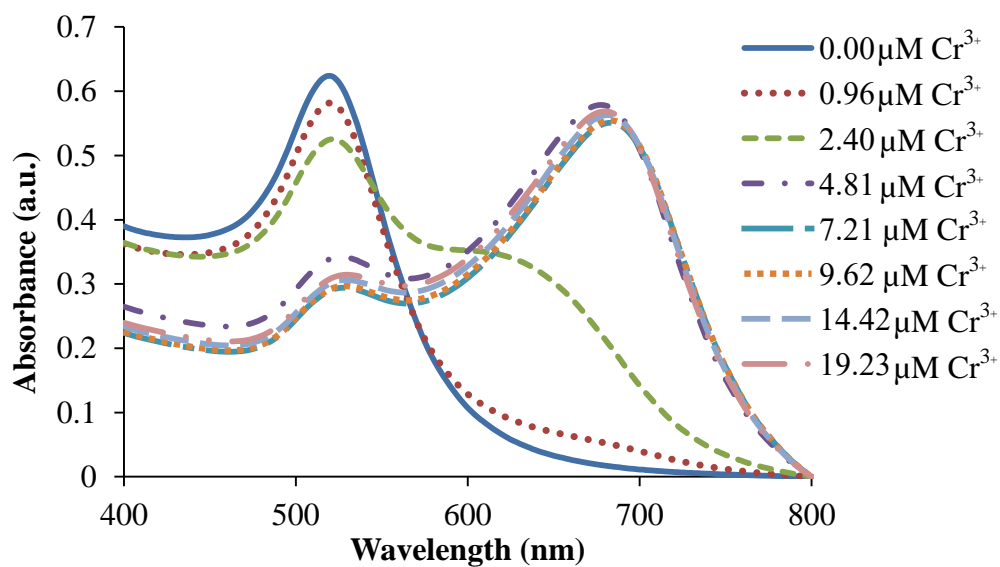


**Figure A1** The UV-Vis absorption spectra of AuNPs on the concentration of  $\text{Cr}^{3+}$  ranged from 0.00 - 19.23  $\mu\text{M}$ .

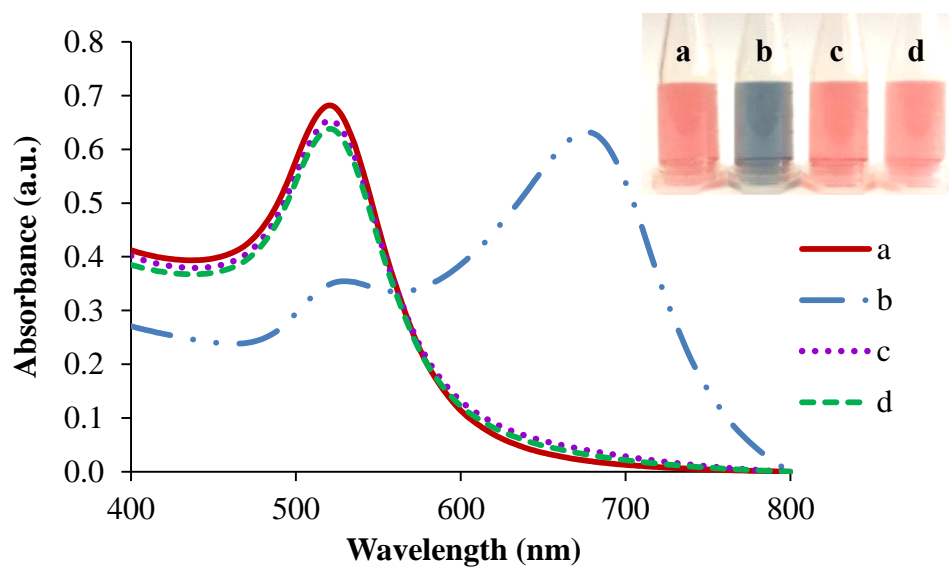


**Figure A2** The UV-Vis absorption spectra of (a) AuNPs, (b) AuNPs + 50  $\mu\text{M}$   $\text{Cr}^{3+}$ , (c) AuNPs + 50  $\mu\text{M}$   $\text{Fe}^{3+}$  and (d) AuNPs + 50  $\mu\text{M}$   $\text{Al}^{3+}$  prepared in 10 mM phosphate buffer (pH 7.0). Inset is the corresponding photograph of a - d.

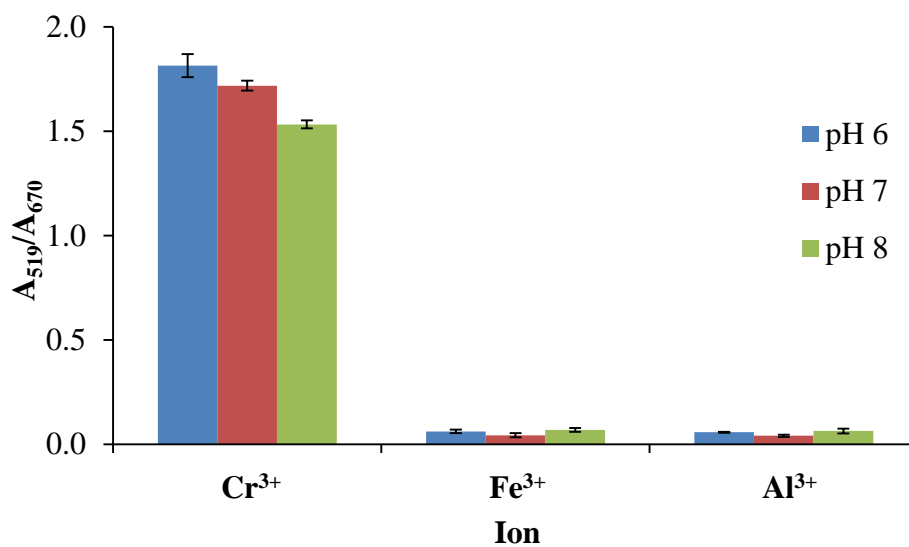


**Figure A3** Effect of pH of phosphate buffer on aggregation of AuNPs in the presence of  $Cr^{3+}$ ,  $Fe^{3+}$  and  $Al^{3+}$ .

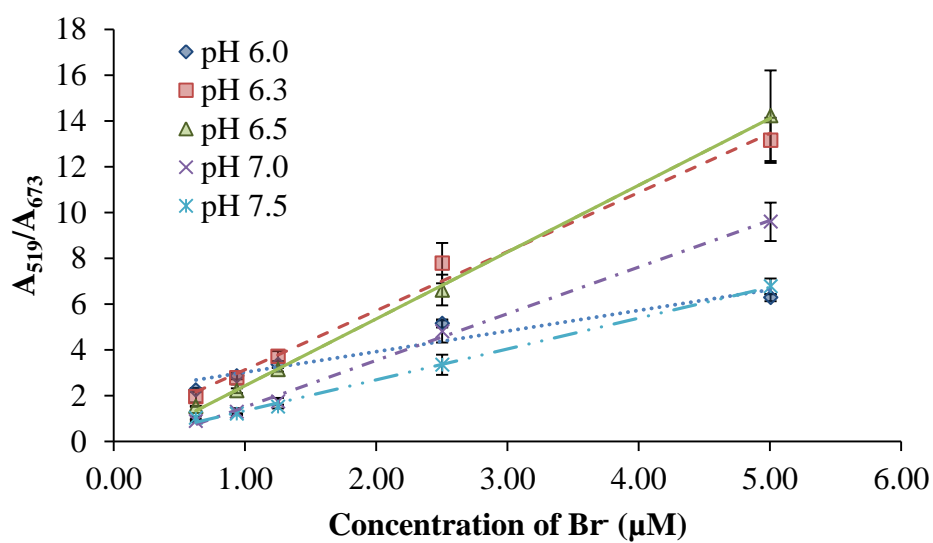


**Figure A4** Effect of pH of phosphate buffer on the linearity curve of  $Br^-$  concentration ranged from 0.63 - 5.01  $\mu M$ .

**Table A1** The corresponding linear equation and coefficient of determination ( $R^2$ ) obtained from the result of the effect of phosphate buffer pH (Figure A2).

pH of buffer	Linear equation	$R^2$
6.0	$y = (0.8986 \pm 0.1563)x + (2.1210 \pm 0.4084)$	$0.9168 \pm 0.5600$
6.3	$y = (2.5815 \pm 0.1429)x + (0.5437 \pm 0.3735)$	$0.9909 \pm 0.5121$
6.5	$y = (2.9188 \pm 0.0482)x - (0.4853 \pm 0.1260)$	$0.9992 \pm 0.1728$
7.0	$y = (2.0373 \pm 0.0655)x - (0.5425 \pm 0.1712)$	$0.9969 \pm 0.2348$
7.5	$y = (1.3484 \pm 0.0416)x - (0.0077 \pm 0.1088)$	$0.9972 \pm 0.1491$

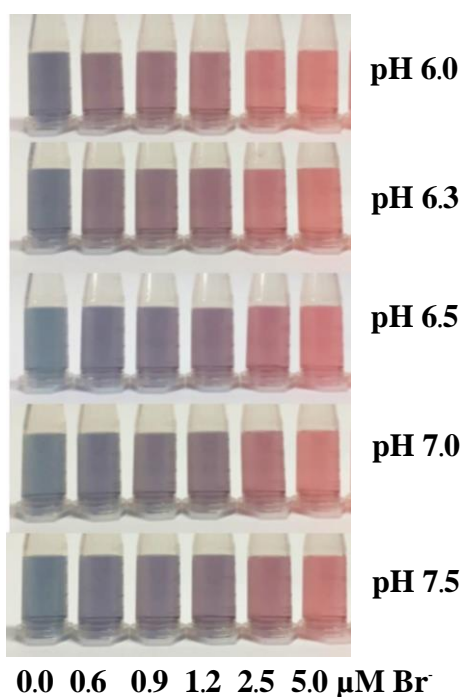


**Figure A5** The color of solution on the effect of pH of phosphate buffer corresponding to the linearity curve of  $Br^-$  concentration ranged from 0.63 - 5.01  $\mu M$   $Br^-$  (Figure A2).



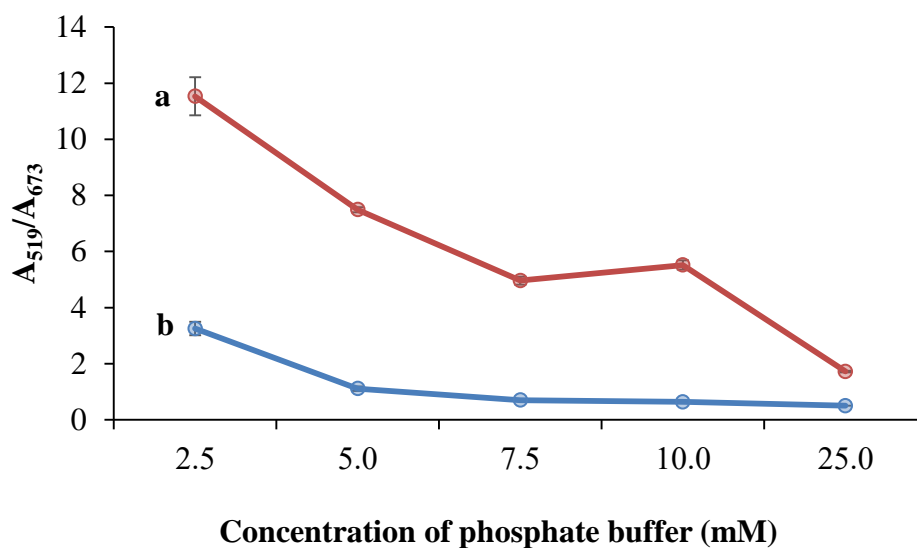


**Figure A6** The effect of phosphate buffer concentration (pH 6.5). (a) Analyte signal ( $0.25 \mu\text{M Br}^-$ ) and (b) Blank signal (no  $\text{Br}^-$ ).

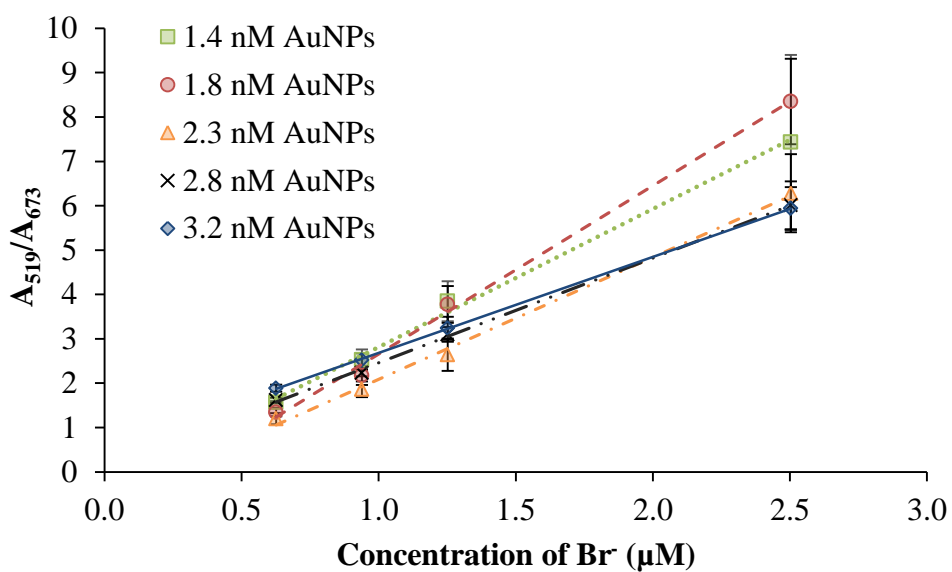


**Figure A7** The effect of concentration of AuNPs on the linearity curve of  $\text{Br}^-$  concentration ranged from  $0.63 - 2.50 \mu\text{M}$ .

**Table A2** The corresponding linear equation and coefficient of determination ( $R^2$ ) obtained from the result of the effect of concentration of AuNPs (Figure A5).

Concentration of AuNPs (nM)	Linear equation	$R^2$
1.4	$y = (3.1129 \pm 0.1415)x - (0.2959 \pm 0.2134)$	$0.9959 \pm 0.2016$
1.8	$y = (3.7940 \pm 0.1572)x - (1.1324 \pm 0.2372)$	$0.9966 \pm 0.2240$
2.3	$y = (2.7518 \pm 0.1062)x - (0.6621 \pm 0.1602)$	$0.9970 \pm 0.1514$
2.8	$y = (2.3613 \pm 0.0513)x + (0.0996 \pm 0.0774)$	$0.9991 \pm 0.0732$
3.2	$y = (2.1662 \pm 0.0166)x + (0.5161 \pm 0.0250)$	$0.9999 \pm 0.0237$



**Figure A8** The color of solution on the effect of concentration of AuNPs corresponding to the linearity curve of  $\text{Br}^-$  concentration ranged from 0.63 - 2.50  $\mu\text{M}$   $\text{Br}^-$  (Figure A5).

**Table A3** The repeatability measurement of blank signal (n = 20)

Time	Absorbance intensity (a.u.)		Absorbance intensity ratio ( $A_{519}/A_{673}$ )
	519 nm ( $A_{519}$ )	673 nm ( $A_{673}$ )	
1	0.2709	0.4795	0.5650
2	0.2986	0.5171	0.5775
3	0.2878	0.5232	0.5501
4	0.2915	0.5036	0.5788
5	0.2928	0.5296	0.5529
6	0.2852	0.5020	0.5681
7	0.2916	0.5290	0.5512
8	0.2802	0.4944	0.5667
9	0.2899	0.5263	0.5508
10	0.2897	0.5259	0.5509
11	0.2971	0.4898	0.6066
12	0.3126	0.4927	0.6345
13	0.3146	0.4847	0.6491
14	0.3140	0.4792	0.6553
15	0.3264	0.4806	0.6792
16	0.3200	0.4953	0.6461
17	0.3174	0.4891	0.6489
18	0.3179	0.4958	0.6412
19	0.3140	0.4975	0.6312
20	0.3125	0.4891	0.6389
<b>Average</b>			<b>0.6021</b>
<b>SD</b>			<b>0.0446</b>

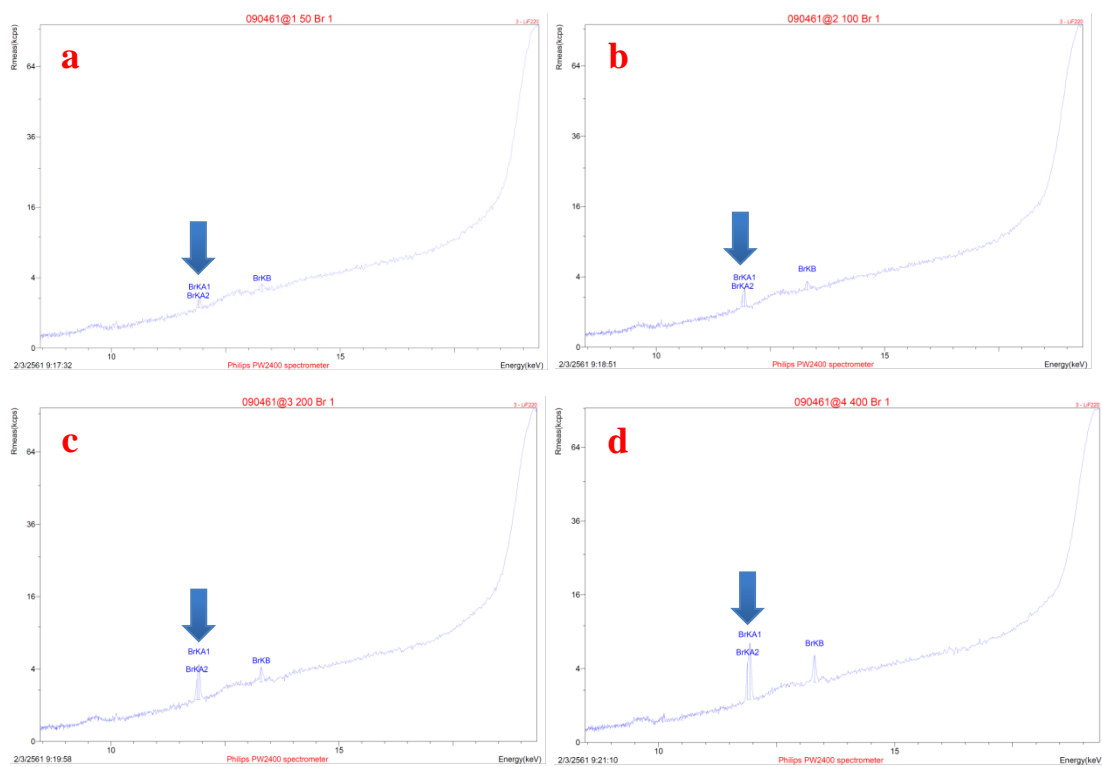


**Figure A9** The XRF spectra of (a) 50, (b) 100, (c) 200 and (d) 400 mg L<sup>-1</sup> Br<sup>-</sup> spiked in the composite rice samples.

## Appendix B

### The calculation of concentration of AuNPs

The concentration of origin AuNPs was calculated according to Beer's Law. The AuNPs were 2.5 times diluted before absorbance measurement (Figure B1).

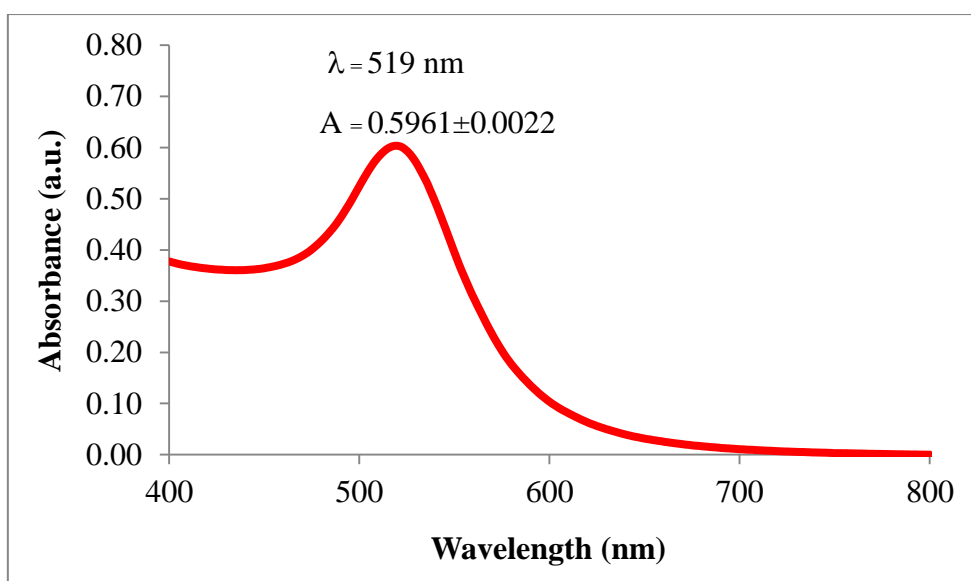


**Figure B1** The UV-Vis adsorption spectrum of diluted AuNPs.

#### Calculation

$$A = \epsilon bc$$

$$c = \frac{0.5961}{1 \times 2.7 \times 10^8}$$

$$c = 2.2078 \text{ nM}$$

$$\text{So; [AuNPs]} = 2.2078 \times 2.5 = 5.52 \text{ nM}$$

When  $A$  : The absorbance of AuNPs solution

$\epsilon$  : The extinction coefficient of AuNPs at 520 nm =  $2.70 \times 10^8 \text{ M}^{-1} \text{ cm}^{-1}$   
(Liu et al., 2011)

$b$  : Path length of cell = 1 cm

$c$  : The concentration of particles

[AuNPs] : Initial concentration of AuNPs

**Appendix C**  
**Publication**

## PAPER

Cite this: *RSC Adv.*, 2018, 8, 21566

# Robust colorimetric detection based on the anti-aggregation of gold nanoparticles for bromide in rice samples†

Siwat Plaisen,<sup>ab</sup> Wilairat Cheewasedtham <sup>b</sup> and Thitima Rujiralai <sup>\*ab</sup>

Inorganic bromide ( $\text{Br}^-$ ) is an important contaminant ion as it can originate from the overuse of illegal methyl bromide as a fumigant in stored rice samples. Herein, we developed a simple and highly sensitive colorimetric sensor for bromide ion detection in rice samples. The sensor is based on the anti-aggregation of gold nanoparticles (AuNPs) by  $\text{Br}^-$  in the presence of  $\text{Cr}^{3+}$ , which made the method more selective than other typical aggregations of nanoparticles. The AuNPs underwent an aggregation process as a result of the coordination of  $\text{Cr}^{3+}$  and the carboxylate group of a citrate ion stabilized the AuNPs, resulting in a red-to-blue color change. When  $\text{Br}^-$  was pre-mixed with the AuNPs and  $\text{Cr}^{3+}$  was added, the solution color changed from blue to red with an increase in the  $\text{Br}^-$  concentration. The anti-aggregation process can be detected with the naked eye and monitored using UV-vis spectrophotometry. The linear calibration curve ranged between 0.31 and 3.75  $\mu\text{M}$   $\text{Br}^-$  with a low LOD and LOQ of 0.04 and 0.13  $\mu\text{M}$ . The recovery was excellent, ranging from 79.9–92.2% with an RSD of less than 4.0%. The good inter-day and intra-day precisions were 2.9–6.4% and 3.1–7.1%, respectively. The developed sensor has proved to provide a robust method for  $\text{Br}^-$  detection in rice samples.

Received 23rd April 2018  
Accepted 28th May 2018

DOI: 10.1039/c8ra03497d

[rsc.li/rsc-advances](http://rsc.li/rsc-advances)

## 1. Introduction

Methyl bromide ( $\text{CH}_3\text{Br}$ ) is a fumigant that is often used for controlling a variety of pests such as insects, mites, moulds, nematodes, weeds, viruses and bacteria, as well as being used in soil disinfection and as a postharvest treatment for stored and dried foodstuffs including rice, tobacco, fresh fruits and vegetables.<sup>1–3</sup> It is dominant over other fumigants due to the fact it is a colorless, odorless (at low concentrations) and non-flammable gas with a high rate of penetration.<sup>2–4</sup> Its toxic effects on human health are (following short-term exposure) headache, dizziness, nausea, vomiting, blurred vision, slurred speech and convulsions. High concentrations of methyl bromide may cause unconsciousness and death. Prolonged exposure to methyl bromide may cause injury to the central nervous system.<sup>4</sup> Furthermore, it can greatly destroy the ozone layer through emission from agricultural pesticide use, from the burning of biomass and leaded gasoline, and from the ocean.<sup>5,6</sup> Thus, the use of methyl bromide is controlled by many organizations and

it is already being phased out. From January 1 2005, the production and use of methyl bromide will be stopped in the U.S.A. with exemptions for emergency and critical use.<sup>5–7</sup> The agricultural use of methyl bromide in China will also be terminated at the end of 2018.<sup>8</sup> The application of methyl bromide in the European Union has been forbidden since 2010, but exceptions are made, especially with regard to the International Standards for Phytosanitary Measures 15.<sup>9</sup>

After food commodities are fumigated, methylated products and inorganic bromide are formed as a result of chemical reactions with some of the constituents of the treated foodstuffs or the breakdown products of methyl bromide.<sup>1–3,10,11</sup> Inorganic bromide has been detected in rice and glutinous rice in the ranges 0.13–11.93  $\text{mg kg}^{-1}$  and 0.20–1.37  $\text{mg kg}^{-1}$ , respectively, and its concentration in all samples were within the Codex maximum residue limit value of 50  $\text{mg kg}^{-1}$ .<sup>2</sup> Methyl bromide residues can persist in nuts and seeds for 10 weeks and in dried fruit for 4 weeks.<sup>1</sup> Cova *et al.* reported that higher concentrations of bromide ions were detected in fumigated pastas with eggs, pastas with eggs and spinach, and rice compared to in those that were unfumigated.<sup>11</sup>

Thailand, as the world's leading rice producer and also one of the largest rice consumers, imported an average of 357.69 and 103.85 tons per year of methyl bromide and a mixture between methyl bromide and chloropicrin, respectively, to eliminate undesired pests before commercializing their products between 2007 and 2012.<sup>2</sup> Due to its toxicity, under the agreement of the Montreal Protocol, Thailand agreed to

<sup>a</sup>Department of Chemistry, Center of Excellence for Innovation in Chemistry, Faculty of Science, Prince of Songkla University, Hat Yai, Songkhla, 90112 Thailand. E-mail: thitima.r@psu.ac.th

<sup>b</sup>Analytical Chemistry and Environment Research Unit, Division of Chemistry, Department of Science, Faculty of Science and Technology, Prince of Songkla University, Pattani, 94000, Thailand

† Electronic supplementary information (ESI) available. See DOI: 10.1039/c8ra03497d



gradually reduce and to phase out the use of methyl bromide by 2015.<sup>12</sup> The Thai Ministry of Public Health has defined the maximum residue limit (MRL) of methyl bromide in rice as 0.01 mg kg<sup>-1</sup> and of bromide ions in rice as 50 mg kg<sup>-1</sup>.<sup>13</sup> In 2013, methyl bromide was not detected in any rice samples ( $n = 13$ ), however the bromide ion concentration in one sample was detected to be 77.2 mg kg<sup>-1</sup> and after 4 days its concentration had decreased to 20.9 mg kg<sup>-1</sup>.<sup>14</sup>

Due to food globalization, rice consumption is also increasing around the world. The determination of methyl bromide and inorganic bromide contamination in rice is, therefore, required as a method for guaranteeing consumer safety. In most cases, bromide ion contamination in rice has been found when food commodities are fumigated with either low or high concentrations of methyl bromide, and are particularly over the limit when they have been fumigated with methyl bromide multiple times.<sup>1-3,11,14,15</sup> Many studies have also focused on inorganic bromide in food in order to assess the daily intake of bromide ions from food and water into the human body.<sup>10,16,17</sup> Therefore, bromide ions are the main target analyte for this work, whether from the accumulation of bromide ions from the environment or from the transformation of methyl bromide.

Prior to the detection step, bromide ions in foodstuffs have been treated using different procedures *e.g.*, low energy microwave digestion,<sup>16</sup> high temperature heating (~850 °C),<sup>18</sup> hydrolysis with alkaline and ashing at 550 °C,<sup>2</sup> and suspension in 6 N sulfuric acid and propylene oxide followed by extraction with ethyl acetate.<sup>15</sup> Subsequently, the pre-treated samples are determined using sophisticated instrumentation such as inductively coupled plasma-mass spectrometry,<sup>16</sup> gas chromatography-electron capture detecting,<sup>2,15</sup> and ion-exchange chromatography with visible light detection.<sup>19</sup> However, these mentioned instrumentations require not only complex sample preparation and long analysis times but also complicated and expensive instruments.

Nowadays, gold nanoparticle (AuNP)-based colorimetric sensors have drawn increasing attention due to their low cost and their rapid, selective and reliable detection.<sup>20-23</sup> In general, AuNPs change from the dispersion to the aggregation state and their color changes from ruby red to purple or blue.<sup>20-23</sup> An absorption band in the visible range with a high extinction coefficient (*e.g.*,  $2.70 \times 10^8 \text{ M}^{-1} \text{ cm}^{-1}$ )<sup>23</sup> appears when the incident photon frequency resonates with the excitation of the conduction electrons. This phenomenon is named surface plasmon resonance (SPR).<sup>20-23</sup> Due to these advantages, AuNPs can be used as a powerful tool for real-time monitoring *via* naked-eye detection, rather than using any advanced instruments. AuNPs have also been applied for the detection of ions,<sup>20-22,24-28</sup> gas<sup>29</sup> and organic residues<sup>30-34</sup> such as Hg<sup>2+</sup>, Cu<sup>2+</sup>, S<sup>2-</sup>, I<sup>-</sup>, SCN<sup>-</sup>, H<sub>2</sub>S, clenbuterol, aflatoxins, tetracycline, amoxicillin and pazufloxacinmesilate, in which the detection mostly depends on the aggregation. It was reported that AuNP aggregation is not selective and can provide false positive results due to the effects of many other external factors in real applications. Thus, the anti-aggregation or re-dispersion of AuNPs has become a good option to utilise in order to improve selectivity.<sup>21,22,25,27,29</sup>

So far, a colorimetric probe based on the AuNP anti-aggregation process has not been found for bromide ion determination in rice samples. In this work, we developed a AuNP colorimetric sensor for the facile, sensitive and selective detection of bromide ions in rice samples. The sensor is based on the fact that bromide ions prevent the aggregation of AuNPs. The addition of Cr<sup>3+</sup> into a AuNP solution resulted in the aggregation of AuNPs with a red-to-blue color change. In the presence of Br<sup>-</sup>, the aggregation of AuNPs was interrupted and the corresponding color of solution changed from blue to red. The concentration of bromide ions in real samples can be easily observed with the naked eye, and also quantitatively measured using UV-visible spectroscopy.

## 2. Material and methods

### 2.1 Chemical and reagents

All chemicals were of analytical grade. Gold(III) chloride trihydrate (HAuCl<sub>4</sub>·3H<sub>2</sub>O) was purchased from Sigma-Aldrich (USA). Chromium(III) nitrate nanohydrate was purchased from Alfa-Aesar (USA). Trisodium citrate and disodium hydrogenphosphate dodecahydrate were purchased from Ajax Finechem (Australia). Hydrochloric acid, potassium hydroxide, ethanol and nitric acid were purchased from RCI Labscan (Thailand). Potassium bromide and sodium dihydrogen phosphate dehydrate were purchased from LobaChem (India). All solutions were prepared using 18 MΩ cm<sup>-1</sup> ultrapure water obtained from ELGA Maxima.

Sodium phosphate buffer (pH 6.5 at 0.01 M) was prepared by mixing 34 mL of 0.02 M sodium dihydrogenphosphate and 16 mL of 0.02 M disodium hydrogenphosphate. Subsequently, the buffer was adjusted by either sodium dihydrogenphosphate or disodium hydrogenphosphate to obtain a pH of 6.5 and the volume was made up to 100 mL with ultrapure water. A stock solution of 12.52 mM bromide ion was prepared from potassium bromide. It was necessary that all the glassware was thoroughly cleaned in freshly prepared aqua regia solution (3 : 1 v/v HCl–HNO<sub>3</sub>), washed with ultrapure water at least twice and then oven-dried at 150 °C before use to avoid aggregation of gold colloids due to any contaminants.

### 2.2 Synthesis of gold nanoparticles (AuNPs)

The gold nanoparticles (AuNPs) were synthesized *via* the trisodium citrate reduction of HAuCl<sub>4</sub> according to the previous method with slight modification.<sup>20</sup> A volume of 250 mL of 0.015% (m/v) HAuCl<sub>4</sub> solution was added into a 500 mL Duran bottle and was heated to boiling with vigorous stirring. Subsequently, 8.75 mL of 1% (w/v) trisodium citrate solution was added rapidly into the boiling solution followed by stirring. The color of the solution changed from pale yellow to wine red in a few minutes as Au<sup>3+</sup> was reduced to Au<sup>0</sup>, indicating the formation of citrate-capped gold nanoparticles (AuNPs). After that, the AuNP solution was continuously boiled for another 15 min to ensure the reaction was completed. It was then allowed to cool down to room temperature under stirring, and the volume was adjusted to 250 mL with ultrapure water in

a volumetric flask. The spectrum of this synthesized AuNP solution was investigated. For further study, this AuNP solution was stored in an amber bottle at 4 °C. After synthesis, the maximum absorbance of the AuNP solution was 1.49 at a surface plasmon resonance (SPR) wavelength of 519 nm with a calculated particle concentration of 5.52 nM (Fig. S1 (ESI<sup>†</sup>)), according to Beer's law using an extinction coefficient of  $2.70 \times 10^8 \text{ M}^{-1} \text{ cm}^{-1}$ .<sup>23</sup> We have proved that AuNPs synthesized *via* the above method can be kept in a fridge for up to 4 months without any loss of sensitivity together with an absorbance of  $1.49 \pm 0.01$  at 519 nm (Fig. S2 (ESI<sup>†</sup>)).

### 2.3 Characterization

The surface plasmon resonance (SPR) spectra of the synthesized AuNP solution were investigated in the range 400–800 nm using a UV-1800 spectrophotometer (Shimadzu, Japan) in a 1.5 mL disposable polystyrene cuvette. The size and shape of the AuNPs were measured using a transmission electron microscope (TEM, JEM-2010, JEOL, Japan) with a 200 kV acceleration voltage. Before TEM measurements, the samples were diluted 3 times with ultrapure water before deposition and 5  $\mu\text{L}$  of the diluted sample was deposited on the carbon-coated copper grid and then evaporated at room temperature. Moreover, the zeta-potential value and size distribution of the synthesized AuNP solution were studied using a zeta potential analyzer (ZetaPALS, Brookhaven, USA).

### 2.4 Colorimetric determination of bromide ions

To increase the selectivity of the developed method, the determination of the bromide ions in this study was based on the anti-aggregation of AuNPs. A volume of 100  $\mu\text{L}$  of different concentrations of  $\text{Br}^-$  was first added to 400  $\mu\text{L}$  of 5.52 nM AuNP solution containing 500  $\mu\text{L}$  of 10 mM phosphate buffer solution (pH 6.5), and the mixture was mixed well using a vortex mixer. After that, 100  $\mu\text{L}$  of 57.70  $\mu\text{M}$   $\text{Cr}^{3+}$  was added to the mixture with vortex mixing and the solution was incubated for 10 min at room temperature ( $25 \pm 2$  °C) to allow for adequate reaction time and to ensure the color had completely developed. After interaction, the color of the solution was observed with the naked eye. Photographs of the resulting solution were taken and the UV-visible spectra of the mixtures from 400–800 nm were recorded immediately. The spiked samples for recovery in pre-treated samples were investigated using the same procedure.

### 2.5 Sample preparation of rice

White rice samples (five commercial brands) were collected randomly from a supermarket in the Hat Yai district, Songkhla province, Thailand and stored in a refrigerator at 4 °C before the experiment. The rice sample was prepared according to the report of Sungwaranond *et al.* with modifications.<sup>2</sup> The rice sample (100 g) was ground using a Ball mill (Retsch MM400, Germany) to obtain a powder ( $\sim 5$   $\mu\text{m}$ ).

Two grams of the rice powder was added into a 50 mL nickel crucible and digested with 5 mL of 1% potassium hydroxide in 50% ethanol. The sample was boiled on a hotplate (by gradually increasing the heating rate to avoid the sample bumping) until

it was dry and no smoke was observed. Next, it was burned in a muffle furnace at 600 °C for 4 h to eliminate the organic residues in the rice samples. After the obtained ash was allowed to cool down, 15 mL ultrapure water was added and the solution was boiled for 15 min on a hotplate in order to dissolve the inorganic bromide, and was filtered with a 0.22  $\mu\text{m}$  Nylon membrane through a 25 mL volumetric flask. The ash residue was placed in a nickel crucible and was again boiled using another 10 mL ultrapure water. This new solution was filtered through the previous volumetric flask and finally diluted with ultrapure water up to the mark. The sample solution was then diluted 1 fold with ultrapure water before the color reaction was performed.

### 2.6 Optimization of the colorimetric detection of bromide ions

To obtain the best sensitivity of the method, the analytical conditions for the detection of  $\text{Br}^-$ , *i.e.*, the concentration of  $\text{Cr}^{3+}$ , the pH and concentration of the phosphate buffer, the concentration of the AuNPs and the reaction time, were optimized. Each parameter was studied using a one step at a time experiment. All experiments were repeated three times with the results reported as mean  $\pm$  standard deviation (SD). The absorbances at 519 and 673 nm were found to be directly related to the dispersed, aggregated and anti-aggregated states of the AuNPs. Therefore, the absorbance intensity ratio of  $A_{519}/A_{673}$  was used for the quantitative determination of  $\text{Br}^-$ . In order to obtain a representative sample for method development and optimization, five different brands of rice were mixed together. All the statistical analyses were performed using Microsoft Office Excel 2007. The ANOVA at a 95% confidence level was used for data analysis.

## 3. Results and discussion

### 3.1 Proposed sensing mechanism

Fig. 1 shows the proposed mechanism for the successful colorimetric sensor of bromide ions based on the anti-aggregation of AuNPs. The AuNP solution presented a maximum SPR absorption at 519 nm (Fig. 2a) with a red wine color (Fig. 1), which was in good agreement with previous reports.<sup>20–22</sup>

In this study, sodium citrate could act as a reductant and a stabilizer of colloidal AuNPs. Thus, the AuNPs were relatively stable due to the strong electrostatic repulsion between the negatively charged citrate ions on the surface of the AuNPs.<sup>35,36</sup> It was reported that  $\text{Cr}^{3+}$  could coordinate with two citrate ions *via* the hydroxyl groups in each citrate ion with a high formation constant of  $3.89 \times 10^{29}$ .<sup>37,38</sup> Thus, citrate can also be used as the ligand for interaction with  $\text{Cr}^{3+}$ , and  $\text{Cr}^{3+}$  can serve as a cross linking agent between the pairs of citrate-coated AuNPs.<sup>36</sup> This ligand exchange is probably strong enough to overcome the electrostatic repulsion imposed by the citrate-AuNPs, thus inducing the aggregation of the AuNPs.

Upon addition of  $\text{Cr}^{3+}$  (Fig. 1A), the intensity of the SPR band of the AuNPs at 519 nm decreased, and a new absorption band

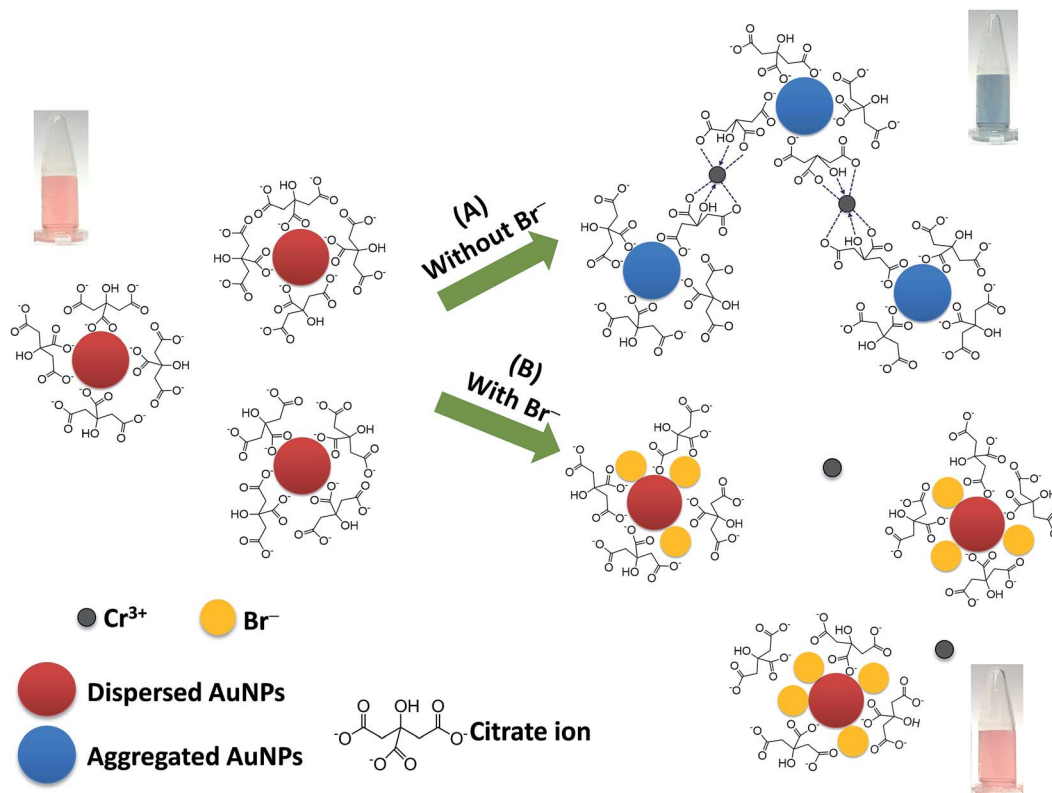


Fig. 1 A proposed mechanism for the colorimetric sensor of bromide ions based on the anti-aggregation of AuNPs.

appeared at 673 nm (Fig. 2b) due to the AuNP aggregation driven by  $\text{Cr}^{3+}$ , demonstrating the successful conjugation of  $\text{Cr}^{3+}$  with the AuNPs. This caused a red-to-blue color change. The result of the aggregation was also confirmed *via* TEM measurement (Fig. 3A). We observed a spherical monodisperse colloid of individual AuNPs before aggregation (Fig. 3A(a)). The average particle size of the prepared AuNPs was  $16.43 \pm 0.81$  nm. In the presence of  $\text{Cr}^{3+}$  (Fig. 3A(b)), heavy aggregation of the AuNPs was observed, confirming that  $\text{Cr}^{3+}$  induced large-scale aggregation of the AuNPs through chelating reactions, resulting in the particle size distribution of the aggregated AuNPs in the presence of  $\text{Cr}^{3+}$  being about 16 times higher than those without  $\text{Cr}^{3+}$  (calculated from the size ratio of 262.30/

16.43 in Fig. 3B(d and e)). A similar phenomenon of aggregation was also reported by Liu and Wang.<sup>39</sup>

When the AuNPs were treated with  $\text{Br}^-$  followed by mixing with  $\text{Cr}^{3+}$  (Fig. 1B), the color of the AuNPs was found to successfully change from blue to wine red, along with

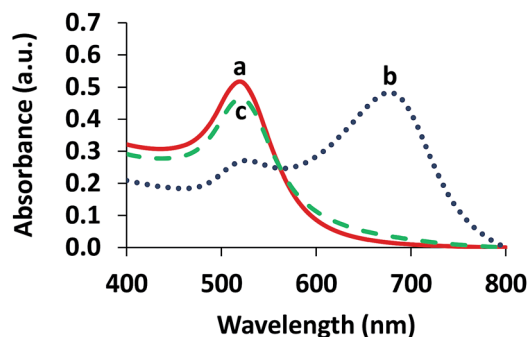


Fig. 2 UV-vis absorption spectra of (a) AuNPs, (b) aggregation of the AuNPs in the presence of  $4.80 \mu\text{M}$   $\text{Cr}^{3+}$  and (c) anti-aggregation of the AuNPs in the presence of  $3.13 \mu\text{M}$   $\text{Br}^-$  and  $4.80 \mu\text{M}$   $\text{Cr}^{3+}$ .

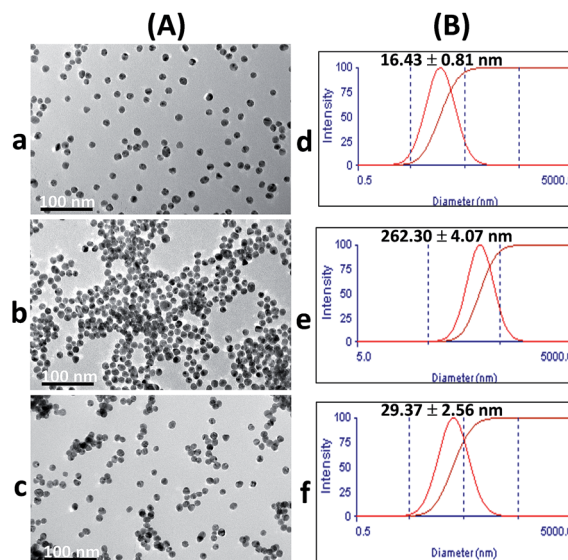


Fig. 3 (A) TEM images and (B) particle size distributions of (a) and (d) AuNPs, (b) and (e) aggregation of the AuNPs in the presence of  $4.80 \mu\text{M}$   $\text{Cr}^{3+}$ , and (c) and (f) anti-aggregation of the AuNPs in the presence of  $3.13 \mu\text{M}$   $\text{Br}^-$  and  $4.80 \mu\text{M}$   $\text{Cr}^{3+}$ .

a decrease in the SPR absorption band at 673 nm and an increase in the band at 519 nm (Fig. 2c). This was called the anti-aggregation of the AuNPs, which was a result of the change of the AuNPs from the aggregation (blue color) to dispersion state (red color).

The anti-aggregation of the AuNPs could be caused by the adsorption of  $\text{Br}^-$  onto the AuNP surface, leading to the prevention of aggregation driven by the  $\text{Cr}^{3+}$ -citrate complex. The bromide ion is a chaotropic anion that can transfer its charge to the AuNP surface and thus, increase electrostatic stabilization.<sup>40</sup> Moreover, the adsorption of  $\text{Br}^-$  on the surface of the AuNPs may prevent aggregation due to a higher stability constant of the Au (1+ or 3+)- $\text{Br}^-$  complex, which is 12.3 and 32.8 for the  $\text{Au}^+$ - and  $\text{Au}^{3+}$ - $\text{Br}^-$  complex, respectively,<sup>41</sup> compared to the lower stability constant of the  $\text{Cr}^{3+}$ - $\text{Br}^-$  complex (-2.66).<sup>42</sup>

The zeta potential values of the AuNPs after addition of 0.63, 2.50 and 4.38  $\mu\text{M}$   $\text{Br}^-$  were also investigated. As shown in Fig. S3 (ESI<sup>†</sup>), the zeta potential values increased in proportion to the concentration of  $\text{Br}^-$ , indicating that colloidal AuNPs are more highly electrically stabilized. The addition of  $\text{Br}^-$  could stabilize the AuNP colloid and enhance the repulsion force between the AuNPs. This increased the repulsion force of each AuNP, which could affect the chelation between  $\text{Cr}^{3+}$  and citrate. As a result, the color of the solution remained red as the  $\text{Br}^-$  concentration increased, relating to the increased dispersion state. The TEM confirmed the observation that the AuNPs remained dispersed with the addition of  $\text{Br}^-$  and  $\text{Cr}^{3+}$ , as well as confirming the decrease in size of the AuNPs compared to their size in the aggregation state as shown in Fig. 3A(c) and (f), respectively. Thus, it suggested that the effective anti-aggregation is induced by  $\text{Br}^-$ .

## 3.2 Optimization of colorimetric detection of bromide ions

**3.2.1 Concentrations of  $\text{Cr}^{3+}$ .** The effect of different concentrations of  $\text{Cr}^{3+}$  in the range 0.96–19.23  $\mu\text{M}$  on the aggregation of AuNPs was investigated (Fig. 4A). With an increasing concentration of  $\text{Cr}^{3+}$ , the color of the suspension gradually changed from red wine to purple and finally to blue, indicating a disruption to the stability of the citrate-capped AuNPs (Fig. 4A, inset picture). Initially, at a concentration of 0.96  $\mu\text{M}$   $\text{Cr}^{3+}$ , the aggregation of the AuNPs was negligible since the excess amount of AuNPs provided a large number of binding sites and a better affinity for the citrate ion over  $\text{Cr}^{3+}$ .<sup>39</sup> At a concentration of 2.40–4.81  $\mu\text{M}$   $\text{Cr}^{3+}$ , the aggregation was enhanced, which can be seen in the colour change from a purple to a blue solution. This may be attributed to the fact that the binding sites of the citrate ion on the surface of the AuNPs were occupied by  $\text{Cr}^{3+}$ , leading to aggregation.

These results reveal the sharp decrease in the absorbance ratio of  $A_{519}/A_{673}$  of 0.96–4.81  $\mu\text{M}$   $\text{Cr}^{3+}$  (Fig. 4A). At a concentration of  $\text{Cr}^{3+}$  higher than 4.81  $\mu\text{M}$ , the ratio became stable, indicating the maximum degree of aggregation. By considering the lowest concentration of  $\text{Cr}^{3+}$  that provided the maximum degree of aggregation, 4.81  $\mu\text{M}$   $\text{Cr}^{3+}$  was chosen as the optimal concentration.

Although  $\text{Cr}^{3+}$  is a toxic substance, it is considered as an essential trace element and is less toxic than  $\text{Cr}^{6+}$ , since  $\text{Cr}^{6+}$  has

high solubility and mobility in biological systems.<sup>43</sup> The selected concentration of  $\text{Cr}^{3+}$  (equal to 4.81  $\mu\text{M}$  or 5.76 nmol  $\text{Cr}^{3+}$ ) used in our test was very low.

Moreover, we have investigated other non-toxic substances such as  $\text{Fe}^{3+}$  and  $\text{Al}^{3+}$  for use as aggregation reagents as shown in Fig. S4 (ESI<sup>†</sup>). This showed that at the same concentration of ions,  $\text{Cr}^{3+}$  provided heavy aggregation of citrate-stabilized gold nanoparticles but  $\text{Fe}^{3+}$  and  $\text{Al}^{3+}$  did not aggregate AuNPs. The optimization of the pH of the phosphate buffer in the range 6.0–8.0 in the presence of  $\text{Cr}^{3+}$ ,  $\text{Fe}^{3+}$  and  $\text{Al}^{3+}$  was also carried out (Fig. S5 (ESI<sup>†</sup>)). Only  $\text{Cr}^{3+}$  gave the response of aggregation of the AuNPs. These two investigations confirmed that  $\text{Cr}^{3+}$  is more specific for  $\text{Br}^-$  detection than other aggregation reagent ions ( $\text{Fe}^{3+}$  and  $\text{Al}^{3+}$ ).

**3.2.2 pH of solution.** The pH of solution affected the anti-aggregation system between  $\text{Br}^-$  and the AuNPs, and thus influenced the  $A_{519}/A_{673}$  ratio. The phosphate buffer was chosen due to its high solubility in water and high buffering capacity in the studied range. Fig. 4B shows the effect of the pH values (6.0 to 7.5) of the phosphate buffer on the sensitivity to  $\text{Br}^-$  concentration in the range 0.63–5.01  $\mu\text{M}$ . This sensitivity value was the slope of linearity plotted between the  $A_{519}/A_{673}$  ratio (y axis) and the  $\text{Br}^-$  concentration (x axis) as shown in Fig. S6 (ESI<sup>†</sup>). The result showed that the sensitivity of bromide detection increased when the pH of the buffer increased from 6.0 to 6.5 (Fig. 4B) and the corresponding solution changed color from blue to red (Fig. S6 (ESI<sup>†</sup>)).

It is known that the  $\text{pK}_{\text{a}1}$ ,  $\text{pK}_{\text{a}2}$  and  $\text{pK}_{\text{a}3}$  values of citric acid are 3.2, 4.8 and 6.4, respectively.<sup>38,44</sup> When the pH value was lower than 6.4, the citric acid group can combine with  $\text{H}^+$ , resulting in the reduction of the chelation interaction between the citrate ion and  $\text{Cr}^{3+}$ . This negatively influenced the aggregation process, and as a result, a decrease in sensitivity was observed.

In the case of pH 6.5 (close to  $\text{pK}_{\text{a}3}$ ), citric acid exists in a trivalent anion and this has the highest ability to chelate  $\text{Cr}^{3+}$ .<sup>37</sup> This pH resulted in an increase in the affinity of chelation between the citrate ion and  $\text{Cr}^{3+}$ . Therefore, high aggregation will lead to a high anti-aggregation process in the studied concentration range of  $\text{Br}^-$  and then maximize sensitivity. When the pH was increased from 7.0–7.5, the sensitivity was reduced in this system because hydrolysis of  $\text{Cr}^{3+}$  probably occurred, resulting in the formation of colloidal  $\text{Cr}(\text{OH})_3$  that could stop the chelating reaction of the citrate-capped-AuNPs with  $\text{Cr}^{3+}$ .<sup>45,46</sup> Another possible reason is that  $\text{Br}^-$  was likely dispersed in the alkaline environment of the solution rather than adsorbed on the AuNP surface. To obtain the maximum response of detection, a phosphate buffer of pH 6.5 was chosen.

**3.2.3 Concentrations of the phosphate buffer.** The influence of the concentration of the phosphate buffer (pH 6.5) in the range 2.5–25.0 mM on the aggregation and anti-aggregation of the AuNPs was performed. We investigated the effect of the buffer concentration by monitoring the change in the intensity ratio of the anti-aggregation signal from the analyte and aggregation signal from the  $\text{Cr}^{3+}$  (Fig. 4C), and all the obtained signals are shown in Fig. S7 (ESI<sup>†</sup>).

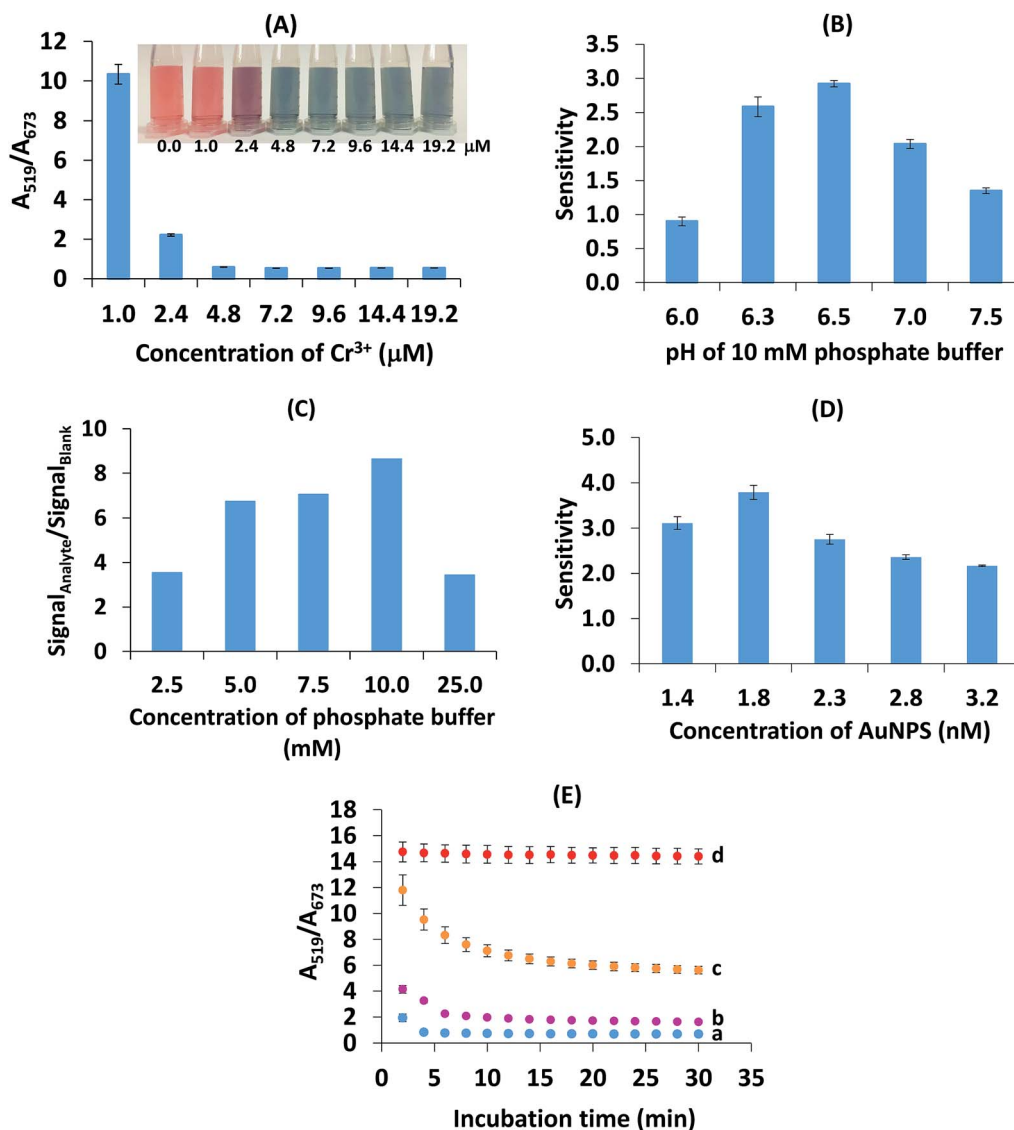


Fig. 4 Optimization of the colorimetric detection of  $\text{Br}^-$ . (A) Concentration of  $\text{Cr}^{3+}$ . (B) pH of 10 mM phosphate buffer. The sensitivity was the slope of linearity plotted between the  $A_{519}/A_{673}$  ratio (y axis) and the  $\text{Br}^-$  concentration in the range 0.62–5.01  $\mu\text{M}$  (x axis). (C) Concentration of the phosphate buffer (pH 6.5). The  $\text{signal}_{\text{Analyte}}$  and  $\text{signal}_{\text{Blank}}$  were the anti-aggregation signal from the analyte and aggregation signal from the  $\text{Cr}^{3+}$ , respectively. (D) Concentration of AuNPs. The sensitivity was the slope of linearity for the  $\text{Br}^-$  concentration in the range 0.63–2.50  $\mu\text{M}$ . (E) Reaction time: (a) blank (without  $\text{Br}^-$ ), (b) 1.25  $\mu\text{M}$   $\text{Br}^-$ , (c) 2.50  $\mu\text{M}$   $\text{Br}^-$  and (d) 5.01  $\mu\text{M}$   $\text{Br}^-$ .

Liu and Wang mentioned that citrate-capped AuNPs would aggregate in aqueous media with high ionic strength.<sup>39</sup> In this study, the maximum tolerable ionic strength was found to be 10.0 mM since this was when the maximum sensitivity was obtained. The results showed that a buffer concentration of 25.0 mM led to a large increase in the ionic strength, which could cause the anti-aggregation to decrease and thus cause the intensity ratio to decrease. By considering the maximal ratio between the signal of the analyte and the blank, 10.0 mM phosphate buffer (pH 6.5) was chosen for the next experiment.

**3.2.4 Concentrations of AuNPs.** The amount of AuNPs is relative to the adsorption of  $\text{Br}^-$  on the AuNP surface. If the concentration of AuNPs increases, it is necessary to increase the amount of  $\text{Br}^-$  to allow for the anti-aggregation of the AuNPs.

Therefore, different final concentrations of the AuNPs ranging from 1.38 to 3.21 nM were tested to obtain the maximum sensitivity of the  $\text{Br}^-$  concentration in the range 0.63–2.50  $\mu\text{M}$  (Fig. 4D). This sensitivity value was the slope of linearity (Fig. S8 (ESI<sup>†</sup>)). When the AuNP concentration was 1.38 nM, it was difficult to observe the color of the solution with the naked eye due to its faded color. The sensitivity increased to be highest in the case of 1.83 nM AuNPs and decreased when the concentration increased above 1.83 nM because an insufficient amount of bromide ions was adsorbed on the high abundance of AuNPs, leading to low anti-aggregation. Therefore, 1.83 nM AuNPs was chosen.

**3.2.5 Reaction time.** The influence of the reaction time in the range 0–30 min on the interaction between AuNPs and  $\text{Br}^-$

at 1.25, 2.50 and 5.01  $\mu\text{M}$  was studied (Fig. 4E). It can be seen that the absorption ratio ( $A_{519}/A_{673}$ ) tended to decrease in the period from 0 to 10 min and was then stable from 10 to 30 min. This indicated that the anti-aggregation was complete after 10 min of reaction time. Thus, a reaction time of 10 min was chosen and all further sensor measurements could be carried out within 10 min.

### 3.3 Method validation

The concentration of bromide ions in a solution was confirmed by comparing its color and absorbance with a standard solution under the same conditions. The degree of anti-aggregation (seen by the color of solutions changing gradually from blue to red) depends on the concentration of  $\text{Br}^-$ . Fig. 5 shows the absorption changes with the addition of  $\text{Br}^-$ , which were further confirmed by looking at the color changes. The absorbance at 673 decreased with an increasing concentration of  $\text{Br}^-$  and the peak at 519 nm increased due to the anti-aggregation of the AuNPs. The absorbance ratio of  $A_{519}/A_{673}$  was used for the quantitative determination of  $\text{Br}^-$  since it was found to be less sensitive to changes caused by different detection conditions.

A good linearity of the standard calibration curve ( $y = 3.4803x - 0.6065$ ,  $R^2 = 0.9970$ ) was found in the range 0.31–3.75  $\mu\text{M}$   $\text{Br}^-$  (Fig. 6a). The limit of detection (LOD) and limit of quantification (LOQ) were the  $\text{Br}^-$  concentrations that gave a signal equal to the blank signal (S/N) plus three and ten standard deviations of the blank, respectively ( $n = 20$ ).<sup>47</sup> The LOD and LOQ were as low as 0.04 and 0.13  $\mu\text{M}$ , respectively. The recovery was investigated by spiking the  $\text{Br}^-$  concentrations of 12.00 to 60.00  $\text{mg kg}^{-1}$  into composite rice samples and then testing them using our developed system. As seen in Table 1, good recoveries ranging from 79.9–92.2% were obtained with a precision (RSD) of less than 4.0% ( $n = 3$ ). The inter-day precision of the three concentration levels of  $\text{Br}^-$  (0.63, 1.25, 3.75  $\mu\text{M}$ ) determined on each of 5 days fell between 3.07 and 7.12% ( $n = 45$ ), whereas the intra-day precision obtained from

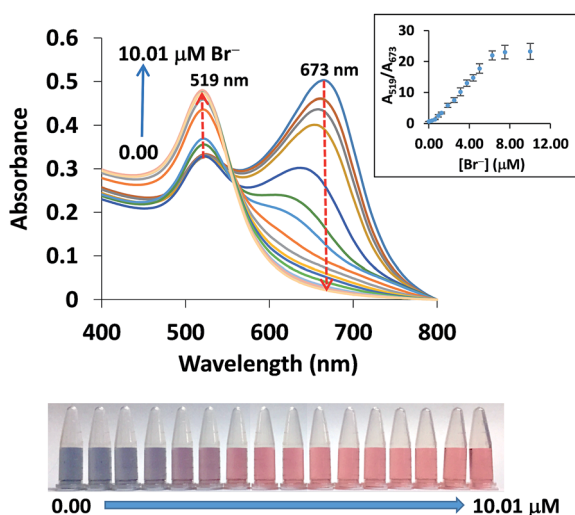


Fig. 5 UV-vis absorption spectra changes of the AuNPs in the presence of 0.00–10.01  $\mu\text{M}$   $\text{Br}^-$ .

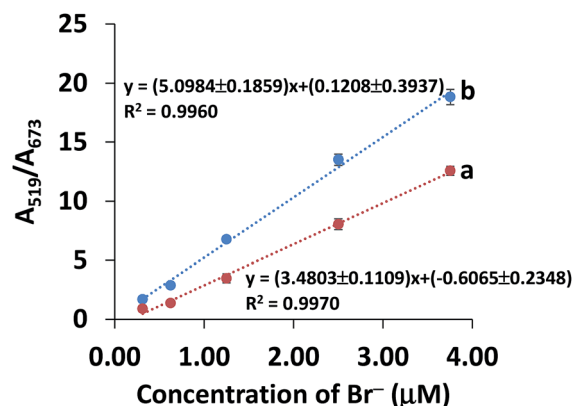


Fig. 6 Curves of (a) the standard calibration curve and (b) the standard addition curve for  $\text{Br}^-$  concentration in the range 0.31–3.75  $\mu\text{M}$ .

the 5 measurements of each of the three concentration levels on the same day ranged from 2.87–6.35% ( $n = 15$ ). These recoveries and precisions were acceptable within the range referred to in the AOAC standard method.<sup>48</sup>

In contrast to the aqueous standard solution, trace quantification of the analyte in real samples can suffer from the effects of the sample matrices, which can cause a positive or negative response by increasing background noise or suppressing the signal response.<sup>49</sup> Hence, the matrix effect was investigated using a standard addition curve (Fig. 6b) in the range 0.31–3.75  $\mu\text{M}$   $\text{Br}^-$  (spiked into rice water extracts), which was compared to a standard calibration curve (Fig. 6a). As shown in Fig. 6, the sensitivity of the standard addition curve (b) was significantly different from that of the standard curve (a) ( $P < 0.05$ ), indicating that the matrix did have an effect on the analysis of  $\text{Br}^-$  in rice samples. Therefore, we used a standard addition curve for accurate determination of  $\text{Br}^-$  in rice samples.

### 3.4 Comparison of the developed sensor with other analytical methods

To further demonstrate the advantages of the developed sensor, the performance of our sensor was compared with other previously reported methods. Table 2 lists the comparison results, including sample amount, linear range, LOD and detection time, of our developed sensor with other methods. The LOD and linearity obtained by our sensor were clearly superior to those obtained in the other studies. In addition, our sensor has a short detection time compared with the expensive

Table 1 Recoveries of spiked  $\text{Br}^-$  in composite rice samples with relative standard deviation (RSD) values ( $n = 3$ )

Spiked ( $\text{mg kg}^{-1}$ )	Detected ( $\text{mg kg}^{-1}$ )	Recovery (%)	RSD (%)
0.00	$2.19 \pm 0.57$	—	—
12.00	$11.78 \pm 0.33$	79.94	2.81
25.00	$23.52 \pm 0.94$	85.35	3.98
50.00	$48.28 \pm 1.86$	92.19	3.85
60.00	$50.42 \pm 1.18$	80.40	2.35

Table 2 Comparison of the developed sensor with other methods applied for Br<sup>-</sup> determination in different samples

Method <sup>a</sup>	Sample	Sample amount	Linear range (μM)	LOD (μM)	Detection time (min)	Reference
LLE-deriv.-GC-μECD	Rice	2 g	62.58–938.63	25.03	20	3
Microwave digestion-ICP-MS	Food	1–2 g	25.03–2503.00	8.51	1	16
Phenol red spectrophotometry	Vegetables	5 g	6.26–56.32	3.13	3	18
LPIEC-visible light detection	Foodstuffs	25 g	0.38–62.58	0.03	7.5	19
Phenol red and chloramine-T colorimetry	Environmental samples	20–300 μL	0.00–375.45	1.38	5	50
Aggregation and anti-aggregation of AgNPs	Water	—	0.99–5.66	1.67	—	51
Total reflection X-ray fluorescence spectrometry	Soil	1 g	15.64–156.44	3.13	25	52
Fluorescent Ag nanocluster detection	Dried kelp	1 g	0.10–50.00	—	60	53
Anti-aggregation of AuNPs	Rice	2 g	0.31–3.75	0.04	<10	This work

<sup>a</sup> LLE-deriv.-GC-μECD: liquid-liquid extraction-derivatization-gas chromatography-micro electron capture detector; ICP-MS: inductive coupled plasma-mass spectrometry; LPIEC: low pressure ion-exchange chromatography.

methods.<sup>3,52,53</sup> Our sensor required a comparable amount of sample to be used for detecting Br<sup>-</sup> in real samples to the methods mentioned in Table 2. Overall, these results confirmed that our method for Br<sup>-</sup> determination based on the anti-aggregation of AuNPs was more efficient and sensitive.

### 3.5 Selectivity study

Other cations and anions in rice samples were investigated as they could probably interfere with the selectivity for Br<sup>-</sup>. It was reported that inorganic anions, *i.e.* F<sup>-</sup>, Cl<sup>-</sup>, NO<sub>2</sub><sup>-</sup>, NO<sub>3</sub><sup>-</sup> and SO<sub>4</sub><sup>2-</sup>, were found in rice samples from four provinces in China using ion chromatography, ranging from not detected to 20.90 mg kg<sup>-1</sup>.<sup>54</sup> Some elements in rice extracts prepared using our alkaline digestion and ashing method were determined using inductively coupled plasma-optical emission spectrometry (ICP-OES) as presented in Table S1 (ESI<sup>†</sup>). It was shown that

the samples had high concentrations of K, Mg, Ca and P in the range 6.66–13 554.17 mg kg<sup>-1</sup> whereas Al, Cr and Se were found in low concentrations (0.20–2.79 mg kg<sup>-1</sup>). The detection of K, Ca, Mg and Al agreed with the data of other reports.<sup>55,56</sup> Thus, the 10 common ions, *i.e.* K<sup>+</sup>, Mg<sup>2+</sup>, Ca<sup>+</sup>, Al<sup>3+</sup>, NO<sub>2</sub><sup>-</sup>, NO<sub>3</sub><sup>-</sup>, PO<sub>4</sub><sup>3-</sup>, SO<sub>4</sub><sup>2-</sup>, F<sup>-</sup>, Cl<sup>-</sup>, were investigated alongside Br<sup>-</sup> under the same optimal conditions. We found that Cu, Fe, Mn, Ni and Zn were not detected, thus they were not included as interferences.

The selectivity was evaluated by testing the absorbance ratio ( $A_{519}/A_{673}$ ) of 5 μM Br<sup>-</sup> to 5000 μM of other ions including K<sup>+</sup>, Mg<sup>2+</sup>, Ca<sup>2+</sup>, Al<sup>3+</sup>, NO<sub>2</sub><sup>-</sup>, NO<sub>3</sub><sup>-</sup>, PO<sub>4</sub><sup>3-</sup>, SO<sub>4</sub><sup>2-</sup>, F<sup>-</sup> and Cl<sup>-</sup>. As shown in Fig. 7, Br<sup>-</sup> (red bar) showed a distinct signal whereas in the absence of Br<sup>-</sup>, the signal of the other ions except for Cl<sup>-</sup> (blue bar) was almost identical to the blank even when their concentrations were 1000-fold higher than Br<sup>-</sup>, suggesting that no anti-aggregation of AuNPs was caused by the other ions. Furthermore, the response of Br<sup>-</sup> in the presence of a mixture of all the ions (violet bar) increased to a level similar to that of Br<sup>-</sup> alone (red bar). This can be explained by the fact that Br<sup>-</sup> is lightly hydrated and has higher polarizability which can be attractive when it is close to the AuNP surface compared to NO<sub>3</sub><sup>-</sup>, SO<sub>4</sub><sup>2-</sup>, F<sup>-</sup> and Cl<sup>-</sup> while the other negative ions are repelled from the surface.<sup>57</sup> Only the addition of 5000 μM Cl<sup>-</sup> can result in anti-aggregation. However, considering that a low abundance of Cl<sup>-</sup> (about 3.05 mg kg<sup>-1</sup>) was detected in the rice sample matrix, the signal caused by Cl<sup>-</sup> can be ignored.

Other anions such as I<sup>-</sup>, S<sup>2-</sup>, SO<sub>3</sub><sup>2-</sup>, and SCN<sup>-</sup> could affect the detection of Br<sup>-</sup>. Thus, the effect of I<sup>-</sup> and SCN<sup>-</sup> on the selectivity of the detection was investigated and the results are shown in Fig. S9 (ESI<sup>†</sup>), and the responses of these ions were similar to that of Br<sup>-</sup>. This means that they interfere with the anti-aggregation of AuNPs because I<sup>-</sup> and SCN<sup>-</sup> are classified as chaotropic anions like Br<sup>-</sup>.<sup>57</sup> However, SCN<sup>-</sup>, S<sup>2-</sup> and SO<sub>3</sub><sup>2-</sup> have never been reported in rice samples, thus they are not of major concern for detection. It was reported that the concentration of I<sup>-</sup> is approximately 185 times lower than that of Br<sup>-</sup> in white rice samples,<sup>55</sup> and therefore, the signal caused by the low abundance of I<sup>-</sup> in real samples can be ignored.

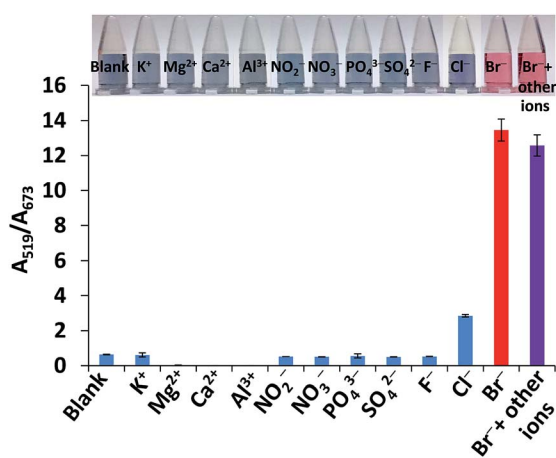


Fig. 7 Selectivity of the Br<sup>-</sup> detection. The absorbance ratio response ( $A_{519}/A_{673}$ ) of the proposed sensor for 5 μM Br<sup>-</sup> (red bar) was plotted against 5000 μM of ion interferences (K<sup>+</sup>, Mg<sup>2+</sup>, Ca<sup>2+</sup>, Al<sup>3+</sup>, NO<sub>2</sub><sup>-</sup>, NO<sub>3</sub><sup>-</sup>, PO<sub>4</sub><sup>3-</sup>, SO<sub>4</sub><sup>2-</sup>, F<sup>-</sup> and Cl<sup>-</sup> (blue bars)) and a mixture of Br<sup>-</sup> and the other ions (violet bar). All signals corresponded to the blank. The photograph is an example of the detection sensor for 5 μM Br<sup>-</sup>, the other ions and a mixture of Br<sup>-</sup> and all the other ions.

These results clearly revealed that the simultaneous presence of other competitive ions even at very high concentrations did not interfere with the determination of  $\text{Br}^-$ . Thus, our colorimetric sensor exhibited a high selectivity for  $\text{Br}^-$  over other ions in rice samples.

### 3.6 Application of the method to rice samples

To further evaluate the feasibility of the developed sensor, five different commercial brands of white rice were collected from supermarkets and examined for  $\text{Br}^-$  residues. The first attempt to prepare the rice sample was made by soaking the rice in water as a simple method and the water extract of the rice was then passed through a solid phase sorbent cartridge (Oasis HLB) and analyzed using colorimetric determination. It appeared that no significant difference in color between the unspiked and spiked sample was observed (both samples presented a red solution), indicating that the interferences, especially organic substances as well as  $\text{Br}^-$ , could dissolve in aqueous extracts.

Srisawat *et al.* examined phenolic or flavonoid compounds in rice water extracts.<sup>58</sup> These compounds could probably interfere with the  $\text{Br}^-$  detection by: (i) adsorbing onto the surface of the AuNPs and hindering the ligand-exchange process in the  $\text{Cr}^{3+}$ -citrate complex and (ii) forming a complex with  $\text{Cr}^{3+}$  instead of with the citrate. Therefore, the removal of the organic interferences is necessary.

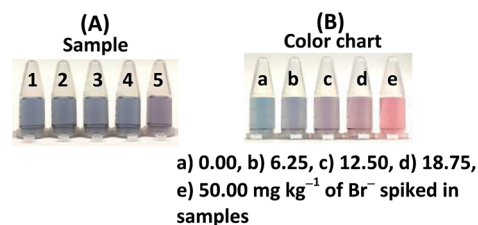
Our sample digestion method using 1% potassium hydroxide in 50% ethanol and our ashing procedure to remove all the organic contents from the rice samples was studied and compared with an acidic digestion using hydrogen peroxide and hydrochloric acid. Metals in all the samples were analyzed using ICP-OES. As seen in Table S1 (ESI<sup>†</sup>), the concentrations of other cations such as  $\text{Mg}^{2+}$ ,  $\text{Ca}^{2+}$  and  $\text{Al}^{3+}$  obtained using our method were much lower than those obtained *via* acidic digestion except that a higher amount of  $\text{K}^+$  was detected. This was due to the addition of KOH for rice digestion; however, it has proved that  $\text{K}^+$  residue does not interfere with colorimetric detection using AuNPs as shown in Fig. 7.

In addition, high recoveries for the sample preparation and detection were obtained (Table 1). Since we used a high temperature (600 °C) for the ashing step, it was possible that  $\text{Br}^-$  could evaporate, and so the remaining  $\text{Br}^-$  in the samples was investigated using the X-ray fluorescence (XRF) technique. The composite rice samples were spiked with  $\text{Br}^-$  concentrations of 50, 100, 200 and 400 M and prepared as mentioned in Section 2.5. After dilution, the solution was adjusted to pH 8.0 with 1 M nitric acid, and was subsequently analyzed using the XRF method. Fig. S10 (ESI<sup>†</sup>) shows the XRF spectra of the sample solutions spiked with  $\text{Br}^-$  concentrations in the range 50–400 M. The peak signals of  $\text{Br}^-$  increased with increasing  $\text{Br}^-$  concentration. This confirmed that  $\text{Br}^-$  will not evaporate at a temperature of 600 °C. Thus, these results confirmed that our alkaline digestion and ashing method can remove some metals and organic interferences without any loss of  $\text{Br}^-$ .

Whereas Sungwaranond *et al.*<sup>2</sup> performed the ashing step for 8 h, leading to a time consuming sample preparation, we further investigated the time for ashing (4 and 8 h). The results

**Table 3** The determination of  $\text{Br}^-$  in the rice samples using the developed sensor ( $n = 3$ ) and ion chromatography ( $n = 2$ ), with (A) the corresponding colorimetric results and (B) a color chart for the sample sensor

Sample	Found ( $\text{mg kg}^{-1}$ )	
	Developed sensor	Ion chromatography
White rice 1	$3.12 \pm 0.83$	$3.41 \pm 1.61$
White rice 2	$4.23 \pm 1.10$	$6.25 \pm 0.80$
White rice 3	$4.07 \pm 1.70$	$3.41 \pm 2.41$
White rice 4	$4.16 \pm 0.48$	$4.00 \pm 2.41$
White rice 5	$5.21 \pm 0.91$	$6.82 \pm 4.82$



showed that statistically insignificant differences in the concentrations of cations with an ashing step of 4 and 8 h were observed in the samples (Table S1 (ESI<sup>†</sup>)). Thus, in this work, the rice samples were treated using the alkaline digestion and ashing method for 4 h.

Table 3 shows the determination of  $\text{Br}^-$  in rice samples using our sensor, together with the corresponding colorimetric results. The color chart, made by adding a  $\text{Br}^-$  standard ranging from 6.25 to 50.00  $\text{mg kg}^{-1}$  into the samples, was made for detection with the naked eye.  $\text{Br}^-$  residues were detected in all the studied samples in the range 3.12–5.21  $\text{mg kg}^{-1}$ , which all fell in the range 0.00–6.25  $\text{mg kg}^{-1}$  shown in the color chart and were higher than those detected by Parengam *et al.* (0.40–1.4  $\text{mg kg}^{-1}$ ).<sup>55</sup> However, the detectable concentrations of  $\text{Br}^-$  did not exceed the MRL limit set by The Thai Ministry of Public Health (50  $\text{mg kg}^{-1}$ ).<sup>13</sup> Moreover, it showed that no interferences due to co-extracted compounds were found as seen in the colorimetric results of the samples (Table 3(A)).

At present, there is no established standard method for the detection of  $\text{Br}^-$  in rice samples. We have validated our developed sensor with the ion chromatographic (IC) technique (Table 3). It was found that the concentrations of  $\text{Br}^-$  detected using the developed sensor were not significantly different from those detected using IC ( $P > 0.05$ ).

These results confirmed that the developed sensor method can be used for the analysis of  $\text{Br}^-$  in real complex samples.

## 4. Conclusions

We have developed a robust colorimetric sensor for bromide ions using citrate-capped AuNPs in the presence of  $\text{Cr}^{3+}$ . The method was simple, highly sensitive and selective, and was based on the anti-aggregation induced by  $\text{Br}^-$ , which results in a color change from blue to red upon the addition of different concentrations of  $\text{Br}^-$ . This system presents a low LOD and LOQ



without any noticeable interfering effects from the other components in rice samples. Satisfying recovery and precision were achieved with our developed colorimetric sensor.

## Conflicts of interest

There are no conflicts of interest to declare.

## Acknowledgements

This work was financially supported by the Research Assistantship (Contract No. 1-2558-02-003), Faculty of Science, Prince of Songkla University, the Department of Chemistry, the Center of Excellence for Innovation in Chemistry (PERCH-CIC), Office of the Higher Education Commission, Ministry of Education (OHEC), and the Graduate School, Prince of Songkla University.

## References

- 1 K. N. T. Norman, *Pest Manage. Sci.*, 2000, **56**, 154–158.
- 2 B. Sungwaranond, P. Jongmeevasana and G. Thoophom, *Bulletin of the Department of Medical Sciences*, 1998, **40**(2), 171–177.
- 3 W. Wittayanan and W. Jongmeevasana, *Bulletin of the Department of Medical Sciences*, 2015, **57**(3), 219–232.
- 4 U.S Department of Health and Human Services, *Occupational health guideline for methyl bromide*, 1978, pp. 1–5.
- 5 United States Environmental Protection Agency (U.S. EPA), Protection of Stratospheric Ozone: Incorporation of Montreal Protocol Adjustment for a 1999 Interim Reduction in Class I, Group VI Controlled Substances. *Fed. Regist.*, 1999, **64**(104), 29240–29245.
- 6 W. B. Thomas, *J. Nematol.*, 1996, **28**(4S), 586–589.
- 7 FAO (1999) Food Agriculture Organization-World Health Organization, Codex maximum limits for pesticide residues, Codex Alimentarius Commission, FAO plant production and protection paper.
- 8 CCM, China reveals a list of newly banned insecticides, <http://www.cnchemicals.com/Press/89543-China%20reveals%20a%20list%20of%20newly%20banned%20insecticides.html>, accessed 18. 11. 2017.
- 9 X. Baur, L. T. Budnik, Z. Zhao, M. Bratveit, R. Djurhuus, L. Verschoor, F. M. Rubino, C. Colosio and J. R. Jepsen, *J. Occup. Med. Toxicol.*, 2015, **10**(19), 1–18.
- 10 M. Miyahara and Y. Saito, *J. Agric. Food Chem.*, 1994, **42**, 1126–1131.
- 11 D. Cova, G. F. Molinari and L. Rossini, *Food Addit. Contam.*, 1986, **3**(3), 235–240.
- 12 The Montreal Protocol on Substances that Deplete the Ozone Layer/Article 2H: Methyl bromide, <http://www.ozone.unep.org/en/handbook-montreal-protocol-substances-deplete-ozone-layer/16>, accessed 9. 04. 2018.
- 13 Notification of the Ministry of Public Health (No. 361) B.E. 2556, 2013, page 5.
- 14 P. Pimpun, Methyl bromide and bromide ion, <http://www.thaipan.org/sites/default/files/file/4%20MB-Br%20.Prapassara.pdf>, accessed 4. 11. 2017.
- 15 A. A. Mahmoud, R. Gouda and L. Ryad, *Journal of Plant Protection and Pathology*, 2014, **5**(11), 1015–1023.
- 16 T. K. D. Nguyen and R. Ludwig, *Anal. Sci.*, 2014, **30**, 1089–1092.
- 17 G. Chiu and R. D. Eubanks, *Microchim. Acta*, 1989, **2**, 145–148.
- 18 E. Baso-Cejas, G. Brito, C. Díaz and E. M. Peña-Méndez, *Bull. Environ. Contam. Toxicol.*, 2007, **78**, 417–420.
- 19 L. Yu, X. Zhang, J. Jin, S. Che and L. Yu, *Czech J. Food Sci.*, 2011, **29**(6), 634–640.
- 20 Y. Zhou, H. Dong, L. Liu, M. Li, K. Xiao and M. Xu, *Sens. Actuators, B*, 2014, **196**, 106–111.
- 21 Y. Li, P. Wu, H. Xu, Z. Zhang and X. Zhong, *Talanta*, 2011, **84**, 508–512.
- 22 M. R. H. Nezhad and S. A. Moayed, *Talanta*, 2014, **129**, 227–232.
- 23 D. Liu, Z. Wang and X. Jiang, *Nanoscale*, 2011, **3**, 1421–1433.
- 24 M. Zhang, Y. Q. Liu and B. C. Ye, *Analyst*, 2011, **136**, 4558–4562.
- 25 T. Lou, L. Chen, C. Zhang, Q. Kang, H. You, D. Shen and L. Chen, *Anal. Methods*, 2012, **4**(2), 488–491.
- 26 G. Wang, Z. Chen, W. Wang, B. Yan and L. Chen, *Analyst*, 2011, **136**(1), 174–178.
- 27 L. Chen, W. Lu, X. Wang and L. Chen, *Sens. Actuators, B*, 2013, **182**, 482–488.
- 28 Z. Zhang, J. Zhang, C. Qu, D. Pan, Z. Chen and L. Chen, *Analyst*, 2012, **137**, 2682–2686.
- 29 Z. Zhang, Z. Chen, S. Wang, C. Qu and L. Chen, *ACS Appl. Mater. Interfaces*, 2014, **6**(9), 6300–6307.
- 30 J. Kang, Y. Zhang, X. Li, L. Miao and A. Wu, *ACS Appl. Mater. Interfaces*, 2016, **8**, 1–5.
- 31 A. Sharma, Z. Matharu, G. Sumana, P. R. Solanki, C. G. Kim and B. D. Malhotra, *Thin Solid Films*, 2010, **519**, 1213–1218.
- 32 Y. Luo, J. Xu, Y. Li, H. Gao, J. Guo, F. Shen and C. Sun, *Food Control*, 2015, **54**, 7–15.
- 33 M. Akhond, G. Absalan and H. Ershadifar, *Spectrochim. Acta, Part A*, 2015, **143**, 223–229.
- 34 S. Kong, M. Liao, Y. Gu, N. Li, P. Wu, T. Zhang and H. He, *Spectrochim. Acta, Part A*, 2016, **157**, 244–250.
- 35 J. Song, F. Wu, Y. Wan and L. Ma, *Food Control*, 2015, **50**, 356–361.
- 36 M. Elavarasi, A. Rajeshwari, N. Chandrasekaran and A. Mukherjee, *Anal. Methods*, 2013, **5**, 6211–6218.
- 37 A. Heller, A. Barkleit, H. Foerstendorf, S. Tsushima, K. Heim and G. Bernhard, *Dalton Trans.*, 2012, **41**, 13969–13983.
- 38 V. I. Kornev and G. A. Mikryukova, *Russ. J. Coord. Chem.*, 2004, **30**(12), 946–950.
- 39 Y. Liu and X. Wang, *Anal. Methods*, 2013, **5**, 1442–1448.
- 40 C. Pfeiffer, C. Rehbock, D. Hühn, C. Carrillo-Carrion, D. J. de Aberasturi, V. Merk, S. Barcikowski and W. J. Parak, *J. R. Soc., Interface*, 2014, **11**(20130931), 1–13.
- 41 G. Senanayake, *Miner. Eng.*, 2004, **17**, 785–801.
- 42 E. G. Vinokurov and V. V. Bondar, *Russ. J. Coord. Chem.*, 2003, **29**(1), 66–72.
- 43 K. Shrivias, S. Sahu, G. K. Patra, N. K. Jaiswal and R. Shankar, *Anal. Methods*, 2016, **8**, 2088–2096.
- 44 M. Chen, H.-H. Cai, F. Yang, D. Lin, P.-H. Yang and J. Cai, *Spectrochim. Acta, Part A*, 2014, **118**, 776–781.

- 45 X. Wang, Y. Wei, S. Wang and L. Chen, *Colloids Surf., A*, 2015, **472**, 57–62.
- 46 L. Spiccia and W. Marty, *Inorg. Chem.*, 1986, **25**, 266–271.
- 47 J. N. Miller and J. C. Miller, *Statistics and Chemometrics for Analytical Chemistry*, Pearson Education Limited, England, UK, 5th edn, 2005, Essex.
- 48 AOAC, *Guidelines for Standard Method Performance Requirements, Appendix F*, 2016, pp. 2–18.
- 49 T. Rujiralai, N. Raekasin, W. Cheewasedtham and C. Cheewasedtham, *Chem. Pap.*, 2014, **68**(8), 1041–1048.
- 50 B. J. Lepore and P. Barak, *Soil Sci. Soc. Am. J.*, 2009, **73**, 1130–1136.
- 51 S. Bothra, R. Kumar, R. K. Pati, A. Kuwar, H.-J. Choi and S. K. Sahoo, *Spectrochim. Acta, Part A*, 2015, **149**, 122–126.
- 52 H. Gallardo, I. Queralt, J. Tapias, L. Candela and E. Margui, *Chemosphere*, 2016, **156**, 294–301.
- 53 L. Fu, C. Li, Y. Li, S. Chen, Y. Long and R. Zeng, *Sens. Actuators, B*, 2017, **240**, 315–321.
- 54 H. Sun, L. Xia, S. Liang and S. Shen, *Food Analytical Methods*, 2014, **7**, 1791–1797.
- 55 M. Parengam, K. Judprasong, S. Srianujata, S. Jittinandana, S. Laoharajanaphand and A. Busamongko, *J. Food Compos. Anal.*, 2010, **23**, 340–345.
- 56 L. Lu, S. Tian, H. Liao, J. Zhang, X. Yang, J. M. Labavitch and W. Chen, *PLoS One*, 2013, **8**(2), e57360.
- 57 V. Merk, C. Rehbock, F. Becker, U. Hagemann, H. Nienhaus and S. Barcikowski, *Langmuir*, 2014, **30**, 4213–4222.
- 58 U. Srisawat, W. Panunto, N. Kaendee, S. Tanuchit, A. Itharat, N. Lerdvuthisopon and P. Hansakul, *J. Med. Assoc. Thailand*, 2010, **93**(7), S83–S91.

## VITAE

**Name** Mr. Siwat Plaisen

**Student ID** 5810220086

### **Educational Attainment**

<b>Degree</b>	<b>Name of Institution</b>	<b>Year of Graduation</b>
Bachelor of Science (Chemistry)	Prince of Songkla University	2015

### **Scholarship Awards during Enrolment**

The Research Assistantship (Contract No. 1-2558-02-003), Faculty of Science, Prince of Songkla University

The Department of Chemistry Faculty of Science, Prince of Songkla University

The Center of Excellence for Innovation in Chemistry (PERCH-CIC), The Office of the Higher Education Commission, Ministry of Education (OHEC)

The Graduate School, Prince of Songkla University

### **List of Poster presentations and Publication**

#### **Poster presentation**

- A highly sensitive colorimetric detection for bromide ion based on anti-aggregation of gold nanoparticles, The PERCH-CIC Congress X, July 4-7, 2018 at Jomtien Palm Beach Hotel, Pattaya, Thailand.

#### **Publication**

- Plaisen, S., Cheewasedtham, W., and Rujiralai, T. 2018. Robust colorimetric detection based on the anti-aggregation of gold nanoparticles for bromide in rice samples. *RSC Advances*, **8**, 21566-21576.